Remote Sensing of Environment 209 (2018) 551–580

Contents lists available at ScienceDirect

Remote Sensing of Environment

journal homepage: www.elsevier.com/locate/rse

Review

Spatially enhanced passive microwave derived soil moisture: Capabilities and opportunities

Sabah Sabaghy[a,*], Jeffrey P. Walker[a], Luigi J. Renzullo[b], Thomas J. Jackson[c]

[a] Department of Civil Engineering, Monash University, Clayton Campus, VIC 3800, Australia
[b] Fenner School of Environment and Society, The Australian National University, Canberra, Australia
[c] U.S. Department of Agriculture ARS, Hydrology and Remote Sensing Laboratory, Beltsville, MD 20705, USA

ARTICLE INFO

Keywords:
Soil moisture
Downscaling
Disaggregation
Subpixel heterogeneity

ABSTRACT

Low frequency passive microwave remote sensing is a proven technology for providing soil moisture estimates, but the coarse resolution of its data restricts the range of applications. Downscaling, otherwise known as disaggregation, has been proposed as the solution to spatially enhance these coarse resolution soil moisture observations, through association with complementary observations, or ancillary information about land surface features at higher spatial resolution. Such information includes solar reflectance, thermal emission, passive microwave emissions at a higher frequency, radar backscatter, soil or surface attributes such as topography and soil properties, and land surface modelling. Each of these ancillary data sources has its own strengths and limitations in terms of, for example, sensitivity to surface soil moisture dynamics and availability. This paper provides an extensive review of the capabilities and opportunities of current soil moisture downscaling approaches which provide a deterministic pattern of soil moisture, together with their strengths and limitations.

1. Introduction

Land-atmosphere interactions are affected by soil moisture on a global scale (e.g. Entekhabi et al., 1996; Petropoulos et al., 2015), thus exerting an impact upon the climate and weather (e.g. Entekhabi, 1995; Western et al., 2002; Seneviratne et al., 2010; Jung et al., 2010; Lakshmi, 2013; Taylor, 2015) by influencing the partitioning of the incoming radiant energy at the land surface into sensible and latent heat fluxes (Xia et al., 2014). Soil moisture variation also controls the water and energy cycle components through the amount of evapotranspiration which affects soil surface wet and dry patterns that in turn affect precipitation (Koster et al., 2004; Hirschi et al., 2011). The volume of surface run-off and groundwater recharge also depends upon the soil moisture by way of the infiltration rate of precipitation into the soil (Tuttle and Salvucci, 2014). Regional characterization of soil moisture variability at short time intervals would therefore greatly assist understanding of the land-atmosphere system.

Obtaining accurate information on soil moisture at an appropriate temporal and spatial scales is challenging to achieve with global coverage using traditional approaches, due to the high spatial and temporal variability of soil moisture. This variation is caused by the heterogeneous nature of soil properties, topography, land cover, and meteorology (e.g. rainfall and evapotranspiration) that vary as a function of scale (e.g. Crow et al., 2012; Vereecken et al., 2008). Meteorological forcing has a dominant control on the soil moisture spatial pattern at watershed, regional and continental scales (Jana, 2010; Crow et al., 2012), unlike the field and point scales at which the soil moisture varies due to land cover, topography and soil properties. Accordingly, multi-scale soil moisture measurements can provide a vital piece of information for economic, social and environmental planning. Development of field and watershed scale soil moisture measurements is of benefit to agricultural production and better understanding of rainfall-runoff responses, respectively (Robinson et al., 2008). Moreover, measurement of soil moisture at regional and continental scales is important for interpreting land-surface-atmosphere interactions (Kerr et al., 2001; Robinson et al., 2008).

Historically, ground sampling was the only possible approach to measuring soil moisture. However, the sparseness of point measurement stations makes the use of in situ measurements for capturing the spatially variable nature of soil moisture impractical due to their high maintenance and operation expenses. The need for global soil moisture monitoring that compliments the sparsely distributed ground measurements has led to the development of space-borne remote sensing (e.g. Entekhabi et al., 1999; Njoku et al., 2002; Entekhabi et al., 2010; Kerr et al., 2012), covering the Earth's surface with a temporal frequency of a few days. Consequently, a number of sensors have been

* Corresponding author.
E-mail address: sabah.sabaghy@monash.edu (S. Sabaghy).

https://doi.org/10.1016/j.rse.2018.02.065
Received 16 March 2017; Received in revised form 18 January 2018; Accepted 22 February 2018
0034-4257/ © 2018 Elsevier Inc. All rights reserved.

launched on space-borne platforms over the past four decades to acquire the electromagnetic emission, reflection and/or scattering from the land surface, but not necessarily designed for soil moisture.

Sensors are classified according to the electromagnetic spectrum in which they monitor the Earth's surface. The regions of the spectrum of greatest interest for soil moisture are the optical and microwave. Optical remote sensing measures the solar reflective (VIS, Near Infrared (NIR), and Short-Wave InfraRed (SWIR) bands) and/or thermal emissive (Thermal InfraRed (TIR) band) regions of the electromagnetic spectrum. These measurements have been used to determine spatial soil moisture variations by monitoring changes in surface albedo (e.g. Liu et al., 2002; Leone and Sommer, 2000; Dalal and Henry, 1986) and soil heat capacity (Petropoulos et al., 2015). While this information can be observed at a 1 km or better spatial resolution on a (cloud free) daily basis, the signal is directly related to only the very top millimetres of the soil surface for bare soil, or to the surface of the leaves if vegetated. Moreover, the relationship to soil moisture typically depends on evaporative demand and/or vegetation variation across seasons, which limits the potential application of optical observations for direct soil moisture retrieval (Petropoulos et al., 2015). These optical observations also suffer from being attenuated by the atmosphere, and are unable to provide useful data under cloudy skies. This makes the interpretation of optically-based soil moisture predictions complicated because data on the surface micro-meteorological and atmospheric information is required for corrections (Zhang and Wegehenkel, 2006). Access to such data is limited at global scale, thus restricting the application of optical remote sensing for direct soil moisture estimation.

The conversion of remotely sensed solar reflection/albedo data to soil moisture is primarily based on the color of the soil or vegetation. Thus, information about soil mineral composition, organic matter, local incidence angle and vegetation type is required (e.g. Wang and Qu, 2009). For bare soil the determination of soil moisture is limited to observing and interpreting changes in soil color, with moist soil being darker than dry soil. When there is a layer of vegetation, observations primarily reflect changes in vegetation color and/or water in the vegetation. Several land surface indices e.g. Normalized Difference Vegetation Index (NDVI) by Rouse et al. (1974), Normalized Difference Water Index (NDWI) by Gao (1996), and Normalized Multiband Drought Index (NMDI) by Wang and Qu (2007) were developed to suppress vegetation and/or plant color impact. However, their application is limited by the factors mentioned previously.

The utility of TIR remote sensing for soil moisture mapping has been demonstrated in several studies (e.g. Schmugge et al., 1980; Friedl and Davis, 1994; Verhoef et al., 1996; Muller and Décamps, 2001; Anderson et al., 2007). These studies have shown that while there is a negative correlation between the diurnal range in surface soil temperature and the surface soil moisture content, moist soil is cooler in daytime and warmer at night-time than dry soil. This is because the presence of water, which has a greater heat capacity, leads to moist soil having a greater resistance to temperature change than dry soil. These TIR techniques, which use the thermal inertia concept for estimation of soil moisture, are often based on using the TIR imagery in energy balance calculations (e.g. Goward et al., 2002) or hydrological models (e.g. Coppola et al., 2007; Minacapilli et al., 2009). The thermal inertia principle correlates changes of soil temperature to changes of soil moisture as well as heat capacity (e.g. Mallick et al., 2009; Van Doninck et al., 2011). Moreover, the TIR data is either used alone or combined with vegetation indices to adjust for the vegetation impact on the degree of heat transferred into the soil (Carlson et al., 1994). For example, Hain et al. (2009) used the TIR-based Atmosphere Land EXchange Inversion (ALEXI) surface energy balance model (Anderson et al., 1997; Mecikalski et al., 1999; Anderson et al., 2007) to estimate available water fraction, from which volumetric soil moisture was indirectly derived.

Microwave emission (collected by passive sensors) and backscatter (from active sensors, otherwise known as radars) are directly related to near surface soil moisture ($<$ 5 cm) through the dielectric contrast between that of liquid water (~80) and dry soil (~4) (Schmugge et al., 1974). The observations can be made under almost all weather conditions due to the atmosphere being transparent at the wavelengths most suitable for soil moisture (X- to L-band). The difference between the active and passive microwave techniques lies in the source of the signal; radar observations measure the proportion of a transmitted signal being backscattered to the sensor proportional to the surface reflectivity and roughness, while the radiometer observations are measurements of a natural emission proportional to the surface emissivity and physical temperature (Ulaby et al., 1981).

Active microwave remote sensing of soil moisture has the advantage of being at high spatial resolution, especially Synthetic Aperture Radar (SAR) which has the capability of observing the earth's surface at resolutions as high as 10 m (Torres et al., 2012). However, this high spatial resolution results in a revisit time of 35 days or longer. The temporal repeat issue has been recently addressed through a constellation of sensors by the European Space Agency (ESA); Sentinel-1 consists of two polar orbiting satellites having a global coverage of at least once every 6 to 12 days in Interferometric Wide Swath (IWS) mode (Wagner et al., 2009). The higher temporal resolution of Sentinel-1 SAR observations compared to that of previous SAR missions improves the feasibility of using SAR radar backscatter for a wider range of soil moisture applications. Nevertheless, its narrow imaging swath cannot achieve the temporal resolution of 3 days or better that is required for many soil moisture mapping needs (e.g. Walker and Houser, 2004; the National Research Council's Decadal Survey). Radar imagery is also highly sensitive to surface roughness, vegetation biomass and vegetation water content, making the direct soil moisture retrieval from radar backscatter alone a complex process. One solution proposed to overcome this problem is to use temporal change detection approach (Engman and Chauhan, 1995; Wagner et al., 1999; Njoku et al., 2002; Moran et al., 2000), which assumes that factors such as surface roughness remain fixed with only the soil moisture varying. However, to date accurate and global soil moisture retrieval from SAR backscatter remains a challenge.

Passive microwave emissions at L-band (e.g. Schmugge et al., 1974; Jackson, 1993; Ulaby et al., 1996; Njoku and Entekhabi, 1996; Schmugge et al., 2002) have been of great interest because of their better sensitivity to soil moisture dynamics (Ulaby et al., 1982) than radar and optical observations, and their favourable signal-to-noise ratio. Consequently, the European Space Agency (ESA) and National Aeronautics and Space Administration (NASA) have launched dedicated soil moisture missions using L-band passive microwave instruments aboard the Soil Moisture and Ocean Salinity (SMOS) satellite in 2009 and Soil Moisture Active Passive (SMAP) satellite in 2015, respectively, to monitor global surface soil moisture at a temporal resolution of at least 3 days. SMOS uses an interferometric radiometer with aperture synthesis by which multi-angular brightness temperature data sets are collected. In contrast, the SMAP radiometer has a scanning real aperture antenna which provides single angle (~40°) but high accuracy brightness temperature observations. Both the SMOS and SMAP satellites have an approximately 40 km resolution of their brightness temperature measurements, due to the trade-offs in antenna (aperture) size needed for high resolution and the technical challenge of launching and operating a large antenna in space. As the 40 km spatial resolution restricts the applications to hydro-climatological studies (Entekhabi et al., 2008b), spatial enhancement approaches are required if the passive microwave missions are to satisfy hydro-meteorological and agricultural applications (Entekhabi et al., 2010). Fig. 1 summarizes the temporal and spatial resolution requirements of soil moisture in a range of application areas.

No remote sensing technique utilizing a single electromagnetic region or approach can by itself satisfy the accuracy, spatial and temporal resolution requirements. While L-band passive microwave can yield accurate estimates of soil moisture content at low resolution, the radar

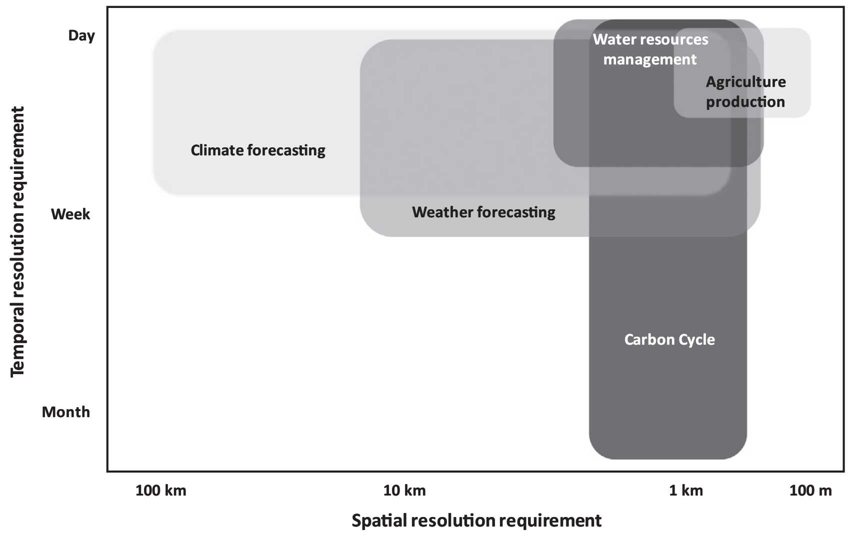

Fig. 1. Summary of spatial and temporal resolution requirement of soil moisture for a range of applications (Dr. Thomas Jackson and Prof. Dara Entekhabi, personal communication).

and optical imagery are capable of high spatial resolution but low accuracy soil moisture; the decreased accuracy of the radar- and optical-based remote sensing of soil moisture is due to the high impact by features such as surface roughness and vegetation canopy. Consequently, the SMAP satellite had included a radar in its design, to produce an approximately 10 km resolution soil moisture by merging the active and passive microwave data sets and permitting a compromise on accuracy. But due to a hardware anomaly, the radar transmitter failed on 7th of July 2015, making the SMAP combination of active and passive microwave observations no longer possible.

Apart from the SMAP active-passive baseline approach (Das et al., 2014), there have been a number of other studies that have proposed leveraging the strengths of passive microwave with that of radar and/or optical observations. This leveraging is possible through a process called downscaling or disaggregation. Downscaling methods combine coarse passive microwave observations with high spatial resolution features obtained from: microwave remote sensing backscatter observations from active microwave sensors (e.g. Piles et al., 2009b; Das et al., 2011; Das et al., 2014; Akbar and Moghaddam, 2015); higher frequency radiometric observations from passive microwave sensors (e.g. Santi, 2010; Gevaert et al., 2015); visible, SWIR and/or TIR observations from optical sensors (e.g. Verhoef et al., 1996; Muller and Décamps, 2001); and/or soil surface attributes (e.g. Pellenq et al., 2003; Ines et al., 2013). More recently, data assimilation has been used to combine coarse passive microwave data into a high resolution hydrological/land surface model (e.g. Reichle et al., 2001; Sahoo et al., 2013; Reichle et al., 2017), and a hydrological/land surface model has been used to train machine learning techniques for soil moisture downscaling (e.g. Srivastava et al., 2013; Chai et al., 2011; Chakrabarti et al., 2015, 2016). One advantage of these model-based prediction approaches is that there is no need for concurrent overpass by other satellites or concern about lost data due to cloud coverage.

There are also statistical-based downscaling approaches (e.g. Parada and Liang, 2003; Loew and Mauser, 2008; Kaheil et al., 2008; Mascaro et al., 2010, 2011; Shi et al., 2014b; and Verhoest et al., 2015), which provide the possible behaviour of the soil moisture using copula probability distributions and/or wavelet coefficients. Camps et al. (2008) and Piles et al. (2009a) have also developed mathematical-based downscaling techniques, which also estimate the possible behaviour of the soil moisture using the Fourier domain. However, such techniques are out of scope of this manuscript, which provides an overview of downscaling techniques that derive a deterministic pattern of soil moisture at higher resolution.

This paper provides a systematic and critical review of existing downscaling techniques for high resolution soil moisture mapping. Strengths and limitations associated with each technique are discussed, specifically in relation to the suitability and/or applicability in terms of the accuracy of soil moisture products, and availability of the land surface feature data, which are the key component in mapping accurate soil moisture. A comprehensive background of the downscaling methods and how they operate to improve soil moisture spatial scale are also provided. Subsequently, there is an overview and discussion on the advantages, drawbacks and knowledge gaps related to each approach to highlight the opportunities and challenges related to the research in this field. This review paper is complimentary to Peng et al. (2017), by providing a detailed description of the limitations of the various downscaling techniques, so as to move forward the development of high resolution soil moisture mapping from coarse passive microwave observations and summarising the accuracy of the different approaches.

2. Review of downscaling methods

Accurate soil moisture maps at moderate spatial resolutions (1–10 km) are required for regional and local earth system applications. Various downscaling techniques have been proposed for meeting the user requirements on spatial scale and accuracy of soil moisture measurements. A schematic of the general approach to downscaling soil moisture is shown in Fig. 2, with Table 1 providing a concise overview of the strengths and weaknesses of each downscaling method by listing each method with its pros/cons. Table 2 provides the reported accuracy of each downscaling technique together with the list of methods, references, main inputs, and improvement of downscaled products over the radiometer only measurements, as suggested by Merlin et al. (2015).

[Tables 1 and 2 (available after the references section) features here].

2.1. Microwave-based downscaling techniques

The capability of active and passive microwave observations has been verified for soil moisture mapping since the 80's (eg. Dobson and Ulaby, 1986; Ulaby et al., 1982). The Advanced SCATterometer (ASCAT) aboard the European METeorological OPerational (METOP) satellite is an example of an operational microwave radar which maps soil moisture globally at coarse resolution of 25 and 50 km (Wagner et al., 2013). The ESA Climate Change Initiative (CCI) active soil moisture data, which is a merged product created from C-band

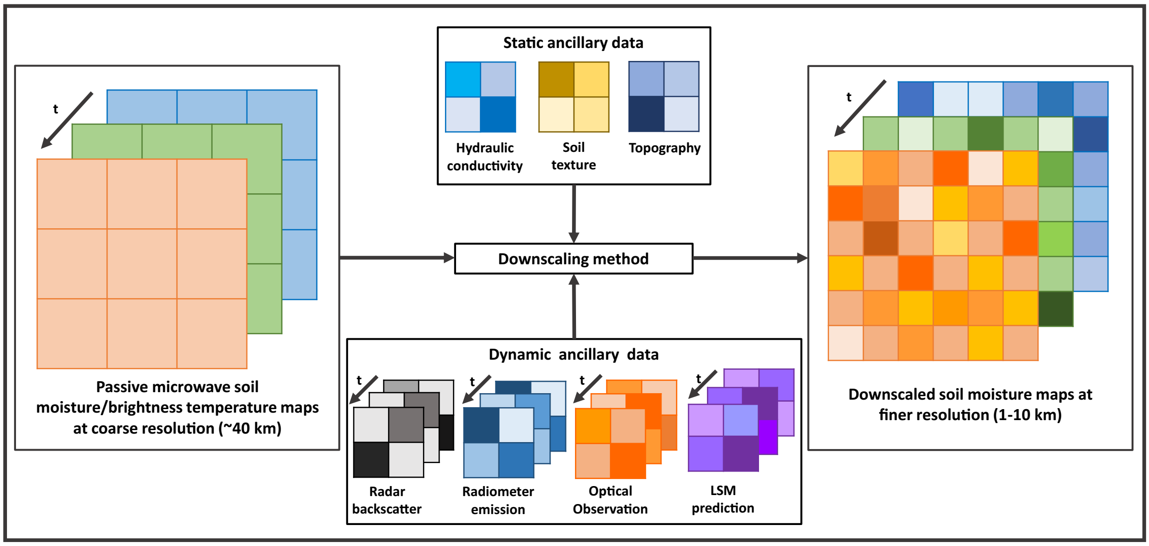

Fig. 2. Schematic of the downscaling concept using spatially detailed information on land surface features to distribute coarse scale soil moisture to fine scale.

scatterometers (ERS-1/2 scatterometer, METOP Advanced Scatterometer), is available at 12.5 km. However, these products cannot satisfy the spatial resolution requirement of soil moisture applications presented in Fig. 1. Advanced Synthetic Aperture Radar (ASAR) also maps soil moisture at 1 km, but this product is only available over Australia, southern and central Africa, and parts of Argentina for the time period between January 2005 and May 2010 (see: http://rs.geo.tuwien.ac.at/data-viewers/). Accordingly, active microwave observations alone have not been able to routinely provide accurate high resolution soil moisture estimates (e.g. Walker et al., 2004; Paloscia et al., 2013) globally, but can contribute valuable information about the geophysical properties of the target scenes (e.g. Chauhan, 1997; Mohanty et al., 2017). Reliable soil moisture retrieval from passive microwave remote sensing is limited to the lower frequencies, namely L-band (~1.4 GHz), C-band (~6.9 GHz) and X-band (~10 GHz). The higher frequencies such as Ka-band are not as sensitive to soil moisture as lower frequencies and respond to a very shallow layer of soil (Calvet et al., 2011; Yee et al., 2017). Conversely, the Ka-band provides observations at much higher resolution than lower frequencies because the Instantaneous Field of View (IFOV) which is a spatial resolution measure of the remote sensing system is proportional to wavelength (Salvia et al., 2011). Therefore, while direct retrieval is unlikely, Ka-band could be a potential source of information about the surface spatial heterogeneity (e.g. Neale et al., 1990; Santi, 2010; Gevaert et al., 2015).

The multi-source concept, in which the strengths of each sensor type

Table 1
Summary of the strengths and weaknesses of each downscaling method listing all the methods and pros/cons.

Downscaling Techniques	Approaches	Pros	Cons
Radar-based	Complimentary radar and radiometer Change detection of radar Fractal interpolation Bayesian Combined radar and radiometer	● Applicable under all-weather condition ● Independent from meteorological and land surface information ● Better sensitivity of radar backscatter to soil moisture dynamics than optical observations	● Lack of concurrent radar and radiometer observations at the same temporal repeat and on the same platforms ● Low temporal coverage of radar imagery ● Active microwave observations are sensitive to vegetation cover and surface roughness
Radiometer-based	Combined high and low frequency radiometer	● Applicable under all-weather condition ● Direct relationship of radiometric emissions to soil moisture dynamics ● Availability of radiometric emissions at higher frequency and at regular repeat coverage	● Spatial scale of soil moisture retrievals is limited to the scale of high frequency radiometric observations ● High frequency microwave observations are sensitive to vegetation cover and rainfall events
Optical-based	Physical Thermal inertia Semi-empirical	● High spatial resolution of optical observations ● High temporal resolution of optical observations	● No availability of optical observations under cloudy sky ● Impacts of vegetation cover on the optical observations makes relating these observations to soil moisture difficult ● Indirect relationship of optical observations to soil moisture variations
Soil surface attributes-based	Statistical	● Reflects soil water dynamic and storage capacity impact/control on soil moisture space-time scaling behaviour	● Limited access to global data on attributes including topography, soil surface properties and their possible rate of change
Data assimilation-based	High resolution model predictions combined with low resolution radiometric observations	● Accounts for both model and measurement uncertainties ● No need to have concurrent overpass by other satellites	● Requires information on meteorological and land surface parameters at high resolution
Machine learning-based	Relationship with surface parameters	● No need to have concurrent overpass by other satellites ● No need for continuous data ● No lost data due to cloud coverage	● Needs parameter optimization ● Computationally demanding ● Training globally

Table 2
Summary table on accuracy of soil moisture downscaling methods including the list of methods, references, and main inputs.

Downscaling techniques	Approaches	References	Main inputs	Accuracy	Improvement over the radiometer only measurements	Range of accuracy parameters
Radar-based	Complimentary radar and radiometer	Ulaby et al. (1983)	• NASA C-130 airborne L-band scatterometer data	± 30% of truth soil moisture	–	RMSE ∈ (0.01,0.029) $m^3 m^{-3}$ R^2 ∈ (0.65,0.99)
		Theis et al. (1986)	• NASA C-130 airborne L- and C-band radiometric data	C-band V-pol R^2 = 0.65, C-band H-pol R^2 = 0.65, L-band H-pol R^2 = 0.95	C-band V-pol ΔR^2 = 0.42, C-band H-pol ΔR^2 = 0.43, L-band H-pol ΔR^2 = 0.26	
		O'neill and Chauhan (1992)	• MACHYDRO '90 experimental AIRSAR L-band radar data • MACHYDRO '90 experimental PBMR L-band radiometric data	RMSE = 0.029 $m^3 m^{-3}$	–	
		O'neill et al., 1996	• MACHYDRO '90 experimental data set including PBMR L-band radiometric and AIRSAR L-band radar data • Washita '92 experimental ESTAR L-band radiometric and GSFC's L-band truck-mounted radar data	MACHYDRO '90: RMSE = 0.028 $m^3 m^{-3}$ R^2 = 0.93 (on average) Washita '92: α = 0: RMSE = 0.016 $m^3 m^{-3}$, R^2 = 0.99 (on average) α ‡ 0: RMSE = 0.01 $m^3 m^{-3}$, R^2 = 0.99 (on average)	–	
		Chauhan (1997)	• MACHYDRO '90 experimental data	Absolute bias on average < 0.05 $m^3 m^{-3}$	–	
	Change detection of radar	Njoku et al. (2002)	• SGP99 L- and S-band PALS experimental data	No report on retrievals analysis, just proposing a method for downscaling	–	RMSE ∈ (0.028,0.052) $m^3 m^{-3}$ R^2 ∈ (0.31,0.85)
		Narayan et al. (2006)	• SMEX02 PALS L-band radiometer data • SMEX02 AIRSAR L-band radar data	RMSE = 0.046 $m^3 m^{-3}$, R^2 = 0.7 (on average) After removing outliers: RMSE = 0.028 $m^3 m^{-3}$, R^2 = 0.85 (on average)	–	
		Narayan and Lakshmi (2008)	• AMSR-E C-band radiometric data • TMI X-band brightness temperature • TRMM-PR Ku-band backscatter data	AMSR-E & TRMM-PR: RMSE = 0.052 $m^3 m^{-3}$, R^2 = 0.31 TMI & TRMM-PR: RMSE = 0.049 $m^3 m^{-3}$, R^2 = 0.45	AMSR-E & TRMM-PR: ΔRMSE = 0.025 $m^3 m^{-3}$, ΔR^2 = 0.14 TMI & TRMM-PR: ΔRMSE = 0.031 $m^3 m^{-3}$, ΔR^2 = 0.08	
	Fractal interpolation	Bindlish and Barros (2002)	• SGP '97 ESTAR L-band radiometric data • SIR-C/X-SAR L-, C-, and X-band data	RMSE = 0.028 $m^3 m^{-3}$	ΔRMSE = 0.004 $m^3 m^{-3}$	
	Bayesian	Zhan et al. (2006)	• L-band OSSE experimental data set	3 km: RMSE = 0.028 $m^3 m^{-3}$(Low noise data) RMSE = 0.038 $m^3 m^{-3}$ (High noise data) 9 km: RMSE = 0.027 $m^3 m^{-3}$(Low noise data) RMSE = 0.044 $m^3 m^{-3}$ (High noise data)	3 km: ΔRMSE = 0.013 $m^3 m^{-3}$(Low noise data) ΔRMSE = 0.022 $m^3 m^{-3}$ (High noise data) 9 km: ΔRMSE = 0.012 $m^3 m^{-3}$(Low noise data) ΔRMSE = 0.028 $m^3 m^{-3}$ (High noise data)	RMSE ∈ (0.013,0.044) $m^3 m^{-3}$ R^2 ∈ (0.1,0.55)
		Wu et al. (2017)	• SMAPEx-3 L-band PLMR and PLIS observations	1 km: RMSE = 0.020 $m^3 m^{-3}$, R^2 = 0.1 3 km: RMSE = 0.017 $m^3 m^{-3}$, R^2 = 0.3 9 km: RMSE = 0.013 $m^3 m^{-3}$, R^2 = 0.55	1 km: ΔRMSE = 0.041 $m^3 m^{-3}$, ΔR^2 = 0.01 3 km: ΔRMSE = 0.023 $m^3 m^{-3}$, ΔR^2 = 0.18 9 km: ΔRMSE = 0.014 $m^3 m^{-3}$, ΔR^2 = 0.35	
	Combined radar and radiometer	Piles et al. (2009b)	• SMEX02 L-band PALS experimental data set	RMSE = 0.027 $m^3 m^{-3}$ (H pol) RMSE = 0.023 $m^3 m^{-3}$ (V pol)	ΔRMSE = 0.02 $m^3 m^{-3}$	RMSE ∈ (0.019,0.12) $m^3 m^{-3}$
		Das et al. (2011)	• L-band OSSE experimental data set	PALS: RMSE = 0.035 $m^3 m^{-3}$ OSSE: RMSE = 0.028 to 0.033 $m^3 m^{-3}$	ΔRMSE ∈ (0.015–0.02) $m^3 m^{-3}$	
		Das et al. (2014)		PALS: RMSE = 0.033 $m^3 m^{-3}$	ΔRMSE > 0.02 $m^3 m^{-3}$	
		Akbar and Moghaddam (2015)	• MEX02 L-band PALS experimental data set • Truck mounted ComRad data	Low noise level: RMSE = 0.039 $m^3 m^{-3}$ (on average) High noise level: RMSE = 0.047 $m^3 m^{-3}$ (on average)	ΔRMSE = 0.006 $m^3 m^{-3}$ (Low noise level, on average) ΔRMSE = 0.002 $m^3 m^{-3}$ (High noise level, on average)	

(continued on next page)

Table 2 (*continued*)

Downscaling techniques	Approaches	References	Main inputs	Accuracy	Improvement over the radiometer only measurements	Range of accuracy parameters
		van der Velde et al. (2015)	• AMSR-E VUA-NASA C-band soil moisture products • PALSAR L-band radar backscatter	1 km: RMSE = 0.067 $m^3 m^{-3}$, R^2 = 0.37 (on average) 5 km: RMSE = 0.068 $m^3 m^{-3}$, R^2 = 0.36 (on average) 10 km: RMSE = 0.069 $m^3 m^{-3}$, R^2 = 0.36 (on average)	1 km: ΔRMSE = 0.126 $m^3 m^{-3}$, ΔR^2 = 0.02 (on average) 5 km: ΔRMSE = 0.125 $m^3 m^{-3}$, ΔR^2 = 0.01 (on average) 10 km: RMSE = 0.124 $m^3 m^{-3}$, ΔR^2 = 0.01 (on average)	
		Wu et al. (2016)	• SMAPEx-3 L-band PLMR and PLIS observations	The baseline active-passive algorithm by Das et al. (2014): 1 km: RMSE = 0.038 $m^3 m^{-3}$ 3 km: RMSE = 0.028 $m^3 m^{-3}$ 9 km: RMSE = 0.019 $m^3 m^{-3}$ The active/passive retrieval algorithm by Das et al. (2011): 1 km: RMSE = 0.042 $m^3 m^{-3}$ 3 km: RMSE = 0.030 $m^3 m^{-3}$ 9 km: RMSE = 0.021 $m^3 m^{-3}$ The change detection approach by Piles et al. (2009b): 1 km: RMSE = 0.044 $m^3 m^{-3}$ 3 km: RMSE = 0.033 $m^3 m^{-3}$ 9 km: RMSE = 0.026 $m^3 m^{-3}$	ΔRMSE = 0.01 $m^3 m^{-3}$ (For each type of downscaling algorithm)	
		Rüdiger et al. (2016)	• AACES L-band PLMR observations • ASAR C-band radar data	RMSE = 0.06 to 0.12 $m^3 m^{-3}$	–	
		Montzka et al. (2016)	• PLMR brightness temperature • F-SAR radar backscatter	The active/passive retrieval algorithm by Das et al. (2011): Juelich: RMSE = 0.083 $m^3 m^{-3}$ Monschau: RMSE = 0.094 $m^3 m^{-3}$ The baseline active-passive algorithm by Das et al. (2014): Juelich: RMSE = 0.066 $m^3 m^{-3}$ Monschau: RMSE = 0.077 $m^3 m^{-3}$ The alternative active-passive algorithm by Montzka et al. (2016): Juelich: RMSE = 0.078 $m^3 m^{-3}$ Monschau: RMSE = not available	–	
Radiometer-based	Combined high and low frequency radiometer	Santi (2010)	• AMSR-E LPRM C-band soil moisture product	Just proposing a method for downscaling/no analysis	–	RMSE ∈ (0.054,0.13) $m^3 m^{-3}$ R^2 ∈ (0.28,0.41)
		Gevaert et al. (2015)	• AMSR-E Ka-band radiometric data	RMSE = 0.13 $m^3 m^{-3}$, R^2 = 0.41[a]	ΔRMSE = 0.01 $m^3 m^{-3}$, ΔR^2 = 0.01[a]	
		de Jeu et al. (2014)		Std. Dev. = 0.05 $m^3 m^{-3}$	ΔStd. Dev. = −0.016 $m^3 m^{-3}$	
		Parinussa et al. (2014)[b]	• AMSR-E LPRM C-band soil moisture product • ALEXI TIR soil moisture products • ASCAT C-band soil moisture products • AMSR-E Ka-band radiometric data	Downscaled ALEXI: RMSE = 0.054 $m^3 m^{-3}$, R^2 = 0.34[a] Downscaled AMSRE: RMSE = 0.06 $m^3 m^{-3}$, R^2 = 0.35[a] Downscaled ASCAT: RMSE = 0.066 $m^3 m^{-3}$, R^2 = 0.28[a]	Downscaled ALEXI: ΔRMSE = 0 $m^3 m^{-3}$, ΔR^2 = −0.01[a] Downscaled AMSRE: ΔRMSE = 0 $m^3 m^{-3}$, ΔR^2 = −0.02[a] Downscaled ASCAT: ΔRMSE = 0.002 $m^3 m^{-3}$, ΔR^2 = −0.02[a]	
Optical-based	Physical	Merlin et al. (2005)	• SGP '97 ESTAR L-band radiometric data • AVHRR optical data set	Std. Dev. = 0.054 $m^3 m^{-3}$	–	RMSE ∈ (0.003,0.211) $m^3 m^{-3}$ R^2 ∈ (0,0.81) UbRMSE[c] ∈ (0.039,0.102) $m^3 m^{-3}$
		Merlin et al. (2008a)	• Monsoon '90 PMBR L-band radiometric data • MODIS products including NDVI and LST	EF based: RMSE = 0.03 $m^3 m^{-3}$, R^2 = 0.62[a] AEF based: RMSE = 0.02 $m^3 m^{-3}$, R^2 = 0.66[a]	–	
		Merlin et al. (2008b)	• NAFE'06 L-band airborne radiometer observations • MODIS products including NDVI and LST	Uniform θ: RMSE = 0.017 $m^3 m^{-3}$, R^2 = 0.42[a] Non-uniform θ: RMSE = 0.0153 $m^3 m^{-3}$, R^2 = 0.58[a]	–	
		Merlin et al. (2010)		RMSE = 0.012 to 0.025 $m^3 m^{-3}$, R^2 = 0.55 to 0.81[a]	–	
		Merlin et al. (2009)	• NAFE'06 L-band airborne radiometer observations	RMSE = 0.062 $m^3 m^{-3}$, R^2 = 0.64	–	

(continued on next page)

Table 2 (*continued*)

Downscaling techniques	Approaches	References	Main inputs	Accuracy	Improvement over the radiometer only measurements	Range of accuracy parameters
			• MODIS products including NDVI and LST • ASTER			
		Merlin et al. (2012)	• SMOS level-2 soil moisture product • MODIS products including NDVI and LST	Austral summer: RMSE = 0.057 $m^3 m^{-3}$, R^2 = 0.49[a] Austral winter: RMSE = 0.138 $m^3 m^{-3}$, R^2 = ~0[a]	–	
		Merlin et al. (2013)	• SMOS level-2 soil moisture product • MODIS products including NDVI and LST • ASTER products including NDVI and LST • Landsat products including NDVI and LST	3 km, used MODIS: RMSE = 0.11 $m^3 m^{-3}$, R^2 = 0.45[a] 100 m, used ASTER: RMSE = 0.0815 $m^3 m^{-3}$, R^2 = 0.50[a] 100 m, used Landsat: RMSE = 0.1 $m^3 m^{-3}$, R^2 = 0.72[a]	3 km, used MODIS: ΔRMSE = 0.01 $m^3 m^{-3}$, ΔR^2 = 0.1[a] 100 m, used ASTER: ΔRMSE = 0.0385 $m^3 m^{-3}$, ΔR^2 = 0.15[a] 100 m, used Landsat: ΔRMSE = 0.2 $m^3 m^{-3}$, ΔR^2 = 0.37[a]	
		Djamai et al. (2015)	• SMOS level-2 soil moisture product • MODIS products including NDVI and LST	Against ground data: RMSE = 0.03 to 0.05 $m^3 m^{-3}$, R^2 = 0.09 to 0.27[a] Against airborne soil moisture: R^2 = 0.24 to 0.64[a]	–	
		Fan et al. (2015)	• Airborne PLMR soil moisture at 700 m resolution • ASTER products including NDVI and LST at 100 m	RMSE = 0.048 $m^3 m^{-3}$, R^2 = 0.37[a]	ΔRMSE = −0.08 $m^3 m^{-3}$, ΔR^2 = N/A	
		Malbéteau et al. (2016)	• AMSR-E level-3 LPRM soil moisture product • SMOS level-3 daily soil moisture product • MODIS products including NDVI and LST • DEM data (gtopo30)	AMSR-E: Ascending: RMSE = 0.076 $m^3 m^{-3}$, R^2 = 0.61[a] Descending: RMSE = 0.092 $m^3 m^{-3}$, R^2 = 0.61[a] SMOS: Ascending: RMSE = 0.079 $m^3 m^{-3}$, R^2 = 0.53[a] Descending: RMSE = 0.068 $m^3 m^{-3}$, R^2 = 0.5[a]	AMSR-E: Ascending: ΔRMSE = 0.019 $m^3 m^{-3}$, ΔR^2 = −0.08[a] Descending: ΔRMSE = 0.025 $m^3 m^{-3}$, ΔR^2 = 0.12[a] SMOS: Ascending: ΔRMSE = 0.011 $m^3 m^{-3}$, ΔR^2 = 0.04[a] Descending: ΔRMSE = 0.016 $m^3 m^{-3}$, ΔR^2 = 0.02[a]	
		Molero et al. (2016)	• SMOS level-3 daily soil moisture product • MODIS products including NDVI and LST • DEM data (gtopo30)	Averaged results from ascending and descending overpasses Yanco: ubRMSE[c] = 0.093 $m^3 m^{-3}$, R^2 = 0.12[a] Murrumbidgee: ubRMSE = 0.102 $m^3 m^{-3}$, R^2 = 0.1[a] Little Washita: ubRMSE = 0.076 $m^3 m^{-3}$, R^2 = 0[a] Walnut Gluch: ubRMSE = 0.039 $m^3 m^{-3}$, R^2 = 0.01[a]	Yanco: ΔubRMSE = −0.018 $m^3 m^{-3}$, ΔR^2 = 0.08[a] Murrumbidgee: ΔubRMSE = −0.021 $m^3 m^{-3}$, ΔR^2 = 0.06[a] Little Washita: ΔubRMSE = −0.014 $m^3 m^{-3}$, ΔR^2 = −0.01[a] Walnut Gluch: ΔubRMSE = −0.007 $m^3 m^{-3}$, ΔR^2 = 0.01[a]	
		Djamai et al. (2016)	• SMOS level-2 soil moisture product • MODIS products including NDVI and LST • OURANOS geophysical data • NARR atmospheric forcing data	Linear: Ascending: RMSE = 0.06 $m^3 m^{-3}$, R^2 = 0.58[a] Descending: RMSE = 0.05 $m^3 m^{-3}$, R^2 = 0.66[a] Non-linear: Ascending: RMSE = 0.06 $m^3 m^{-3}$, R^2 = 0.49[a] Descending: RMSE = 0.06 $m^3 m^{-3}$, R^2 = 0.52[a]	Linear: Ascending: ΔRMSE = 0.04 $m^3 m^{-3}$, Δ R^2 = 0.13[a] Descending: ΔRMSE = 0.06 $m^3 m^{-3}$, ΔR^2 = −0.03[a] Non-linear: Ascending: ΔRMSE = 0.04 $m^3 m^{-3}$, ΔR^2 = 0.04[a] Descending: ΔRMSE = 0.05 $m^3 m^{-3}$, ΔR^2 = −0.17[a]	
		Chen et al. (2017)		May: NRSD: RMSE = 0.04 $m^3 m^{-3}$,	May: NRSD: ΔRMSE = 0 $m^3 m^{-3}$	

(*continued on next page*)

Table 2 (*continued*)

Downscaling techniques	Approaches	References	Main inputs	Accuracy	Improvement over the radiometer only measurements	Range of accuracy parameters
			• SMAP radiometer-derived soil moisture products • MODIS land surface reflectance products	$R^2 = 0.15$[a] DisPATCh: RMSE = 0.07 $m^3\,m^{-3}$, $R^2 = 0.13$[a] September: NRSD: RMSE = 0.12 $m^3\,m^{-3}$, $R^2 = 0.06$[a] DisPATCh: RMSE = 0.17 $m^3\,m^{-3}$, $R^2 = 0.04$[a]	DisPATCh: ΔRMSE = −0.03 $m^3\,m^{-3}$ September: NRSD: ΔRMSE = 0.02 $m^3\,m^{-3}$ DisPATCh: ΔRMSE = −0.03 $m^3\,m^{-3}$	
		Kim and Hogue (2012)	• AMSR-E Level 3 soil moisture product from NSIDC • MODIS products including NDVI and LST	RMSE = 0.051 $m^3\,m^{-3}$, $R^2 = 0.073$[a]	ΔRMSE = 0.003 $m^3\,m^{-3}$, $\Delta R^2 = 0.067$[a]	
		Zhou et al. (2015)	• AMSR2 Level 3 soil moisture products • MODIS products including NDVI and LST	Merlin et al. (2008a, 2008b, 2009): RMSE = 0.032 $m^3\,m^{-3}$, $R^2 = 0.55$[a] Kim and Hogue (2012): RMSE = 0.038 $m^3\,m^{-3}$, $R^2 = 0.58$[a]	–	
		Peng et al. (2015)	• ESA CCI multi-mission soil moisture product • MODIS products including NDVI and LST • MSG SEVIRI data	MODIS based: RMSE = 0.076 $m^3\,m^{-3}$, ubRMSE[c] = 0.042 $m^3\,m^{-3}$, $R^2 = 0.34$[a] SEVIRI based: RMSE = 0.072 $m^3\,m^{-3}$, ubRMSE = 0.04 $m^3\,m^{-3}$, $R^2 = 0.38$[a]	MODIS based: ΔRMSE = 0.034 $m^3\,m^{-3}$, ΔubRMSE = 0.008 $m^3\,m^{-3}$, $\Delta R^2 = 0.06$[a] SEVIRI based: ΔRMSE = 0.038 $m^3\,m^{-3}$, ΔubRMSE = 0.01 $m^3\,m^{-3}$, $\Delta R^2 = 0.1$[a]	
		Peng et al. (2016)	• ESA CCI multi-mission soil moisture products • MODIS products including NDVI/EVI and LST	LST/NDVI: RMSE = 0.099 $m^3\,m^{-3}$, $R^2 = 0.38$[a] LST/EVI: RMSE = 0.103 $m^3\,m^{-3}$, $R^2 = 0.36$[a] $LST_{day\text{-}night}$/NDVI: RMSE = 0.078 $m^3\,m^{-3}$, $R^2 = 0.56$[a] $LST_{day\text{-}night}$/EVI: RMSE = 0.091 $m^3\,m^{-3}$, $R^2 = 0.45$[a]	LST/NDVI: ΔRMSE = −0.042 $m^3\,m^{-3}$, $\Delta R^2 = -0.23$[a] LST/EVI: ΔRMSE = −0.046 $m^3\,m^{-3}$, $\Delta R^2 = -0.25$[a] $LST_{day\text{-}night}$/NDVI: ΔRMSE = −0.021 $m^3\,m^{-3}$, $\Delta R^2 = -0.05$[a] $LST_{day\text{-}night}$/EVI: ΔRMSE = −0.034 $m^3\,m^{-3}$, $\Delta R^2 = -0.16$[a]	
		Kim et al. (2017) **	• Merged active-passive ESA CCI soil moisture products • MODIS 16-day NDVI composite	REMEDHUS: RMSE = 0.11 $m^3\,m^{-3}$, ubRMSE[c] = 0.05 $m^3\,m^{-3}$, $R^2 = 0.24$[a] CONUS: Arid: RMSE = 0.074 $m^3\,m^{-3}$, ubRMSE = 0.054 $m^3\,m^{-3}$, $R^2 = 0.29$[a](median values) Temperate: RMSE = 0.105 $m^3\,m^{-3}$, ubRMSE = 0.079 $m^3\,m^{-3}$, $R^2 = 0.14$[a](median values) Cold: RMSE = 0.091 $m^3\,m^{-3}$, ubRMSE = 0.074 $m^3\,m^{-3}$, $R^2 = 0.23$[a](median values)	REMEDHUS: ΔRMSE = 0 $m^3\,m^{-3}$, ΔubRMSE = 0.01 $m^3\,m^{-3}$, $\Delta R^2 = -0.1$[a] CONUS: Arid: ΔRMSE = 0 $m^3\,m^{-3}$, ΔubRMSE = −0.003 $m^3\,m^{-3}$, $\Delta R^2 = -0.03$ [a] Temperate: ΔRMSE = −0.006 $m^3\,m^{-3}$, ΔubRMSE = −0.008 $m^3\,m^{-3}$, $\Delta R^2 = -0.01$[a] Cold: ΔRMSE = −0.002 $m^3\,m^{-3}$, ΔubRMSE = −0.004 $m^3\,m^{-3}$, $\Delta R^2 = 0$[a]	
		Wang et al. (2016)	• Microwave products of soil moisture produced by Dorigo et al. (2012) • MODIS products including EVI and LST	On average: RMSE = 0.211 $m^3\,m^{-3}$	On average: ΔRMSE = −0.022 $m^3\,m^{-3}$	
		Hemakumara et al. (2004)	• AMSR-E C-band radiometric data • MODIS and AVHRR LST and NDVI	No report on retrievals analysis, just proposing a method for downscaling	–	
	Thermal inertia	Fang and Lakshmi (2014b)	• AMSR-E soil moisture estimated using the single channel algorithm (SCA) • SMOS Daily Level-3 soil moisture product • MODIS products including NDVI and	SMOS: RMSE = 0.042 $m^3\,m^{-3}$, ubRMSE[c] = 0.045 $m^3\,m^{-3}$ (on average) AMSR-E: RMSE = 0.0385 $m^3\,m^{-3}$, ubRMSE = 0.045 $m^3\,m^{-3}$ (on average)	SMOS: ΔRMSE = 0.001 $m^3\,m^{-3}$, ΔubRMSE = −0.002 $m^3\,m^{-3}$ (on average) AMSR-E: ΔRMSE = 0.006 $m^3\,m^{-3}$, ΔubRMSE = −0.003 $m^3\,m^{-3}$ (on average)	RMSE ∈ (0.027,0.146) $m^3\,m^{-3}$ UbRMSE[c] ∈ (0.026,0.045) $m^3\,m^{-3}$ R^2 ∈ (0.22,0.56)

(*continued on next page*)

Table 2 (*continued*)

Downscaling techniques	Approaches	References	Main inputs	Accuracy	Improvement over the radiometer only measurements	Range of accuracy parameters
			land surface temperature ● AVHRR and SPOT NDVI ● NLDAS model outputs including LST and soil moisture			
		Mallick et al. (2009)	● MODIS and ASTER optical data set ● AMSR-E C-band radiometric product	Fractional vegetation cover < 0.5: RMSE = 0.027 $m^3 m^{-3}$, R^2 = 0.56[a] Fractional vegetation cover > 0.5: RMSE = 0.06 $m^3 m^{-3}$, R^2 = 0.22[a]	–	
			Fang et al. (2013)	● AMSR-E C-band radiometric data ● NLDAS model outputs including LST and soil moisture ● MODIS products including NDVI and LST ● AVHRR NDVI	Mesonet data: RMSE = 0.146 $m^3 m^{-3}$, ubRMSE[c] = 0.042 $m^3 m^{-3}$ Micronet data: RMSE = 0.063 $m^3 m^{-3}$, ubRMSE = 0.026 $m^3 m^{-3}$	
			Mesonet data: ΔRMSE = −0.005 $m^3 m^{-3}$, ΔubRMSE = 0.0 $m^3 m^{-3}$ Micronet data: ΔRMSE = −0.015 $m^3 m^{-3}$, ΔubRMSE = −0.001 $m^3 m^{-3}$			
	Fang and Lakshmi (2014a)		● AMSR-E C-band radiometric data ● NLDAS model outputs including LST and soil moisture ● MODIS products including NDVI and LST	NP89: RMSE = 0.056 $m^3 m^{-3}$, ubRMSE[c] = 0.039 $m^3 m^{-3}$ LP92: RMSE = 0.056 $m^3 m^{-3}$, ubRMSE = 0.04 $m^3 m^{-3}$	NP89: ΔRMSE = −0.001 $m^3 m^{-3}$, ΔubRMSE = −0.001 $m^3 m^{-3}$ LP92: ΔRMSE = −0.001 $m^3 m^{-3}$, ΔubRMSE = −0.002 $m^3 m^{-3}$	
	Semi-empirical	Chauhan et al. (2003)	● SSM/I K-band radiometric data ● AVHRR products including NDVI and LST	RMSE = 0.05 $m^3 m^{-3}$	ΔRMSE = −0.024 $m^3 m^{-3}$	RMSE ∈ (0.043,0.13) $m^3 m^{-3}$ ubRMSE[c] ∈ (0.03,0.07) $m^3 m^{-3}$ R^2 ∈ (0.016,0.79)
		Choi and Hur (2012)	● AMSR-E LPRM soil moisture products ● MODIS products including NDVI, LST and albedo	RMSE = 0.12 $m^3 m^{-3}$, R^2 = 0.22[a](on average)	REMEDHUS: ΔRMSE = 0.03 $m^3 m^{-3}$, ΔR^2 = 0.05[a](on average)	
		Zhao and Li (2013a)[b]	● LPRM AMSR-E soil moisture product ● MSG SEVIRI optical data including NDVI and LST	Zhao and Li, 2013a) model: RMSE = 0.099 $m^3 m^{-3}$, R^2 = 0.057[a](on average) Chauhan et al. (2003) model: RMSE = 0.106 $m^3 m^{-3}$, R^2 = 0.016[a](on average)	Zhao and Li, 2013amodel: ΔRMSE = $m^3 m^{-3}$, ΔR^2 = Chauhan et al. (2003) model:	
		Piles et al. (2011)	● SMOS level-2 soil moisture product ● MODIS products including NDVI and LST	1 km: RMSE = 0.13 $m^3 m^{-3}$, R^2 = 0.21 10 km: RMSE = 0.09 $m^3 m^{-3}$, R^2 = 0.3	1 km: ΔRMSE = 0.03 $m^3 m^{-3}$, ΔR^2 = −0.11 10 km: ΔRMSE = 0.07 $m^3 m^{-3}$, ΔR^2 = −0.03	
		Piles et al. (2012)		RMSE = 0.085 $m^3 m^{-3}$, R^2 = 0.54 (on average)	ΔRMSE = −0.005 $m^3 m^{-3}$, ΔR^2 = −0.26	
		Piles et al. (2013)		RMSE = 0.06 $m^3 m^{-3}$, ubRMSE[c] = 0.04 $m^3 m^{-3}$, R^2 = 0.24[a]	ΔRMSE = −0.01 $m^3 m^{-3}$, ΔubRMSE = −0.01 $m^3 m^{-3}$, ΔR^2 = −0.06	
		Piles et al. (2014)		Morning orbits: RMSE = 0.07 $m^3 m^{-3}$, ubRMSE[c] = 0.03 $m^3 m^{-3}$, R^2 = 0.17[a] Afternoon orbits: RMSE = 0.05 $m^3 m^{-3}$, ubRMSE = 0.04 $m^3 m^{-3}$, R^2 = 0.34[a]	Morning orbits: ΔRMSE = 0.01 $m^3 m^{-3}$, ΔubRMSE = 0.0 $m^3 m^{-3}$, ΔR^2 = −0.08[a] Afternoon orbits: ΔRMSE = 0.02 $m^3 m^{-3}$, ΔubRMSE = −0.01 $m^3 m^{-3}$, ΔR^2 = 0.0[a]	
		Sánchez-Ruiz et al. (2014)		Morning orbits: RMSE = 0.07 $m^3 m^{-3}$, ubRMSE[c] = 0.043 $m^3 m^{-3}$,	Morning orbits: ΔRMSE = 0.0 $m^3 m^{-3}$, ΔubRMSE = 0.003 $m^3 m^{-3}$,	

(*continued on next page*)

Table 2 (*continued*)

Downscaling techniques	Approaches	References	Main inputs	Accuracy	Improvement over the radiometer only measurements	Range of accuracy parameters
				R^2 = 0.37[a](on average) Afternoon orbits: RMSE = 0.051 $m^3 m^{-3}$, ubRMSE = 0.04 $m^3 m^{-3}$, R^2 = 0.52[a](on average)	ΔR^2 = 0.1[a](on average) Afternoon orbits: ΔRMSE = 0.0 $m^3 m^{-3}$, ΔubRMSE = 0.004 $m^3 m^{-3}$, ΔR^2 = 0.11[a](on average)	
		Song et al. (2014)	• AMSR-E Ku-band brightness temperature • MODIS NDVI and LST products	RMSE = 0.091 $m^3 m^{-3}$, R^2 = 0.62 (on average)	–	
		Song et al. (2012)		RMSE = 0.047 $m^3 m^{-3}$, R^2 = 0.74	–	
		Pablos et al. (2016)	• SMOS BEC level-3 soil moisture product • MODIS products including NDVI and LST	LST day: ubRMSE[c] = 0.04 to 0.06 $m^3 m^{-3}$, R^2 = 0.3 to 0.72[a] (on average) LST night: ubRMSE = 0.04 to 0.07 $m^3 m^{-3}$, R^2 = 0.2 to 0.64[a] (on average) Ensemble of day and night LST: ubRMSE = 0.04 to 0.07 $m^3 m^{-3}$, R^2 = 0.3 to 0.72[a] (on average)	–	
		Piles et al. (2016)	• SMOS BEC level-3 soil moisture product • MSG SEVIRI products including NDVI and LST	REMEDHUS: Instant: RMSE = 0.043 $m^3 m^{-3}$, ubRMSE[c] = 0.04 $m^3 m^{-3}$, R^2 = 0.67[a] Daytime: RMSE = 0.063 $m^3 m^{-3}$, ubRMSE = 0.06 $m^3 m^{-3}$, R^2 = 0.45[a] SMOSMANIA: Instant: RMSE = 0.1 $m^3 m^{-3}$, ubRMSE = 0.051 $m^3 m^{-3}$, R^2 = 0.41[a] Daytime: RMSE = 0.109 $m^3 m^{-3}$, ubRMSE = 0.062 $m^3 m^{-3}$, R^2 = 0.26[a] VAS: Instant: RMSE = 0.065 $m^3 m^{-3}$, ubRMSE = 0.031 $m^3 m^{-3}$, R^2 = 0.79[a] Daytime: RMSE = 0.072 $m^3 m^{-3}$, ubRMSE = 0.051 $m^3 m^{-3}$, R^2 = 0.45[a]	REMEDHUS: Instant: ΔRMSE = 0.013 $m^3 m^{-3}$, ΔubRMSE = −0.04 $m^3 m^{-3}$, ΔR^2 = 0.06[a] Daytime: ΔRMSE = −0.007 $m^3 m^{-3}$, ΔubRMSE = −0.024 $m^3 m^{-3}$, ΔR^2 = −0.16[a] SMOSMANIA: Instant: ΔRMSE = −0.021 $m^3 m^{-3}$, ΔubRMSE = −0.01 $m^3 m^{-3}$, ΔR^2 = −0.18[a] Daytime: ΔRMSE = −0.03 $m^3 m^{-3}$, ΔubRMSE = −0.021 $m^3 m^{-3}$, ΔR^2 = −0.33[a] VAS: Instant: ΔRMSE = 0.005 $m^3 m^{-3}$, ΔubRMSE = 0.014 $m^3 m^{-3}$, ΔR^2 = −0.09[a] Daytime: ΔRMSE = −0.002 $m^3 m^{-3}$, ΔubRMSE = −0.006 $m^3 m^{-3}$, ΔR^2 = −0.26[a]	
Knipper et al. (2017)		• SMOS CATDS Level 3 soil moisture products • SMAP Level 3 (L3_SM_P) soil moisture products • MODIS products including LST, EVI and Albedo	Chauhan et al. (2003): SMOS: ubRMSE[c] = 0.042 $m^3 m^{-3}$, R^2 = 0.31 SMAP: ubRMSE = 0.036 $m^3 m^{-3}$, R^2 = 0.39 Piles et al. (2011): SMOS: ubRMSE = 0.043 $m^3 m^{-3}$, R^2 = 0.31 SMAP: ubRMSE = 0.037 $m^3 m^{-3}$, R^2 = 0.35 Chauhan et al. (2003): SMOS: ubRMSE = 0.046 $m^3 m^{-3}$, R^2 = 0.32 SMAP: ubRMSE = 0.037 $m^3 m^{-3}$, R^2 = 0.37	Chauhan et al. (2003): SMOS: ΔubRMSE = 0.008 $m^3 m^{-3}$, ΔR^2 = −0.06 SMAP: ΔubRMSE = −0.004 $m^3 m^{-3}$, ΔR^2 = −0.13 Piles et al. (2011): SMOS: ΔubRMSE = 0.007 $m^3 m^{-3}$, ΔR^2 = −0.06 SMAP: ΔubRMSE = −0.005 $m^3 m^{-3}$, ΔR^2 = −0.17 Chauhan et al. (2003): SMOS: ΔubRMSE = 0.004 $m^3 m^{-3}$, ΔR^2 = −0.05 SMAP: ΔubRMSE = −0.005 $m^3 m^{-3}$, ΔR^2 = −0.15		
Soil surface attributes-based	Statistical	Kim and Barros (2002a)	• SGP '97 experimental ESTAR L-band radiometric data • DEM and rainfall data set • AVHRR NDVI products • Soil texture derived from AVHRR observations	Variance = 0.24 $m^3 m^{-3}$ (on average)	–	RMSE ∈ (0.0224,0.033) $m^3 m^{-3}$ R^2 ∈ (0.023,0.86)

(*continued on next page*)

Table 2 (*continued*)

Downscaling techniques	Approaches	References	Main inputs	Accuracy	Improvement over the radiometer only measurements	Range of accuracy parameters
		Pellenq et al. (2003)	• High resolution DEM data • High resolution soil moisture maps from time domain reflectometry • Soil temperature profile measurements • Soil heat flux and meteorological measurements including rainfall • Surface roughness measurements • Soils information including field saturated hydraulic conductivity and soil depth	$R^2 = 0.67$[a]	–	
		Wilson et al. (2005) Perry and Niemann (2007) Busch et al. (2012)	• High resolution soil moisture data • Terrain attributes • Soil and vegetation properties • High resolution DEM data • Topographic attributes including wetness index and variables that are contained in the wetness index (slope and lnSCA)	Std. Dev. = 0.027 $m^3 m^{-3}$ (on average) RMSE and R^2 are not reported as measures of agreement.	ΔStd. Dev. = 0.011 $m^3 m^{-3}$ (on average)	
		Coleman and Niemann (2013)	• High resolution DEM • Topographic indices • Vegetation and soil properties			
		Ranney et al. (2015)	• High resolution DEM • Topographic indices • High resolution vegetation and soil properties	Topography: EMT: RMSE = 0.028 $m^3 m^{-3}$ EOF: RMSE = 0.027 $m^3 m^{-3}$ Topography and soil: EMT + VS: RMSE = 0.029 $m^3 m^{-3}$ EOF: RMSE = 0.027 $m^3 m^{-3}$		
		Cowley et al. (2017) Hoehn et al. (2017)	• High resolution DEM • Topographic indices • High resolution vegetation and soil properties • Precipitation and potential evapotranspiration data	RMSE and R^2 are not reported as measures of agreement. The accuracy of downscaled soil moisture products is not provided at fine resolution, but at the resolution of coarse soil moisture after averaging the values within the scale of coarse soil moisture.	–	
		Temimi et al. (2010)	• AMSR-E Ka-band radiometric data • MODIS LAI product • Topographic attributes from STRM Digital Elevation Model	Fort Chipewyan A: Dynamic TWI: $R^2 = 0.49$[a] (on average) Classic TWI: $R^2 = 0.14$[a](on average) Prairie River: Dynamic TWI: $R^2 = 0.18$[a](on average) Classic TWI: $R^2 = 0.023$[a](on average)	Fort Chipewyan A: Dynamic TWI: $\Delta R^2 = 0.24$[a] Classic TWI: $\Delta R^2 = -0.11$[a] Prairie River: Dynamic TWI: $\Delta R^2 = -0.09$[a] Classic TWI: $\Delta R^2 = -0.0247$[a]	
		Ines et al. (2013)	• SGP'97 experimental ESTAR L-band radiometric data • Synthetic data set (Walnut Creek WC11) • Soil hydraulic properties of Mualem-van Genuchten functions	FD bottom-boundary conditions: RMSE = 0.0224 $m^3 m^{-3}$, $R^2 = 0.86$[a](on average) Variable groundwater conditions: RMSE = 0.0327 $m^3 m^{-3}$, $R^2 = 0.74$[a](on average)	–	
		Shin and Mohanty (2013)	• SGP'97 experimental ESTAR L-band radiometric data	LW 13: MBE = −0.203 to −0.169 $m^3 m^{-3}$, $R^2 = 0.52$ to 0.83[a]	–	

(*continued on next page*)

Table 2 (*continued*)

Downscaling techniques	Approaches	References	Main inputs	Accuracy	Improvement over the radiometer only measurements	Range of accuracy parameters
			• Synthetic data set (little Washita-LW 13 and 21, Oklahoma) • Soil hydraulic properties of Mualem-van Genuchten functions	LW 21: MBE = -0.165 to $-0.122\ m^3\,m^{-3}$, R^2 = 0.12 to 0.76[a]		
Data assimilation-based	High resolution model predictions combined with low resolution radiometric observations	Reichle et al. (2001)	• SGP97 experimental ESTAR L-band radiometric data • Synthetic L-band radiometric data • Outputs of a land surface hydrologic model by (Reichle, 2000)	RMSE = 0.03 to $0.038\ m^3\,m^{-3}$	–	RMSE ∈ (0.03, 0.09) $m^3\,m^{-3}$ R^2 ∈ (0.07,0.86) ubRMSE[c] ∈ (0.0012,0.083)
		Draper et al. (2009)	• LPRM AMSR-E C-band soil moisture • Outputs of ISBA model	RMSE > $0.09\ m^3\,m^{-3}$	–	
		Sahoo et al. (2013)	• AMSR-E X-band radiometer data • Outputs of Noah land surface model by Mahrt and Pan (1984)	RMSE = $0.03\ m^3\,m^{-3}$, R^2 = 0.69[a]	ΔRMSE = $0.02\ m^3\,m^{-3}$, ΔR^2 = 0.23[a]	
		Kornelsen et al. (2015)	• Simulated brightness temperature using CMEM • Dense soil moisture measurements from experimental watersheds	Little River: RMSE = $0.04\ m^3\,m^{-3}$ Little Washita: RMSE = $0.06\ m^3\,m^{-3}$	Little River: ΔRMSE = $0.01\ m^3\,m^{-3}$ Little Washita: ΔRMSE = $0.03\ m^3\,m^{-3}$	
		Lievens et al. (2015)	• SMOS Level 3 CATDS soil moisture • Outputs of VIC model • Precipitation, 2-m air temperature, pressure, vapour pressure, wind speed, and incoming shortwave and longwave radiation	Mean: RMSE = $0.076\ m^3\,m^{-3}$, R^2 = 0.51[a] SD: RMSE = $0.078\ m^3\,m^{-3}$, R^2 = 0.47[a] • CDF: RMSE = $0.077\ m^3\,m^{-3}$, R^2 = 0.48[a]	Mean: ΔRMSE = $-0.001\ m^3\,m^{-3}$, ΔR^2 = -0.02[a] SD: ΔRMSE = $-0.004\ m^3\,m^{-3}$, ΔR^2 = -0.06[a] • CDF: ΔRMSE = $-0.004\ m^3\,m^{-3}$, ΔR^2 = -0.05[a]	
		Draper and Reichle (2015)	• Level 3 LPRM AMSR-E X-band soil moisture products • Outputs of the NASA's Catchment Land Surface Model	UbMSE[c] = $0.0012\ m^3\,m^{-3}$ (on average)		
		Reichle et al. (2017)	• SMAP L1C_TB brightness temperature observations • Surface meteorological forcing data from the GEOS-5 atmospheric assimilation system, Corrected with precipitation observation • Outputs of the NASA's Catchment Land Surface Model	All sites: ubRMSE[c] = $0.038\ m^3\,m^{-3}$ REMEDHUS: ubRMSE = $0.034\ m^3\,m^{-3}$ Reynolds Creek: ubRMSE = $0.03\ m^3\,m^{-3}$ Yanco: ubRMSE = $0.05\ m^3\,m^{-3}$ Carman: ubRMSE = $0.05\ m^3\,m^{-3}$ Walnut Gulch: ubRMSE = $0.032\ m^3\,m^{-3}$ Little Washita: ubRMSE = $0.034\ m^3\,m^{-3}$ Fort Cobb: ubRMSE = $0.038\ m^3\,m^{-3}$ Little River: ubRMSE = $0.038\ m^3\,m^{-3}$ St Josephs: ubRMSE = $0.05\ m^3\,m^{-3}$ South Fork: ubRMSE = $0.048\ m^3\,m^{-3}$ Monte Buey: ubRMSE = $0.029\ m^3\,m^{-3}$ Tonzi Ranch: ubRMSE = $0.037\ m^3\,m^{-3}$ Kenaston: ubRMSE = $0.038\ m^3\,m^{-3}$ Valencia:	–	

(continued on next page)

Table 2 (*continued*)

Downscaling techniques	Approaches	References	Main inputs	Accuracy	Improvement over the radiometer only measurements	Range of accuracy parameters
				ubRMSE = 0.023 $m^3 m^{-3}$ Niger: ubRMSE = 0.033 $m^3 m^{-3}$ Benin: ubRMSE = 0.047 $m^3 m^{-3}$ Yanco: ubRMSE = 0.041 $m^3 m^{-3}$		
		Lievens et al. (2017)	• SMAP L1C_TB brightness temperature observations • Sentinel-1 C-band backscatter • Surface meteorological forcing data from the GEOS-5 atmospheric assimilation system, Corrected with precipitation observation • Outputs of the NASA's Catchment Land Surface Model	Radiometer only assimilation: Core sites: ubRMSE[c] = 0.048 $m^3 m^{-3}$, R^2 = 0.44[a] REMEDHUS: ubRMSE = 0.037 $m^3 m^{-3}$, R^2 = 0.28[a] Yanco: ubRMSE = 0.049 $m^3 m^{-3}$, R^2 = 0.85[a] Twente: ubRMSE = 0.083 $m^3 m^{-3}$, R^2 = 0.27[a] Little Washita: ubRMSE = 0.035 $m^3 m^{-3}$, R^2 = 0.64[a] Fort Cobb: ubRMSE = 0.038 $m^3 m^{-3}$, R^2 = 0.55[a] South Fork: ubRMSE = 0.052 $m^3 m^{-3}$, R^2 = 0.38[a] Valencia: ubRMSE = 0.024 $m^3 m^{-3}$, R^2 = 0.24[a] Nigerc: ubRMSE = 0.049 $m^3 m^{-3}$, R^2 = 0.22[a] Benind: ubRMSE = 0.056 $m^3 m^{-3}$, R^2 = 0.55[a] TxSON: ubRMSE = 0.039 $m^3 m^{-3}$, R^2 = 0.69[a] HOBE: ubRMSE = 0.051 $m^3 m^{-3}$, R^2 = 0.53[a] Sparse networks: ubRMSE = 0.054 $m^3 m^{-3}$, R^2 = 0.44[a] SCAN: ubRMSE = 0.056 $m^3 m^{-3}$, R^2 = 0.41[a] USCRNF: ubRMSE = 0.053 $m^3 m^{-3}$, R^2 = 0.44[a] Oklahoma Mesonetg: ubRMSE = 0.058 $m^3 m^{-3}$, R^2 = 0.45[a] OzNet: ubRMSE = 0.062 $m^3 m^{-3}$, R^2 = 0.71[a] SMOSMANIA: ubRMSE = 0.045 $m^3 m^{-3}$, R^2 = 0.38[a] Complementary radar and radiometer assimilation: Core sites: ubRMSE = 0.046 $m^3 m^{-3}$, R^2 = 0.49[a] REMEDHUS: ubRMSE = 0.035 $m^3 m^{-3}$, R^2 = 0.36[a] Yanco: ubRMSE = 0.049 $m^3 m^{-3}$, R^2 = 0.86[a] Twente: ubRMSE = 0.08 $m^3 m^{-3}$, R^2 = 0.38[a] Little Washita: ubRMSE = 0.035 $m^3 m^{-3}$, R^2 = 0.62[a] Fort Cobb: ubRMSE = 0.037 $m^3 m^{-3}$, R^2 = 0.55[a] South Fork: ubRMSE = 0.05 $m^3 m^{-3}$, R^2 = 0.45[a] Valencia:	–	

(continued on next page)

Table 2 (*continued*)

Downscaling techniques	Approaches	References	Main inputs	Accuracy	Improvement over the radiometer only measurements	Range of accuracy parameters
				ubRMSE = 0.024 $m^3 m^{-3}$, R^2 = 0.26[a] Nigerc: ubRMSE = 0.045 $m^3 m^{-3}$, R^2 = 0.29[a] Benind: ubRMSE = 0.056 $m^3 m^{-3}$, R^2 = 0.58[a] TxSON: ubRMSE = 0.039 $m^3 m^{-3}$, R^2 = 0.67[a] HOBE: ubRMSE = 0.046 $m^3 m^{-3}$, R^2 = 0.69[a] Sparse networks: ubRMSE = 0.053 $m^3 m^{-3}$, R^2 = 0.46[a] SCAN: ubRMSE = 0.055 $m^3 m^{-3}$, R^2 = 0.41[a] USCRNF: ubRMSE = 0.053 $m^3 m^{-3}$, R^2 = 0.44[a] Oklahoma Mesonetg: ubRMSE = 0.057 $m^3 m^{-3}$, R^2 = 0.45[a] OzNet: ubRMSE = 0.061 $m^3 m^{-3}$, R^2 = 0.72[a] SMOSMANIA: ubRMSE = 0.042 $m^3 m^{-3}$, R^2 = 0.44[a]		
Machine learning-based	Relationship with surface parameters	Srivastava et al. (2013)	• SMOS L-band radiometric data • MODIS LST product	ANN: RMSE = 0.011 $m^3 m^{-3}$, R^2 = 0.75 RVM: RMSE = 0.013 $m^3 m^{-3}$, R^2 = 0.69 SVM: RMSE = 0.013 $m^3 m^{-3}$, R^2 = 0.69 GLM: RMSE = 0.013 $m^3 m^{-3}$, R^2 = 0.69	ANN: ΔRMSE = 0.006 $m^3 m^{-3}$, ΔR^2 = 0.33 RVM: ΔRMSE = 0.004 $m^3 m^{-3}$, ΔR^2 = 0.27 SVM: ΔRMSE = 0.004 $m^3 m^{-3}$, ΔR^2 = 0.27 GLM: ΔRMSE = 0.004 $m^3 m^{-3}$, ΔR^2 = 0.27	RMSE ∈ (0.006, 0.16) $m^3 m^{-3}$ R^2 ∈ (0.37,0.96)
		Chai et al. (2011)	• NAFE'05 experimental PLMR L-band radiometric data • MODIS products including surface reflectance, LST and emissivity	RMSE = 0.018 to 0.035 $m^3 m^{-3}$	–	
		Chai and Goh (2013)		RMSE = 0.0233 $m^3 m^{-3}$, R^2 = 0.89	–	
		Chakrabarti et al. (2015)	• MicroWEXs meteorological forcing data • Land cover map	PRI method: RMSE = 0.006 $m^3 m^{-3}$ UTD method: RMSE = 0.079 $m^3 m^{-3}$	–	
		Chakrabarti et al. (2016)	• Synthetic data set simulated by using a coupled LSP-DSSAT model	RMSE < 0.02 $m^3 m^{-3}$	–	
		Park et al. (2015)	• AMSR2 C-band LPRM daily soil moisture products • MODIS products including surface albedo, LST, NDVI, EVI, LAI and evapotranspiration	Random forest: RMSE = 0.06 $m^3 m^{-3}$, R^2 = 0. 96 Ordinary least square: RMSE = 0.16 $m^3 m^{-3}$, R^2 = 0.47	–	
		Im et al. (2016)	• AMSR-E C-band LPRM Level 3 daily soil moisture products • MODIS products including surface albedo, LST, NDVI, EVI, LAI and evapotranspiration	Random forest: South Korea: RMSE = 0.049 $m^3 m^{-3}$, R^2 = 0.50[a] Australia: RMSE = 0.057 $m^3 m^{-3}$, R^2 = 0.71[a] Boosted regression trees: South Korea: RMSE = 0.052 $m^3 m^{-3}$, R^2 = 0.56[a] Australia: RMSE = 0.078 $m^3 m^{-3}$, R^2 = 0.59[a] Cubist: South Korea: RMSE = 0.051 $m^3 m^{-3}$, R^2 = 0.49[a]	Random forest: South Korea: ΔRMSE = 0.059 $m^3 m^{-3}$, ΔR^2 = 0.28[a] (on average) Australia: ΔRMSE = −0.004 $m^3 m^{-3}$, ΔR^2 = 0.45[a] (on average) Boosted regression trees: South Korea: ΔRMSE = 0.056 $m^3 m^{-3}$, ΔR^2 = 0.34[a] (on average) Australia: ΔRMSE = −0.025 $m^3 m^{-3}$, ΔR^2 = 0.33[a] (on average) Cubist: South Korea:	

(*continued on next page*)

Table 2 (*continued*)

Downscaling techniques	Approaches	References	Main inputs	Accuracy	Improvement over the radiometer only measurements	Range of accuracy parameters
				Australia: RMSE = $0.063\,m^3\,m^{-3}$, $R^2 = 0.37$[a]	$\Delta RMSE = -0.057\,m^3\,m^{-3}$, $\Delta R^2 = 0.27$[a] (on average) Australia: $\Delta RMSE = -0.01\,m^3\,m^{-3}$, $\Delta R^2 = 0.11$[a] (on average)	
		Jiang et al. (2017)	• LPRM, JAXA, and NASA AMSR-E soil moisture products • JAXA AMSR2 soil moisture products • SMOS CATDS Level 3 soil moisture products	NASA AMSR-E: RMSE = $0.15\,m^3\,m^{-3}$, $R^2 = 0.55$[a] LPRM AMSR-E: RMSE = $0.12\,m^3\,m^{-3}$, $R^2 = 0.69$[a] JAXA AMSR-E: RMSE = $0.081\,m^3\,m^{-3}$, $R^2 = 0.72$[a] JAXA AMSR2: RMSE = $0.055\,m^3\,m^{-3}$, $R^2 = 0.86$[a] Ascending SMOS: RMSE = $0.081\,m^3\,m^{-3}$, $R^2 = 0.41$[a] Descending SMOS: RMSE = $0.047\,m^3\,m^{-3}$, $R^2 = 0.77$[a]	NASA AMSR-E: $\Delta RMSE = -0.012\,m^3\,m^{-3}$, $\Delta R^2 = 0.18$[a] LPRM AMSR-E: $\Delta RMSE = -0.001\,m^3\,m^{-3}$, $\Delta R^2 = -0.02$[a] JAXA AMSR-E: $\Delta RMSE = 0.037\,m^3\,m^{-3}$, $\Delta R^2 = -0.05$[a] JAXA AMSR2: $\Delta RMSE = 0.071\,m^3\,m^{-3}$, $\Delta R^2 = 0.11$[a] Ascending SMOS: $\Delta RMSE = 0.01\,m^3\,m^{-3}$, $\Delta R^2 = 0.1$[a] Descending SMOS: $\Delta RMSE = 0.004\,m^3\,m^{-3}$, $\Delta R^2 = 0.09$[a]	

Note: negative values of both ΔR^2 and $\Delta RMSE$ means that coarse passive microwave observations have provided better estimates of soil moisture than the downscaled products.
[a] The R^2 (coefficient of determination) has been calculated by squaring values in R (correlation coefficient).
[b] Indicates studies where their accuracy parameters have been obtained from digitizing the results shown in figure.
[c] ubRMSE and ubMSE values are not included in the summary and discussion section. They are added to this table for the information of readers.

are utilized, could potentially improve the soil moisture estimation in terms of both accuracy and spatial scale. Several studies have therefore suggested that the remotely sensed soil moisture from the passive microwave observations at lower (L- and C-band) frequencies be combined with backscatter or passive microwave emission at higher (Ka-band) frequency. These combination techniques are briefly introduced in the radar- and radiometric-based sections below.

2.1.1. Radar-based downscaling techniques

The combination of active/passive microwave observations has been a preferred approach to downscaling because both sensors respond to changes in the dielectric properties of the soil. Ulaby et al. (1983) conducted one of the first investigations based on this approach using L-band radiometer and C-band radar soil moisture estimates over bare soil and corn fields. They found that it could reduce the estimation error by up to 30% of the reference soil moisture value. Findings from this pioneering work motivated Theis et al. (1986), O'Neill and Chauhan (1992), O'Neill et al. (1996) and Chauhan (1997) to propose approaches using active and passive microwave techniques in compliment to each other, to optimize the accuracy of the final soil moisture estimates. Theis et al. (1986) used L-band scatterometer data to compensate for the surface roughness impact on the response of L- and C-band radiometers to soil moisture. This complimentary combination significantly improved the passive microwave remote sensing of soil moisture over bare fields, especially for L-band soil moisture retrievals, with R^2 equal to 0.95. In order to utilize active and passive microwave data sets in combination, O'neill and Chauhan (1992) retrieved soil moisture from a radiative transfer model with radar-derived ancillary data on the vegetation attenuation parameter. This analysis, which was made for a single field covered by corn, demonstrated that the radar-derived vegetation attenuation could increase the accuracy of radiometric remote sensing of soil moisture. In another study, O'neill et al. (1996) used L-band radar determination of vegetation transmissivity and scattering in a radiative transfer model to estimate soil moisture. They reported successful retrieval of soil moisture within about $0.02\,m^3\,m^{-3}$ of the ground measurements. A dielectric-soil moisture relation was also employed by Chauhan (1997) to estimate soil moisture from Fresnel reflectivity, derived from radar-based estimation of vegetation and surface roughness parameters. The capability of passive microwave remote sensing in delivering soil moisture maps consequently improved, with an averaged absolute bias of less than $0.05\,m^3\,m^{-3}$.

Besides using combined passive and active observations as a means of improving the retrieval of soil moisture measurement, investigations were made for combined radar-radiometer downscaling techniques. This technique attempts to recover the spatial detail of the coarse soil moisture/brightness temperature through the association of the sub-pixel distribution of land surface features embedded in the radar imagery. However, the sensitivity of backscatter to surface roughness and vegetation is the key limitation for applying this technique to radiometric soil moisture downscaling (Njoku et al., 2001).

To explore this concept, a radar-radiometer data set was collected by the Passive-Active L-/S-band (PALS) sensor during the Southern Great Plains Experiment in 1999 (SGP99). This data set was used by Njoku et al. (2002) to design a change detection based downscaling algorithm that employed a linear relationship between the backscatter and volumetric soil moisture (e.g. Dobson and Ulaby, 1986). The use of relative changes in backscatter reduces the impact of surface roughness and vegetation on radar signals, and thus on soil moisture estimates (e.g. Quesney et al., 2000; Wagner and Scipal, 2000; Moran et al., 2000). Narayan et al. (2006) modified the Njoku et al. (2002) method by using the relative radar response to soil moisture suggested by Du et al. (2000).

In order to conduct a comprehensive assessment of the algorithm's applicability, coincident active observations and passive microwave derived soil moisture products were simulated to mimic the gradual wetting and drying conditions. The spatial variability in soil moisture and vegetation water content were assumed to be the only factors influencing temporal changes in the radar signals. This method was used by Narayan and Lakshmi (2008) to downscale space-borne soil moisture estimates from the Advanced Microwave Scanning Radiometer (AMSR-E) and Tropical Rainfall Measuring Mission (TRMM) Microwave Imager

(TMI) with backscatter from the Precipitation Radar (PR). This study demonstrated the applicability of the radar-based downscaling technique to represent soil moisture spatial variability. Through intercomparison between downscaled TMI and AMSR-E, temporal coincidence between radar and radiometer observations was found to exist, providing credence to this approach; soil moisture products from the TMI sensor on the same platform as the TRMM-PR radar were much better enhanced spatially than those from the AMSR-E.

Research on the integration of radar and radiometer observations for spatially enhanced soil moisture mapping has not been limited to the physically based approach of Njoku et al. (2002). For example, Bindlish and Barros (2002) also produced sub-scale brightness temperature prior to soil moisture retrieval by applying a fractal interpolation methodology, combining radar and radiometric observations. In this approach, the ratio between high resolution HH-polarized backscatter, and aggregated backscatter to the scale of the coarse brightness temperature observation, was used as a weighting coefficient to estimate brightness temperature at the same resolution as the backscatter observations. In a further approach, Zhan et al. (2006) developed a Bayesian disaggregation method that merges radar and radiometer observations with an initial background soil moisture field. In this study, using synthetic data from an Observation System Simulation Experiment (OSSE), the background states of soil moisture were first derived using direct inversion of coarse brightness temperature. The uncertainties in the initial soil moisture estimate and the satellite observations were then used to merge observed and calculated brightness temperature and backscatter from the background soil moisture using emission and backscatter models, to get an updated soil moisture field. Wu et al. (2017) subsequently applied this technique to a time series of experimental aircraft-based radar/radiometer observations collected during the SMAPEx-3 field campaign (Panciera et al., 2014) in south-eastern Australia to produce 1, 3 and 9 km resolution soil moisture maps. Findings from this study revealed that: i) the performance of the Bayesian method depended on the accuracy of the radar model, and that ii) the Bayesian merging technique performed best over grassland areas with the radar model used in that study.

The development of radar-based downscaling techniques entered a new phase with the announcement of a dedicated active/passive satellite for soil moisture, SMAP, in response to the National Research Council's Decadal Survey. The SMAP satellite was designed to measure temporally coincident surface emission and backscatter from a radiometer/radar using a single large mesh antenna with a conical scan configuration. The concept of having a radar and radiometer integrated into a single system was first introduced by Njoku et al. (2000). The conical scan provides measurements of the Earth's surface at constant incidence angle and antenna pattern characteristics across the entire swath. Accordingly, the data processing, interpretation, and geophysical retrieval become simplified. The SMAP mission aimed to combine the strengths of the respective radar and radiometer observations - high spatial resolution for the radar and high sensitivity to soil moisture for the radiometer - to optimally estimate soil moisture content at an intermediate resolution.

The change detection method of Piles et al. (2009b) was among the first alternative techniques to derive active/passive merged products. Piles et al. (2009b) made use of the linear correlation between backscatter and soil moisture content for formulating a disaggregation algorithm which derived relative changes of soil moisture. This approach produced the spatial variability of soil moisture by updating the radiometer soil moisture retrieval from the previous observation with the corresponding temporal changes in high resolution backscatter. The approach was applied to airborne data from PALS for the SMEX02 campaign, and to an OSSE. The change detection approach revealed superiority to radiometer only estimations in terms of both the accuracy and spatial heterogeneity of soil moisture products.

The active/passive optional algorithm developed by Das et al. (2011) is an extension to the Piles et al. (2009b) change detection approach. This technique was also developed based on the linear regression between backscatter and volumetric soil moisture. The major enhancement of the active/passive retrieval method over the change detection technique was the estimation of an absolute soil moisture. Being based on the linear relationship between backscatter and passive-based soil moisture products, the successful application of these techniques depends to a great extent on how well backscatter and soil moisture are correlated (Wu et al., 2014), and how sensitive they are to soil moisture changes.

The SMAP active/passive baseline algorithm by Das et al. (2014), which established a linear regression between backscatter and brightness temperature for estimation of absolute soil moisture at 9 km, was an extension of the active/passive optional retrieval algorithm developed by Das et al. (2011). The baseline algorithm downscaled observed brightness temperature and then performed the soil moisture retrieval, as opposed to the optional active/passive retrieval algorithm that downscaled derived soil moisture at coarse resolution as described above. An important aspect of the baseline algorithm is that it considers vegetation and surface roughness heterogeneity in time and space when calibrating the main downscaling factor β [K/dB] as an added value to the active/passive retrieval algorithm. The processing steps of the baseline model currently used by the SMAP science team are described in Fig. 3.

Wu et al. (2016) applied the active/passive optional (Das et al., 2011), baseline (Das et al., 2014) and change detection (Piles et al., 2009b) retrieval algorithms to the SMAPEx-3 airborne simulation (Wu et al., 2015) of the SMAP data stream to test the robustness of alternate radar-radiometer combination algorithms over a semi-arid region. Findings of this study revealed that all the alternate algorithms had only small differences in average Root-Mean-Square-Error (RMSE) and could effectively increase the spatial resolution of soil moisture retrievals from 36 to 9 km. However, the active/passive retrieval algorithm by Das et al. (2011) showed the best correlation with the reference soil moisture map. Consequently, Wu et al. (2016) recommended application of the optional active/passive retrieval algorithm by Das et al. (2011) for global soil moisture mapping.

Montzka et al. (2016) developed a linear relationship between radar- and radiometer- only soil moisture estimates for calibrating a disaggregation algorithm which enhances the spatial resolution of passive-based soil moisture retrievals. This approach was applied to L-band radar and radiometer airborne data from the Tereno campaign (Montzka et al., 2012). Performance of this method was compared against the active/passive optional (Das et al., 2011) and baseline (Das et al., 2014) retrieval algorithms. This analysis revealed superiority of the baseline algorithm in delivering more accurate high resolution soil moisture to the optional technique and the new combined radar/radiometer-only soil moisture technique by Montzka et al. (2016). However, the spatial pattern of retrieved soil moisture from the new combined radar/radiometer-only soil moisture technique by Montzka et al. (2016) was reported to be similar to that of the baseline retrievals.

Recently, Rüdiger et al. (2016) downscaled an airborne simulation of the coarse-scale L-band brightness temperature at 50 km using ESA's C-band Advanced Synthetic Aperture Radar (ASAR) backscatter aggregated to 2 km. This technique included two changes to the active/passive optional algorithm: i) calibration of the downscaling factor at higher resolution than the coarse scale of L-band observations in order to have an adequate number of regression points for establishing a linear relationship, ii) the establishment of a linear regression between the radiometric emissivities and radar backscatter sensitivities instead of between soil moisture and radar backscatter. The intention of using backscatter sensitivities and radiometric emissivities was to preserve the information of vegetation heterogeneity in the downscaling products and to remove the surface temperature impacts, respectively. This downscaling approach resulted in soil moisture estimates with errors of 0.06 to 0.12 $m^3 m^{-3}$, which are comparable to other downscaling techniques.

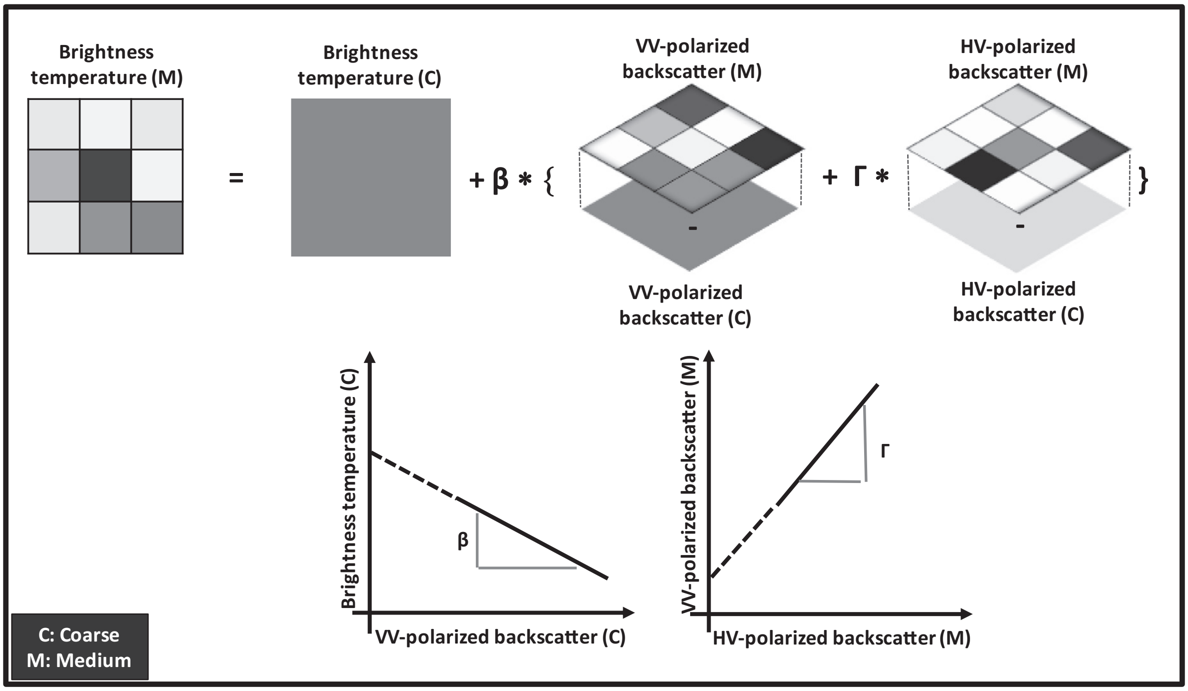

Fig. 3. Schematic diagram of the SMAP active/passive baseline algorithm (adapted from Dr. Xiaoling Wu personal communication).

Akbar and Moghaddam (2015) proposed a Combined Active-Passive (CAP) algorithm based on a joint cost function with adaptive regularization by Monte Carlo numerical simulations. To increase the reliability of soil moisture retrievals in terms of accuracy, CAP gave more weight to radiometric soil moisture but without discarding the complimentary radar-based soil moisture estimates. The novelty of the CAP model was the merging of the same-scaled and coincident radar and radiometric soil moisture. This approach was demonstrated using airborne PALS and tower Combined Radar Radiometer (ComRad) acquisitions, resulting in soil moisture retrievals with accuracy of 0.038 $m^3\,m^{-3}$ for low noise level measurement scenario.

2.1.2. Radiometer-based downscaling techniques

The downscaling of coarse passive microwave data has not been limited to the use of backscatter. The use of passive microwave observations at higher frequencies has also been introduced, with several systems using the same antenna for multi-frequency measurements; higher spatial resolutions are available from the higher frequencies. One such methodology is based on the multi-sensor image fusion technique known as Smoothing Filter-based Intensity Modulation (SFIM) by Liu (2000), initially applied for increasing the spatial resolution of multi-spectral optical data. The approach was subsequently applied by Santi (2010) for downscaling brightness temperature observations from the Advanced Microwave Scanning Radiometer-Earth Observing System (AMSR-E). Applying the SFIM on pairs of simultaneous Ka- and C-band acquisitions from the AMSR-E sensor, Santi (2010) reported on the SFIM's potential for disaggregating approximately 50 km resolution C-band (6.9 GHz) brightness temperature to 10 km. Unravelling of spatial variability in soil moisture using this technique is through heterogeneity captured by the Ka-band (36.5 GHz) brightness temperature at 10 km resolution in the disaggregation procedure.

The performance of this method for soil moisture downscaling was further evaluated by de Jeu et al. (2014) and Parinussa et al. (2014). While these studies reported on the algorithm success in enhancing the spatial variability of soil moisture and in capturing dry and wet regions, their analysis revealed that geophysical accuracy of the high resolution products remained on the same level as that of coarse AMSR-E soil moisture products. Their analysis also revealed that rainfall impacts on the Ka-band observations could diminish the accuracy of downscaled soil moisture products. Gevaert et al. (2015) recently corrected the Ka-band observations for precipitation prior to their use in the SFIM method. This modification involved the application of a precipitation mask to the Ka-band observations to remove them from the processing. Disaggregated soil moisture products at 10 km resolution were subsequently retrieved from the downscaled brightness temperature (see Fig. 4).

2.2. Optical-based downscaling techniques

The association of land surface temperature and vegetation parameters with soil moisture conditions (Nemani et al., 1993) provides the basis for optical downscaling. Carlson et al. (1994) and Gillies and Carlson (1995) developed the universal triangle concept (Fig. 5) which relates VIS/IR parameters, such as the NDVI and Land Surface Temperature (LST), to the soil moisture status. The sensitivity of surface temperature change in response to soil moisture is considered to be different depending upon the surface conditions (e.g. canopy type, density of vegetation cover). This linkage creates a scatter plot of vegetation index - surface temperature in the shape of a triangle (or a four-sided polygon in the case that wet and dry edges cross beyond the maximum NDVI value), yielding boundaries of the wet and dry conditions. However, this concept cannot act as a direct methodology for soil moisture retrieval, due to attenuation of reflected solar radiation from the soil surface by the opaque overlaying media (e.g. atmosphere and vegetation), lack of micro-meteorological and atmospheric information, and the optical observations being affected by clouds.

Several researchers have used the triangle concept as a tool to improve the scale of passive microwave based soil moisture products (e.g. Merlin et al., 2006, 2008a, 2008b; Piles et al., 2011; Merlin et al., 2012, 2013; Fang et al., 2013), with land surface temperature and vegetation parameters derived from optical observations at high resolution being the key factor in the downscaling process. These optical-based downscaling techniques combine the strengths of optical and radiometric observations (i.e. high spatial resolution optical data and high accuracy passive microwave derived soil moisture). While the high spatial

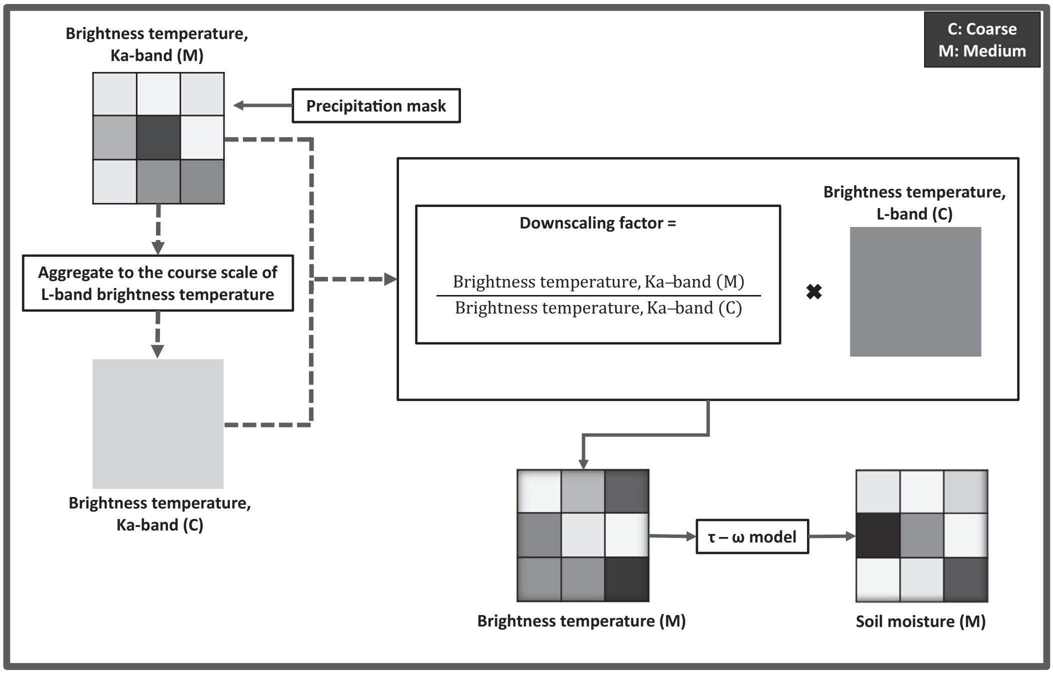

Fig. 4. Schematic of the SFIM technique for downscaling coarse passive microwave brightness temperature to yield a medium resolution soil moisture retrieval.

resolution of optical observations provides information on heterogeneity of surface features, they have limited application due to being highly affected by cloud coverage and vegetation.

To calculate soil moisture variations at 1 km resolution, Chauhan et al. (2003) used optical observations from the Advanced Very High Resolution Radiometer (AVHRR) to infer spatial variability of surface features for downscaling coarse soil moisture from the Special Sensor Microwave Imager (SSM/I), which is not a particularly good frequency to use, for the Southern Great Plains (SGP-97) campaign. Chauhan et al. (2003) calibrated a model through which an ensemble of satellite-derived vegetation index, surface albedo and land surface temperature with soil moisture at the coarse scale of SSM/I, led to reasonable estimates of fine scaled soil moisture in terms of accuracy (0.05 $m^3 m^{-3}$). In this model, which was based on the model by Zhan et al. (2002), a simple linear average equation was applied to the pixel values of AVHRR within the passive grid scale. This model was then applied to high resolution surface feature parameters to retrieve soil moisture maps at 1 km resolution. The advantage of this approach was its modest requirement of ancillary data for disaggregation. Later, Choi and Hur (2012) applied this model to downscale AMSR-E soil moisture products from 25 to 1 km over a study area in Korea. Disaggregated soil moisture products in this study were reported to have slightly lower RMSE and higher correlation of coefficient to ground-based measurements than those of the coarse AMSR-E soil moisture. This technique was also used by Zhao and Li (2013a) to downscale AMSR-E soil moisture retrievals from 25 to 5 km using the METEOSAT Second Generation – Spinning

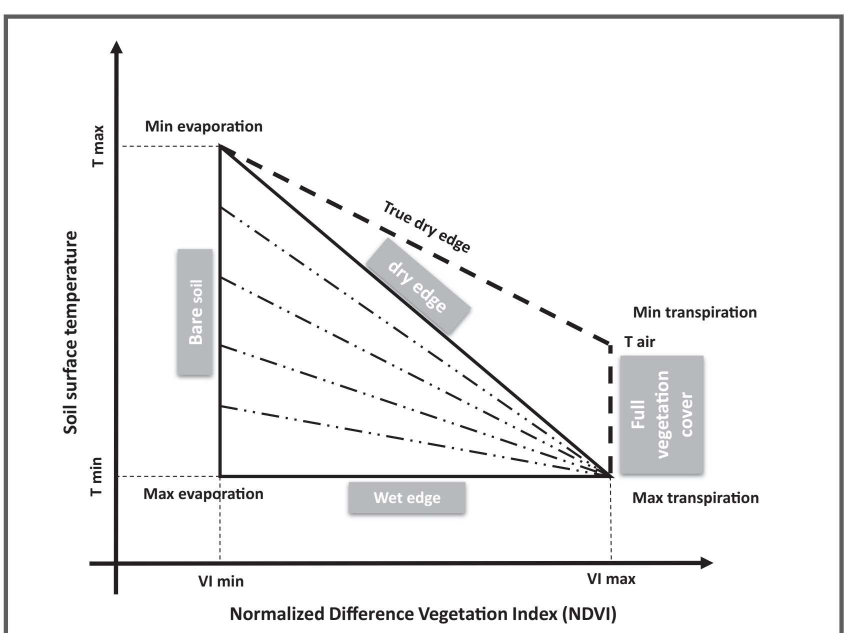

Fig. 5. Triangle/Trapezoid concept of the LST/VI feature space (adapted from Petropoulos et al., 2015 and Merlin et al., 2012).

Enhanced Visible and Infrared Imager (MSG SEVIRI) geostationary satellite data. The fact that geostationary satellites continuously monitor the land surface, facilitates capturing of temporal variation of LST which was correlated to soil moisture instead of an absolute value of LST in this study. Use of change in LST over time was suggested by Stisen et al. (2008) as a solution for reducing the mean error in the thermal information and the impact it had on the accuracy of downscaled soil moisture products. The two LST temporal variation parameters used in this study were mid-morning temperature rising rate and maximum temperature time, which are strongly related to soil moisture (Zhao and Li, 2013b). Retrievals from this downscaling technique revealed no improvement over the AMSR-E soil moisture products when compared against ground based measurements of soil moisture; however, they showed better agreement with in situ measurements than the retrievals from Chauhan et al. (2003) method. Piles et al. (2014) expanded the approach to use the polarimetric multi-angular brightness temperature observations of SMOS to reflect precipitation impact on changes in soil moisture. An early version of the Piles et al. (2014) downscaling scheme was presented in Piles et al. (2011) to downscale SMOS derived soil moisture maps to 1 km resolution. Piles et al. (2011) recommended: i) to capitalize the synergy between SMOS and MODerate resolution Imaging Spectro-radiometer (MODIS) observations instead of other optical observations such as the AVHRR and Landsat, and ii) to average pixel values of MODIS within the SMOS grid scale that were not masked by clouds. While Piles et al. (2011) suggested the use of brightness temperature for better estimates of high resolution soil moisture maps, it was Piles et al. (2012) that added polarimetric and multi-angular brightness temperature into the model. This adjustment made the downscaling algorithm more reliable by increasing the temporal correlation and reducing error retrievals from 0.05 to 0.03 $m^3 m^{-3}$. A schematic of this downscaling model is shown in Fig. 6. Sánchez-Ruiz et al. (2014) used MODIS Normalized Difference Water Index (NDWI) at the higher spatial resolution of 500 m, rather than the 1 km NDVI in Piles et al. (2014), to derive a better agreement of downscaled soil moisture with in situ measurements, particularly during periods of high vegetation activities.

The work of Piles et al. (2014) is capable of downscaling SMOS soil moisture products from a spatial resolution of 25 km to 1 km. However, this technique lacks the ability to preserve the temporal resolution of passive microwave soil moisture data; the temporal resolution of its retrievals is hampered by the availability of MODIS observations and their cloudiness. The shortcomings of this model were overcome by using the MSG SEVIRI optical data in place of MODIS data (Piles et al., 2016). The Piles et al. (2016) model provided 3 km temporally averaged soil moisture estimates using MSG geostationary satellite observations, to provide instantaneous soil moisture estimates at time increments of 15 minutes. The proposed downscaling technique not only estimated high resolution soil moisture with a similar quality to SMOS soil moisture, but also minimised the impact of clouds by using observations throughout the daytime.

Merlin et al. (2005) proposed the use of a physical downscaling model to derive the spatial variability of the top 0–5 cm soil moisture at 1 km resolution. This model disaggregates the surface soil moisture according to fine-scale information provided by radiometric surface temperature and surface coverage condition. Merlin et al. (2006) tested this algorithm over a semi-arid area and found that the model performed best for high solar radiation and low vegetation density. Merlin et al. (2008a) then translated space- and time-based anomalies of soil moisture indices at fine-scale into high resolution soil moisture from SMOS, by establishing a linear relationship to calibrate a time-invariant slope at the SMOS scale. Evaporative Fraction (EF; the ratio of evapotranspiration to the total energy available at the surface) and Soil Evaporative Efficiency (SEE; the ratio of actual to potential evaporation), were chosen as the Soil Moisture Indexes (SMIs) for downscaling. The choice of EF and SEE for soil moisture downscaling was not only because of their direct dependency on soil moisture dynamics, but also their constant diurnal characteristic. Both SMIs provided a fine-scale distribution of soil moisture; however, SEE resulted in more accurate estimates of 1 km scale soil moisture, due to the higher correlation with surface soil moisture. The superior performance of this algorithm was reported for dry-end soil moisture controls and clear sky only condition. An expansion of this algorithm was presented in Merlin et al. (2008b), whereby the relationship between SEE and surface soil moisture was considered to be variable and a function of soil type, wind speed, and SMOS-scale near-surface soil moisture. Relating the spatially averaged MODIS thermal observations to 10 km, linearity of the SEE - soil moisture relationship was improved because sensitivity of coarse thermal observations to soil moisture was considerably higher. Merlin et al. (2009) introduced intermediate resolutions, with the range of 3 to 5 km being optimal for soil moisture products in terms of accuracy. They also suggested a sequential downscaling procedure with the use of multi-resolution thermal imagery. This procedure improved the spatial scale of SMOS retrievals from 40 km to 4 km resolution using the aggregated MODIS observations at 4 km, and subsequently used Advanced Scanning Thermal Emission and Reflection (ASTER) radiometer data to disaggregate retrievals to 500 m soil moisture maps. However,

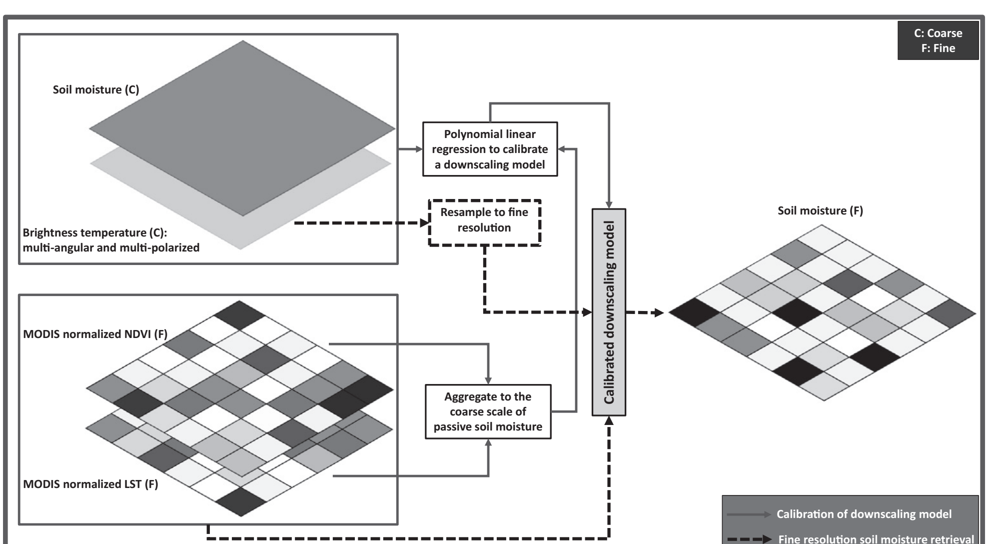

Fig. 6. Schematic of the downscaling model structure developed by Piles et al. (2012).

application of this sequential downscaling model concept was not recommended since combined use of MODIS and ASTER increased uncertainty of soil moisture retrievals compared to MODIS only disaggregated soil moisture. The low temporal repeat of ASTER observations was another factor that reduced the functionality of this approach. Use of the exponential-based SEE model, as opposed to cosine-based suggested by Merlin et al. (2010), led to improved spatial representation of downscaled soil moisture. Developing a Taylor series of soil moisture with respect to projected SEE was also implemented to improve accuracy and robustness of the disaggregation model.

Ongoing efforts to improve performance of the SEE-based disaggregation model (Merlin et al., 2008b) led to the emergence of the Disaggregation based on Physical And Theoretical scale Change (DisPATCh) model by Merlin et al. (2012), in which the use of the universal trapezoid (Fig. 5) instead of the universal triangle concept was recommended for better soil moisture disaggregation. However, the DisPATCh model performance is still related to seasonal and climatic variations because the strength of the coupling between soil moisture and surface temperature varies on a seasonal basis. The strength of this coupling over semi-arid areas during summer resulted in a temporal correlation of 0.7 when compared to point-measurements. This result is in stark contrast to the correlation of downscaled soil moisture content over temperate climate during winter, which had a correlation of zero. The latest version of the DisPATCh model, including the use of vegetation water stress (Moran et al., 1994) and correction for elevation effects on temperature, was introduced by Merlin et al. (2013). That study contrasted the DisPATCh model with the linear and non-linear behaviour of the SEE variable in relation to multi-resolution retrieval of soil moisture, and revealed preference for the SEE linear behaviour over non-linear for kilometre resolution. However, the assumption of a linear relationship between the SEE and soil moisture resulted in poorer performance at metre resolution. These results also confirmed that atmospheric evaporative demand with seasonal variation is the main factor controlling the quality of the DisPATCh downscaled soil moisture retrieval. This method is illustrated in Fig. 7 to provide a clear understanding of how it works.

Using the DisPATCh technique to downscale AMSR-E and SMOS over the Murrumbidgee catchment in Australia, Malbéteau et al. (2016) reported that downscaled soil moisture could provide opportunities for reducing the negative impact of scale mismatch on validation of satellite soil moisture applications. Malbéteau et al. (2016) also showed that DisPATCh was efficient in increasing the correlation coefficient of satellite soil moisture retrievals, especially in semi-arid regions. For example, in the semi-arid region of Yanco, the correlation coefficient of SMOS for afternoon overpasses increased from 0.37 to 0.63 after disaggregation. Djamai et al. (2016) proposed combining DisPATCh derived soil moisture with the Canadian LAnd Surface Scheme (CLASS) simulations of soil moisture in order to estimate a continuous time series of 1 km soil moisture maps for cloudy and cloud-free days. In that study, the DisPATCh derived soil moisture was compared with the CLASS soil moisture simulation for cloud-free days to develop a robust slope correction function. Results from the application of this calibration function - assumed to be valid under cloudy sky - indicated the potential of a DisPATCh/CLASS combination for soil moisture retrieval under cloudy skies.

The soil evaporative efficiency has also been utilized in a different approach by Fang and Lakshmi (2014a), for downscaling AMSR-E soil moisture. In the first step of their soil moisture downscaling procedure, North American Land Data Assimilation System (NLDAS)-derived soil temperature was disaggregated to 1 km resolution using the MODIS LST and fractional vegetation cover. From the disaggregated NLDAS soil temperature, SEE was estimated using the model of Merlin et al. (2010). The 1 km SEE estimates were then converted to soil moisture maps at 1 km resolution using models developed by Noilhan and Planton (1989) and Lee and Pielke (1992). The difference between the AMSR-E derived soil moisture and up-scaled 1 km soil moisture to the resolution of AMSR-E were then added to each 1 km soil moisture pixel to estimate high resolution soil moisture.

Instead of the SEE, which was used in the physical-based downscaling technique by Merlin et al. (2010, 2012), Chen et al. (2017) used

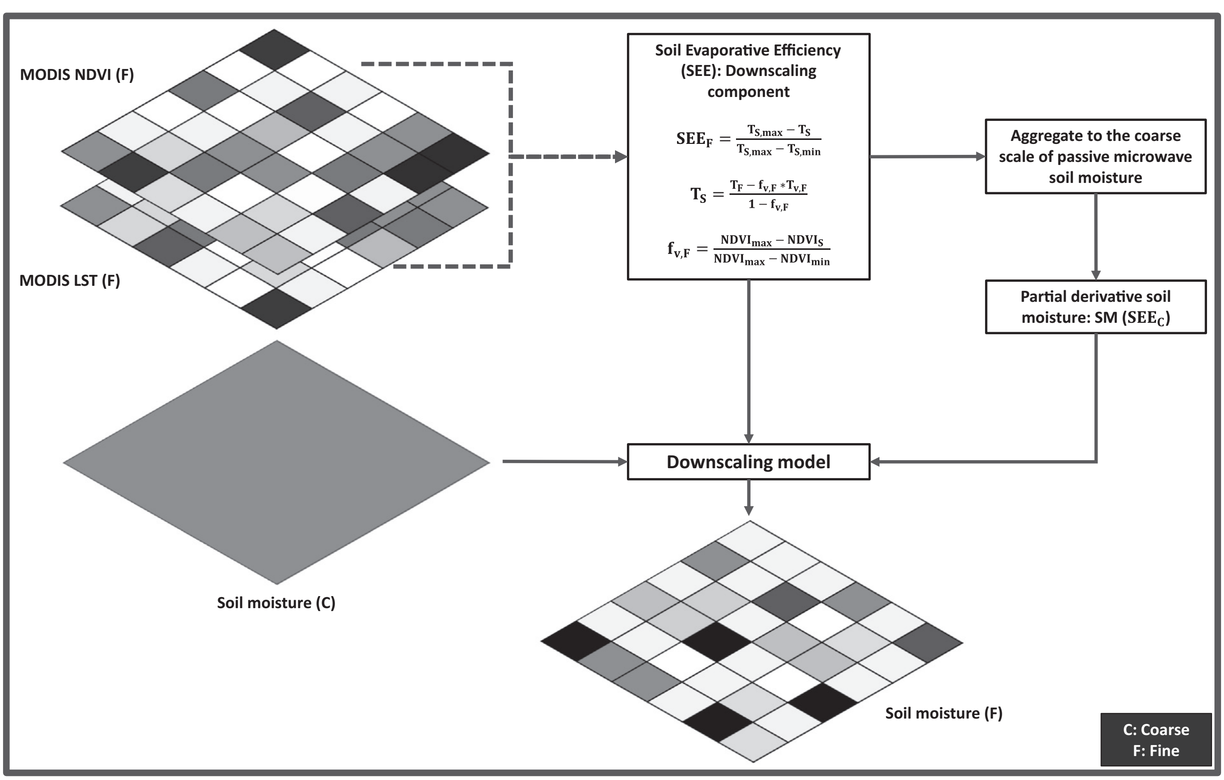

Fig. 7. Schematic of DisPATCh downscaling method which combines accurate but coarse passive microwave observations with high resolution optical observations.

the Normalized Soil Moisture Index (NSMI) as a variance indicator of soil moisture in space. The dimensionless NSMI with resolution of 250 m was derived using the MODIS NIR and red-band land surface reflectance products. This downscaling technique, named Near InfraRed-Red (NIR-Red) Spectral-based Disaggregation (NRSD), was developed using a semi-physical relationship which related the NIR-Red triangle space (Huete et al., 1985; Richardson and Wiegand, 1977) to the soil moisture status. The NRSD technique was formalized to downscale 36 km SMAP radiometer-derived soil moisture to 250 m using the first-order Taylor series (Merlin et al., 2012) through which the SMAP soil moisture was corrected with respect to the converted variance of the NSMI to soil moisture. Accuracy, spatial resolution, and application scope of downscaled soil moisture products from the NRSD were reported to outperform the retrievals from DisPATCh.

The contribution of SWI as a weighting factor to disaggregate coarse AMSR-E surface soil moisture products was evaluated by Kim and Hogue (2012). The coarse C-band AMSR-E observations were multiplied by the ratio of the MODIS-scaled SWI to the mean of MODIS-based SWI over the AMSR-E footprints. To estimate SWI, the algorithm applied the Jiang and Islam (2003) model to MODIS temperature and Enhanced Vegetation Index (EVI) products. The selection of EVI over NDVI was intended to minimise the soil background interference in the vegetation index. The performance of this algorithm resulted in a better approximation of soil moisture than that of the coarse AMSR-E soil moisture over a semi-arid region in the San Pedro River basin. In addition, the model showed better performance than the triangle-based downscaling techniques developed by Chauhan et al. (2003) and Carlson et al. (1994). However, the correlation of estimates from the Kim and Hogue (2012) approach with in situ soil moisture measurements was at lower level than products from the physical based model of Merlin et al. (2008b, and 2009).

By combining LST retrieval from passive microwave brightness temperature algorithm (McFarland et al., 1990) with an empirical relationship (Choudhury et al., 1987; Meesters et al., 2005; Mao et al., 2012) between the Microwave Polarization Difference Index (MDPI, Pampaloni and Paloscia, 1985) and NDVI, Song et al. (2014) developed a downscaling method which involved brightness temperature downscaling prior to soil moisture retrieval. This model was applied to the AMSR-E Ku-band observations available at 25 km to derive soil moisture maps at 1 km over the Maque monitoring network in China. Retrievals from this downscaling technique had a similar temporal trend to the in situ measurements with RMSE less than 0.12 $m^3 m^{-3}$. This technique was suggested to have better performance over bare and sparsely vegetated soil surfaces where the soil has dry or moderately wet condition.

Hemakumara et al. (2004) and Peng et al. (2016) found that the Vegetation Temperature Condition Index (VTCI; Wan et al., 2004) had a positive correlation with soil moisture, and so developed a VTCI-based downscaling algorithm similar to Kim and Hogue (2012). Downscaled soil moisture from the VTCI-based algorithm showed spatially consistent agreement with in situ measurements and land cover, while maintaining the accuracy of coarse soil moisture products. To increase the operational efficiency of this approach, Peng et al. (2015) examined how the VTCI-based algorithm performed when the index is retrieved from a geostationary optical sensor such as the MSG SEVIRI. The capability of geostationary sensors to capture optical acquisitions at shorter time intervals increases the chance of providing more cloud-free observations, thus leading to a greater continuity of downscaled soil moisture. However, it comes with a sacrifice on spatial resolution because the current geostationary optical observations are only available at the scale of 3 to 5 km. A new VI-based downscaling technique was recently developed by Kim et al. (2017), which established a linear relationship between NDVI and temporally averaged coarse passive microwave derived soil moisture data. For developing this downscaling model, Kim et al. (2017) used the ESA CCI merged active-passive soil moisture data available at 25 km together with aggregated 1 km MODIS NDVI 16-day composite to 25 km. Validation results showed that NDVI can replace the required LST information for disaggregation when the LST product is not available or comes with a poor-quality due to cloud coverage. Therefore, use of the NDVI composite allows to downscale soil moisture without the cost of losing the temporal variability of coarse soil moisture due to lack of NDVI information under cloudy skies.

Wang et al. (2016) swapped the SWI downscaling parameter in the Kim and Hogue (2012) model for Temperature Vegetation Drought Index (TVDI, Sandholt et al., 2002) to downscale long time series of passive microwave observations of soil moisture produced by Dorigo et al. (2012). The TVDI is a dryness index which was derived from MODIS LST and NDVI products (Patel et al., 2009). Compared with retrievals from the triangle based downscaling model by Carlson et al. (1994), the physical model by Merlin et al. (2009, 2010), and the Kim and Hogue (2012) model, TVDI-based downscaling retrievals showed superiority in terms of both accuracy and consistency of temporal variability with field measurements.

Another soil moisture disaggregation method is based on the thermal inertia principle, which correlated changes of soil temperature to changes of soil moisture as well as heat capacity (Mallick et al., 2009). This technique produced absolute volumetric soil moisture at 1 km resolution by converting Soil Wetness Index (SWI) to soil moisture using prior knowledge on total water capacity and minimum soil moisture content based on soil type. Compared with a dry soil, water has a greater heat capacity and thus a greater resistance to temperature change. The presence of higher moisture content in the soil, therefore, leads to lower thermal conductivity, with wet soil having a lower day-night temperature difference than for dry soil. However, it is easier to apply this linear relationship between soil moisture and diurnal change of surface temperature to bare soil conditions (Maltese et al., 2013). When the vegetation layer masks the soil surface, canopies interfere with fluctuations of soil moisture through water uptake.

Thermal inertia is also the basic concept behind the physically based optical-passive combination technique developed by Fang et al. (2013). Relating a time series of daily averaged soil moisture estimates to diurnal changes of soil temperature, derived from NLDAS land surface modelling, Fang et al. (2013) calibrated a model for soil moisture downscaling. Calibration lines were fitted on a monthly basis to reduce the impact of varied vegetation biomass on retrievals. Increments of 0.3 in NDVI values were used for further modulation of the surface temperature and soil moisture relationship. Using this model, AMSR-E based soil moisture retrievals at 1 km were derived and corrected by applying the differences between the original coarse AMSR-E soil moisture products and high resolution retrievals within the AMSR-E grid scale. Fang and Lakshmi (2014b) adjusted the temperature difference between passive microwave and optical sensors (SMOS and MODIS, respectively), caused by different overpass time, to achieve better performance of this algorithm. For this purpose, a polynomial regression was fitted to diurnal changes of hourly NLDAS surface temperature and their corresponding time. The model was used to estimate surface temperature at MODIS and SMOS overpass time at NLDAS spatial scale to calculate temperature difference between them. MODIS LST was then adjusted by adding this temperature difference to MODIS LST pixels within each NLDAS pixel.

2.3. Soil surface attributes-based downscaling techniques

The soil moisture state is determined by precipitation, but it also reflects space-time scaling behaviour in response to soil surface attributes and structure such as topography and soil properties (e.g. soil texture, and vegetation cover) (Kim and Barros, 2002b). Consequently, such information has been used in several disaggregation schemes (e.g. Kim and Barros, 2002a; Pellenq et al., 2003) to determine the spatial distribution of soil moisture. Topography provides information about soil water dynamics controlling soil moisture distribution, while soil properties provide information about soil water storage capacity and possible rates of change. However, the limited access to data on these properties at global scale imposes a limitation on the development of these downscaling techniques for global application.

Findings by Kim and Barros (2002b) supported the idea that the fractal interpolation method proposed by Kim and Barros (2002a), which used topography, soil texture and vegetation cover, could be an effective downscaling method. An Empirical Orthogonal Function (EOF) analysis to assess the impact of ancillary data sets on downscaling results showed a close association of soil moisture variability with soil hydraulic conductivity. However, topography and vegetation cover were dominant in downscaling results during wet periods and persistence of dry-down, respectively. Through the coupling of a radiative transfer model to a hydrological model, Pellenq et al. (2003) developed a downscaling methodology that captured disaggregated soil moisture patterns as a function of topographic index and soil depth. Using the infiltration and evaporation concept, the soil moisture profile was simulated by a radiative transfer model and subsequently coupled with a hydrological model to explain how soil moisture behaviour in space is affected by the topography and soil depth. The estimation of soil moisture patterns based on this approach was in general satisfactory, but it revealed a weak point-scale correlation between simulations and observations.

Wilson et al. (2005) implicitly developed a topographic attribute-based downscaling technique for soil moisture estimation at 10 to 40 m from a spatially averaged ground based soil moisture. Using historic high resolution soil moisture measurement data, Wilson et al. (2005) first developed an empirical relationship between an ensemble of soil moisture, topographic attributes (such as elevation, specific contributing area, slope, wetness index, potential solar radiation index, lowness index, and a multiresolution valley bottom flatness index), and the residuals patterns. Second, the topographic attributes and residuals were weighted based on the averaged soil moisture to map high resolution soil moisture for each day. However, such relationships were site specific.

Similarly, Perry and Niemann (2007) used the EOF analysis to decompose the priori high resolution soil moisture maps into spatial patterns of EOF covariation, time series of expansion coefficients (ECs) and the spatial-average soil moisture. Due to the existence of a strong relationship between ECs and spatial-average soil moisture, ECs were estimated from the spatial average soil moisture. A combination of spatial-average soil moisture, ECs, and time-invariant EOFs was used to downscale soil moisture. Busch et al. (2012) further developed the Perry and Niemann (2007) EOF-based downscaling technique such that it did not require priori information about the high resolution soil moisture. Busch et al. (2012) deployed high resolution topographic attributes from a DEM as the only source of information to estimate the EOF because findings by Perry and Niemann (2008) showed that EOFs were strongly related to topographic attributes. Such a relationship was constructed and applied to catchments, revealing that the relationships were site specific.

An Equilibrium Moisture from Topography (EMT; Coleman and Niemann, 2013) model, which is based on a conceptual water balance of the hydrologically active soil layer, is another downscaling technique using topographic indices for spatial resolution enhancement of soil moisture retrieval. This model performance outweighed the EOF method and required only a few soil moisture observations for calibration (Werbylo and Niemann, 2014). Vegetation and soil parameters were included in the EMT model for downscaling temporal soil moisture patterns over the Tarrawarra catchment; however, the fine resolution variations of these properties were not taken into account. Ranney et al. (2015) improved the performance of the EMT downscaling technique by including information about the spatial variation in vegetation and soil characteristics, and named it the Equilibrium Moisture from Topography, Vegetation, and Soil (EMT + VS). Vegetation data were found to be a valuable source of information for soil moisture downscaling. However, fine spatial scale soil data were able to further enhance the performance of EMT + VS downscaling technique. While this model showed good performance for a catchment with a topographic relief of less than 125 m, there is no evidence of its performance over regions with larger ranges of elevation. Large relief, which has impacts on spectral variation of precipitation (e.g. Cowley et al., 2017; Lloyd, 2005; Kyriakidis et al., 2001) and potential evapotranspiration (PET, e.g. Cowley et al., 2017; Shi et al., 2014a; Vanderlinden et al., 2008; Shevenell, 1999) will also control the spatial patterns of soil moisture (Cowley et al., 2017). Accordingly, Cowley et al. (2017) added temporal average PET and precipitation downscaling methods to the Ranney et al. (2015) ETM model, in order to take the spatial patterns of both variables into account for enhancing the coarse soil moisture downscaling. In the process of developing precipitation downscaling techniques the spatial heterogeneity of precipitation was assumed to be linearly related to topographic elevation (e.g. Castro et al., 2014) and topographic orientation (e.g. Franke et al., 2008). An interaction between precipitation, topographic elevation and topographic orientation was also assumed (Hanson, 1982). The PET downscaling method was based on a linear relationship between PET and air temperature (Blaney and Criddle, 1950) which decreases with altitude. Downscaling of PET, which has a predictable temporal pattern, showed more improvement in soil moisture estimates than precipitation downscaling did.

Values of fine scale parameters used in previous versions of the EMT + VS model were the same for all fine pixels lying within the coarse grid cell of soil moisture. Hoehn et al. (2017) used the shifting window to calculate fine scale parameters that vary over the coarse footprint of soil moisture to take development of the EMT + VS model a step further. The shifting window that provided the spatially varied fine scale parameters had the spatial scale of the coarse soil moisture and was centred on each fine grid cell to be calculated. The shifting window method estimated accurate fine resolution soil moisture for a situation where the generated errors of coarse soil moisture from a normal distribution had a standard deviation of 0.01 $m^3 m^{-3}$ or larger. Otherwise, the accuracy of soil moisture estimates from the original EMT + VS model – based on a fixed window method that applied the same value for all the fine pixels lying within the coarse grid – was higher than that of soil moisture estimates from the shifting window procedure. Unlike the fixed window procedure, the shifting window could not maintain the value of coarse soil moisture in its original state.

Using the temporally dynamic Topography-based Wetness Index (TWI), Temimi et al. (2010) developed a new topography-based soil wetness downscaling solution. This study included, for the first time, a vegetation index at VIS wavelength (the MODIS Leaf Area Index product) in the TWI retrieval model, to capture its variation in time. This technique downscaled the soil wetness index derived from the AMSR-E 37-GHz observations having the greatest sensitivity to soil moisture changes (Temimi et al., 2007) to help improve estimation of the soil moisture spatial distribution. Temimi et al. (2010) used TWI as a wetness potential index to spatially disaggregate the soil wetness index and demonstrated that dynamic TWI is an effective index to increase the soil wetness correlation to precipitation occurrence by 0.3, on average.

In studies by Ines et al. (2013) and Shin and Mohanty (2013), subpixel variation of remotely sensed soil moisture was estimated using the heterogeneity of soil texture and vegetation cover. The algorithm presented by Shin and Mohanty (2013) was inspired by the combined simulation-optimization approach of Ines et al. (2013), which downscaled remotely sensed soil moisture products using effective soil hydraulic properties (e.g. saturated soil moisture, saturated hydraulic conductivity, tortuosity in the soil) at subpixel scale, and fraction of soil/vegetation. The Shin and Mohanty (2013) inversion model produced soil moisture with satisfactory quality under various hydrologic and climate conditions using a genetic algorithm, which minimized the difference between observed and simulated soil moisture and evapotranspiration. For example, correlation coefficients of subpixel soil moisture to in situ measurements and mean bias error were reported to vary between 0.343 and 0.845, and -0.165 to $-0.122\,m^3\,m^{-3}$ for a silty loam soil covered by winter wheat and short native grass, respectively. While Ines et al. (2013) used soil characteristics and soil-vegetation fraction without assigning their location within a pixel, Shin and Mohanty (2013) specified the location of soil characteristics and vegetation cover. Shin and Mohanty (2013) also scaled evapotranspiration maps to infer soil moisture distribution, given that a strong correlation exists between evapotranspiration and soil moisture. While retrievals from this approach matched well with the in situ truth soil moisture content, qualified input data on the environmental factors (e.g. weather forcing, soil texture, and vegetation) were required under appropriate weather conditions to achieve such a performance.

2.4. Model/Data-based downscaling techniques

The downscaling of coarse resolution soil moisture observations has not been limited to the use of remote sensing data and/or soil surface attributes. Model predictions have also been used in model/data-based disaggregation schemes to spatially enhance soil moisture observations. These techniques, namely data assimilation- and machine learning-based, have no limitations related to the need for concurrent satellite overpasses or lost data due to cloud coverage. Descriptions of these techniques are briefly provided in the data assimilation- and machine learning-based sections below.

2.4.1. Data assimilation-based downscaling techniques

Data assimilation has been used to improve profile soil moisture estimates (e.g. Walker et al., 2001; De Lannoy and Reichle, 2016b) from surface soil moisture observations. Moreover, the physically based hydrological models at the heart of data assimilation have been used to predict the spatial distribution of soil moisture at high resolution (Reichle et al., 2001). A four-dimensional (spatial update using multi-temporal observations) data assimilation, which can combine noisy high resolution model predictions with accurate low resolution observations, was first introduced by Reichle et al. (2001) as a quasi downscaling technique to overcome limitations in deriving fine-scaled information on soil moisture from passive microwave observations. Downscaling techniques based on the data assimilation concept are distinguished from other approaches by accounting for both model and satellite measurement uncertainties and their independence to either sources of information. Moreover, the philosophy behind this method is to use spatially coarse soil moisture observations to constrain a high resolution dynamic model. The RMSE of downscaled soil moisture products from the assimilation-based downscaling techniques is reported to be $\sim 0.06\,m^3\,m^{-3}$ on average (see Table 2), which does not meet the accuracy requirement of soil moisture missions.

Draper et al. (2009) focused on AMSR-E C-band soil moisture assimilation into the Interactions between Surface, Biosphere, and Atmosphere (ISBA) model, which was the land surface scheme in Météo-France's Aire Limitée Adaptation Dynamique développement InterNational (ALADIN) Numerical Weather Prediction (NWP) model. This model has an irregular spatial resolution, but its estimates were available at 9.5 km over most of European regions where this study was conducted. This two-dimensional (spatial update for a single soil layer) Simplified Ensemble Kalman Filter (SEKF) developed by Mahfouf et al. (2009) and Balsamo et al. (2004), yielded modelled high resolution surface soil moisture at $\sim$9 km and with RMSE values larger than $0.09\,m^3\,m^{-3}$.

Sahoo et al. (2013) disaggregated the 25 km gridded AMSR-E soil moisture products through assimilation into the 1 km resolution NOAH land surface model using a three-dimensional ensemble Kalman filter. Increasing the spatial correlation from 0.7 on average to 0.77, the approach resulted in well matched surface soil moisture retrievals to the in situ data, including also lower RMSE values. Similar to the Ensemble Bias corrected Kalman Filter-2 (EnBKF-2) in De Lannoy et al. (2007), coarse satellite observations were rescaled to the model climatology prior to the assimilation. The RMSE of downscaled soil moisture without bias correction prior to data assimilation was reported to be in the range of 0.08 to $0.17\,m^3\,m^{-3}$, while with the bias correction was between 0.01 and $0.09\,m^3\,m^{-3}$.

As an extension to data assimilation systems that apply bias correction as a common practice, Kornelsen et al. (2015) developed a bias correction technique for soil moisture downscaling. In developing this downscaling procedure, precipitation and evapotranspiration were acknowledged as a derivative of soil moisture changes. The assumption of uniform precipitation over a radiometer scale was also made without making the distribution of soil moisture uniform in that scale. Having verified the temporal stability of brightness temperature and soil moisture, a simple mean-variance matching approach – a bias correction procedure – was applied to the simulated soil moisture over the SGP97's experimental watersheds. The analysis revealed the dependency of successful application of the bias correction technique to availability of priori information about the land surface conditions.

SMOS soil moisture products were also assimilated into the Variable Infiltration Capacity (VIC, Liang et al., 1994, 1996, 1999) by Lievens et al. (2015) to improve the accuracy and spatial resolution of SMOS soil moisture estimates from 25 to 12.5 km. This three-dimensional Ensemble Bias corrected Kalman Filter resulted in reduction of the RMSE of the simulated soil moisture from $0.058\,m^3\,m^{-3}$ to $0.046\,m^3\,m^{-3}$ and increase of the correlation from 0.56 to 0.71.

Being aware that assimilation can improve the surface soil moisture estimates at sub-seasonal time frame, Draper and Reichle (2015) assimilated a long record of AMSR-E X-band soil moisture at 25 km into the NASA's Catchment Land Surface Model (Koster et al., 2000), which was run on the 9 km EASE grid for North America. A one-dimensional bias-blind ensemble Kalman filter was used in this assimilation procedure by applying the coarse scale observations onto the higher resolution underlying model grid. Results from this study showed that for four test sites, assimilating a long record of soil moisture not only improved the ability of the model to represent long-term events such as droughts, but also increased the spatial skill of the model.

Since 2015, SMAP has provided a Level 4 soil moisture product, which has surface and root-zone soil moisture values at 9 km. The Goddard Earth Observing System version 5 (GEOS-5) Land Data Assimilation System (LDAS, Reichle et al., 2014; De Lannoy and Reichle, 2016a, 2016b), which is a three-dimensional EnKF based assimilation technique, assimilates the SMAP 36 km brightness temperature (from L1C_TB; Chan et al., 2016) into the NASA GEOS-5 Catchment Land Surface Model (Koster et al., 2000) for soil moisture estimation. The overall unbiased RMSE (ubRMSE) of the SMAP L4 surface soil moisture was reported by Reichle et al. (2017) to be $0.037\,m^3\,m^{-3}$, which meets the SMAP mission accuracy requirements. Results from this study are not included in the summary section, because they are not consistent with the other studies which reported regular RMSE values. Using this technique, Lievens et al. (2017) assimilated Sentinel-1 (Geudtner and Torres, 2012; Geudtner, 2012; Torres et al., 2012) C-band backscatter simultaneously with SMAP 36 km L-band brightness temperature to enhance the accuracy of soil moisture estimates. The complementary assimilation of radar backscatter and radiometer brightness temperature improved the performance, resulting in better surface soil moisture estimation than when only radiometer observations were assimilated.

2.4.2. Machine learning-based downscaling techniques

The machine learning approach seeks to learn the relationship between the soil moisture and available information on surface parameters without requiring continuous data. This makes it a useful tool for integrating different sources of information about soil moisture (Notarnicola et al., 2008). Consequently, the way that artificial intelligence deals with noisy data from dynamic and non-linear systems (Remesan et al., 2009) makes it a potential technique to improve the scale of soil moisture (Chai et al., 2009). Through a comprehensive analysis, Srivastava et al. (2013) demonstrated the feasibility of using the machine learning technique as a downscaling tool. The aim of this study was to derive a high spatial resolution soil moisture from SMOS using MODIS land surface temperature in a more functional way than optical-based downscaling, which its application is hampered by the sensitivity of optical observations to clouds. They evaluated the performance of a variety of artificial intelligence techniques, including Artificial Neural Network (ANN), Support Vector Machine (SVM), and Relevance Vector Machine (RVM). Among these techniques, the ANN showed considerable potential for deriving accurate soil moisture at higher resolution, especially when applied to data sets divided based on growing and non-growing seasons.

Earlier, Chai et al. (2011) had also used the ANN model to downscale air-borne passive microwave observations from the National Airborne Field Experiment held in Australia in 2005 (NAFE'05). Basing their ANN model on the linear downscaling algorithm (Merlin et al., 2008b), they acquired soil moisture retrievals with a root mean square error of 0.018 to 0.035 $m^3 m^{-3}$. This accuracy, together with the fact that the approach does not rely on a large number of input data, was reported by Chai et al. (2011) to be the main advantages of the ANN model. Chai and Goh (2013) continued to explore the ANN performance for soil moisture disaggregation within an ensemble scheme. The ensemble scheme was recommended to reduce estimation errors through the combination of results from multiple neural network models. This finding concurred with the Hansen and Salamon (1990) suggestion that optimization of neural network models is possible by ensemble scheme.

Based on a machine learning approach called the Self-Regularize Regressive Models (SRRMs), Chakrabarti et al. (2016) has delivered high resolution soil moisture maps at 1 km resolution with an RMSE of less than 0.02 $m^3 m^{-3}$. Utilizing a regularized clustering and kernel regression, the SRRM technique was capable of deriving the desired variables for all pixels covering the study area. This technique was reported to be efficient in terms of computational time, number of required samples for training, and accuracy when compared to the earlier machine learning technique developed by Chakrabarti et al. (2015). It used a Bayesian transformation process which related the high resolution auxiliary information to coarse soil moisture through a probabilistic relationship on the basis of the Principle of Relevant Information (PRI). Both SRRM and PRI techniques were developed and tested with the use of multiscale synthetic data from a coupled Land Surface Process-Decision Support System for Agrotechnology Transfer (LSP-DSSAT) model.

Park et al. (2015) enhanced the spatial resolution of AMSR2 soil moisture products, retrieved using the VUA-NASA algorithm (Owe and Van De Griend, 2001; Owe et al., 2008), from 25 km to 1 km using MODIS optical products in two different machine learning techniques: i) random forest and ii) ordinary least squares. Both approaches associated evapotranspiration and multiplication of LST and NDVI (LST × NDVI) in their process for soil moisture estimation. The random forest approach, which had flexibility in randomization and adopted an ensemble approach, outperformed this technique over the other machine learning approach. Similar to this study, Im et al. (2016) investigated the spatial downscaling of AMSR-E soil moisture data from 25 km to 1 km using MODIS 1 km products, including land surface temperature, surface albedo, NDVI, EVI, Leaf Area Index, and evapotranspiration. The intention of this study was to evaluate the performance of three different machine learning-based downscaling approaches including random forest, boosted regression trees, and Cubist approaches over two regions (South Korea and Australia). Among these techniques, the random forest showed superiority to the other techniques, yielding a higher correlation coefficient (0.71 and 0.84 for South Korea and Australia, respectively) of 1 km soil moisture with in situ measurements than that of the original AMSR-E soil moisture products.

The effective simulation of the nonlinear relationship between soil moisture and LST/VI by Back-Propagation Neural Network (BPNN) motivated Jiang et al. (2017) to use it as a tool to improve the scale of coarse passive microwave soil moisture products. Assuming that the relationship between soil moisture and LST/VIs was scale-invariant, the BPNN was trained by taking different combinations of coarsely aggregated MODIS LST and VIs, including NDVI, EVI, and NDWI as the input, and the coarse soil moisture retrievals from AMSR-E, AMSR2, and SMOS as the output. The best trained BPNN model was then applied to the inputs at the MODIS scale to estimate fine scaled soil moisture. Optimal downscaled products, which showed significant correlation larger than 0.6 with in situ soil moisture data from the central Tibetan Plateau Soil Moisture/Temperature Monitoring Network (SMTMN), were achieved when the BPNN was trained using the combination of LST and EVI.

3. Discussion

This paper seeks to provide a critical review of the available soil moisture downscaling methods, including an evaluation of the strengths and weaknesses of their strategies as well as existing challenges in soil moisture downscaling. As presented, several downscaling methods exist for combining accurate passive microwave observations with high spatial resolution information on soil surface features which include vegetation coverage, soil surface attributes, soil temperature, etc. to derive high spatial resolution soil moisture. Some of the techniques are able to retrieve soil moisture estimates at an accuracy of 0.04 $m^3 m^{-3}$, which is the soil moisture accuracy requirement – in the top 5 cm of the soil for vegetation water content ≤5 $kg.m^{-2}$ – suggested by the SMAP science team for a wide range of applications (Entekhabi et al., 2008a).

Existing downscaling approaches are reported to have a range of accuracy under differing weather and climate conditions. A rigorous inter-comparison of different downscaling methods would be beneficial to clarify advantages and disadvantages of each downscaling method. However, until now there has been no study to thoroughly compare the various downscaling techniques for a specific set of conditions. Fig. 8

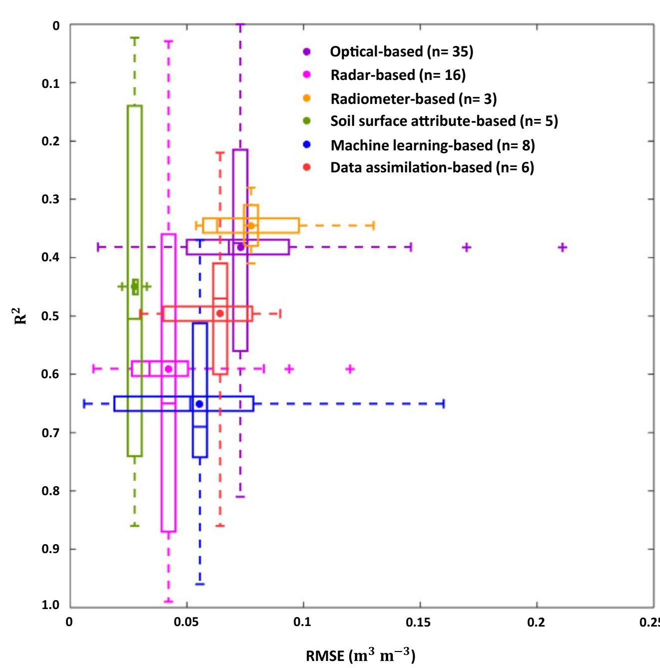

Fig. 8. Summary of accuracy statistics from different downscaling techniques presented as boxplot that contains the interquartile ranges, the sample median (bar), and outliers associated with the mean (dot). * n indicates the number of validation studies that reported the accuracy of retrieval in terms of R or R^2 and RMSE for the particular downscaling approach, and were thus used to make this figure.

presents a summary of Table 2 in order to give a concise overview of the performance of each downscaling technique in terms of reported accuracy. The performance variation of individual approaches may lie in the disparate characteristics of the data and field sites utilized for the soil moisture disaggregation evaluation. However, study domains and seasons are not distinguished in this study, as downscaling techniques should be applicable for a wide range of surface and climate conditions if they are to be applied operationally. Moreover, there is a wide variation between approaches, with each having its own advantages and limitations, and conditions where it works best. For example, the radar-radiometer microwave combination could be the most promising and/or robust technique to retrieve soil moisture values under homogeneous roughness and low vegetation density conditions as it is unaffected by meteorology, but the lack of concurrent radar and radiometer observations at the same frequency and platform currently limits its application.

The radar-based downscaling techniques have been shown to outperform the optical-based techniques (see Fig. 8), in terms of RMSE ($0.04\,m^3\,m^{-3}$ vs. $0.072\,m^3\,m^{-3}$ on average for radar- and optical-based downscaling techniques, respectively), due to the greater sensitivity of microwave observations to soil moisture dynamics under all-weather conditions. However, the trade-off between wavelength and temporal coverage of currently available radar imagery, and the impact of clouds on optical observations require consideration when evaluating their effectiveness in estimating accurate soil moisture from coarse passive microwave observations. The use of geostationary based optical sensors could alleviate some of the meteorological limitations of typical polar orbiting sensors due to high frequency optical acquisitions (0–30 minutes), increasing the chance of obtaining cloud-free observations (Zhang et al., 2014; Piles et al., 2016). However, it comes at the cost of estimating soil moisture at the lower spatial scale of the geostationary based optical sensors (being on order of 3 to 5 km) than typical polar orbiting sensors (being on order of 1 km resolution).

Radiometric emissions at higher microwave frequencies (i.e. Ka-band) can penetrate through non-raining clouds similar to radar observations. Their advantage over the backscatter method is the availability at regular repeat coverage and reduced impact of surface roughness. These characteristics make them a potentially more reliable source of information on surface spatial heterogeneity for mapping variability of soil moisture compared with optical and radar observations. However, the radiometer-based downscaling technique has so far been found to result in less accurate soil moisture products than the radar-based technique. While the radiometer-based technique has shown similar performance to the optical-based downscaling techniques (Fig. 8), optical observations have the advantage of producing disaggregated soil moisture at finer resolution (1 km) than currently available Ka-band passive microwave observations (10 km) when there is no cloud coverage. The superiority of radiometer-based to optical-based downscaling lies in the applicability of the radiometer-based technique under all weather and climate conditions, unlike the optical-based techniques that are more applicable to areas where there is no such limitation (Garcia et al., 2014). Using a bigger antenna for scanning brightness temperature at Ka-band, or developing methods to resample the Ka-band observations to resolutions finer than 10 km while preserving the accuracy of medium scaled Ka-band brightness temperature observations, could be potential solutions to overcome this drawback and make the radiometer-based techniques operational.

Providing that spatially detailed information on soil surface attributes and a universal relationship was available at the global scale, the soil surface attributes-based downscaling technique could be a suitable alternative to the radar-based technique for disaggregation of soil moisture. This technique owes its performance to the information about soil water dynamics and soil water storage capacity, which are represented in the soil moisture downscaling process through the use of topography and soil properties, respectively. As shown in Fig. 8, soil surface attributes-based downscaling technique is a more accurate technique in terms of RMSE than either the radiometer- or optical-based techniques, with an averaged accuracy of $0.028\,m^3\,m^{-3}$.

Use of high resolution land surface models together with data assimilation and/or machine learning could provide a more robust downscaling approach, as there are no limitations related to the need for concurrent satellite overpasses, or lost data due to cloud coverage. Moreover, the advantages of a data assimilation-based downscaling technique may outweigh the machine learning-based technique because dynamically varying uncertainties of both the model predicted and satellite observed soil moisture, and the temporal interpolation of coarse soil moisture retrievals, are implicitly included. Data assimilation has the additional advantage of providing root zone soil moisture content. However, based on the available literature the machine learning technique (with RMSE of $0.056\,m^3\,m^{-3}$ on average) seems not only to be superior to the data assimilation-based technique but also superior to the other currently available downscaling techniques, apart from radar-based techniques in terms of RMSE. The performance of the machine learning technique also appears to be superior to other downscaling techniques in terms of correlation between the downscaled and in situ soil moisture. However, further testing and research are required to increase the computational efficiency of this technique and to overcome its global training requirements before it could be considered for use operationally.

In addition to the further development requirements of the above-mentioned, there are several unresolved challenges facing soil moisture downscaling that need to be addressed. In order to meet the spatial resolution requirement of agricultural production and efficient management of water resources, there is a need to improve the spatial scale of downscaled products to higher than 1 km (Fig. 1). This highlights the need for high resolution ancillary data which usually dictates the spatial scale of downscaled products. These ancillary data should not only be at a high spatial resolution, but should also be precise in order to assure an accurate disaggregation of soil moisture.

Reduction of uncertainty in the coarse passive soil moisture retrieval process is another key factor for downscaled soil moisture improvement. The radiative transfer models used for soil moisture retrieval from passive microwave remote sensing has reached a mature level (Das et al., 2011). However, the variation of ancillary parameters (e.g. vegetation properties, surface roughness and scattering albedo) in space and time make the model parameterization and retrievals uncertain. Evaluation of the radiative transfer model across a wide range of climate and land surface conditions may assist in quantifying and clarifying such uncertainties.

For satisfactory application of high resolution soil moisture in agriculture and water resources management, continuous time series of soil moisture are required at temporal frequencies better than 3 days. The development of downscaling techniques that are applicable to multi-satellite coarse soil moisture data could potentially be a pragmatic solution to satisfying this demand. In this case, merged multi satellite soil moisture products could be developed, and be downscaled across all the low resolution passive microwave satellites using the best downscaling methodology. A harmonized ensemble of disaggregated soil moisture products from different retrieval algorithms might provide another solution, with the added value of providing more frequent soil moisture than the individual downscaled products alone. An ensemble of downscaled soil moisture products might also result in more accurate soil moisture products, recognising strengths of alternative products under varying climate and land surface conditions.

4. Summary

This paper has provided a comprehensive discussion of alternative soil moisture downscaling techniques. While the reasons and motivation for downscaling soil moisture and the concept behind each downscaling technique have been extensively described, this study has also provided an overview of the resources required for each disaggregation technique and the expected accuracy of the approach.

This paper argues that downscaling techniques can deliver substantially greater spatial detail about soil moisture spatial variability, as compared to the original remotely sensed passive microwave data, to meet the requirements of a growing number of applications. Moreover, the combination of remotely sensed land surface features with passive microwave observations has been successful in deriving fine-scaled soil moisture with reasonable accuracy. A considerable contribution to combined techniques was made by the optical acquisitions that are available at high resolution on a daily basis, but cloudy skies and seasonality significantly affect the functionality of optical-based downscaling methods. The use of geostationary based optical sensors which process a much higher (every ~10–15 minutes) imaging capability than their polar orbiting counterparts could help alleviate the issues, thus increasing the chance of providing cloud-free observations. However, combined L-band radar and radiometer (radar-based) downscaling approaches have demonstrated the best success in deriving multi-sensor soil moisture maps, but at a resolution of approximately 10 km. Aggregation of fine resolution SAR radar observations to medium resolution, to decrease the impact of speckle noise, provides an opportunity for downscaled soil moisture to be derived at medium resolution with reasonable accuracy, but is limited by the time interval of repeat overpasses and the current wavelengths available.

Utilizing the soil surface attributes and structure, including topography and soil texture, is also beneficial to the space-time scaling of soil moisture. Topography and soil texture impacts the soil water dynamic and thus distribution of soil moisture. Both soil water dynamics and storage capacity exert effective impact on soil moisture variation. However, the limited access to such data imposes a limit on the application and development of these downscaling techniques for global soil moisture monitoring.

Alternative downscaling approaches that use high resolution model predictions together with data assimilation of coarse scale observations – and/or machine learning-based techniques – provide an opportunity to overcome issues related to the lack of concurrent overpasses by required satellites or lost data due to cloud coverage. However, there is considerably more work required to increase the accuracy of high resolution soil moisture prediction models, the computational efficiency of these innovative techniques, and the global training required for the machine learning technique.

Soil moisture downscaling to spatial resolutions higher than 1 km should also be considered an issue for advancing the practical use of soil moisture in agriculture and water resources management. These must also be provided at the time scale of 1 to 3 days in order to provide information about the temporal dynamics of soil moisture. The development of applicable downscaling techniques under all weather and climate conditions and across all current passive microwave observations will hopefully fill this gap. Prior to reaching this milestone, the merger of multi satellite soil moisture products should reach a level of maturity. Thus, harmonized downscaled soil moisture products from different downscaling techniques could be able to produce a consistent time series of high resolution soil moisture.

Acknowledgements

This study has been conducted within the framework of an ARC Discovery Project (MoistureMonitor, DP140100572). The authors would like to acknowledge the Monash University contributions towards a postgraduate scholarship for Sabah Sabaghy to pursue her PhD.

References

Akbar, R., Moghaddam, M., 2015. A combined active-passive soil moisture estimation algorithm with adaptive regularization in support of SMAP. IEEE Trans. Geosci. Remote Sens. 53, 3312–3324.

Anderson, M.C., Norman, J.M., Diak, G.R., Kustas, W.P., Mecikalski, J.R., 1997. A two-source time-integrated model for estimating surface fluxes using thermal infrared remote sensing. Remote Sens. Environ. 60, 195–216.

Anderson, M.C., Norman, J.M., Mecikalski, J.R., Otkin, J.A., Kustas, W.P., 2007. A climatological study of evapotranspiration and moisture stress across the continental United States based on thermal remote sensing: 1. Model formulation. J. Geophys. Res. Atmos. 112.

Balsamo, G., Bouyssel, F., Noilhan, J., 2004. A simplified bi-dimensional variational analysis of soil moisture from screen-level observations in a mesoscale numerical weather-prediction model. Q. J. R. Meteorol. Soc. 130, 895–915.

Bindlish, R., Barros, A.P., 2002. Subpixel variability of remotely sensed soil moisture: an inter-comparison study of SAR and ESTAR. IEEE Trans. Geosci. Remote Sens. 40, 326–337.

Blaney, H.F., Criddle, W.D., 1950. Determining water requirements in irrigated areas from climatological and irrigation data, USDA SCS-TP-96. U.S. Dept. of Agric, Washington, D. C.

Busch, F.A., Niemann, J.D., Coleman, M., 2012. Evaluation of an empirical orthogonal function–based method to downscale soil moisture patterns based on topographical attributes. Hydrol. Process. 26, 2696–2709.

Calvet, J.-C., Wigneron, J.-P., Walker, J., Karbou, F., Chanzy, A., Albergel, C., 2011. Sensitivity of passive microwave observations to soil moisture and vegetation water content: L-band to W-band. IEEE Trans. Geosci. Remote Sens. 49, 1190–1199.

Camps, A., Vall-Llossera, M., Piles, M., Torres, F., Corbella, I., Duffo, N., 2008. Improving the Spatial Resolution of Synthetic Aperture Radiometer Imagery using Auxiliary Information: Application to the Smos Mission. In: IEEE International Geoscience and Remote Sensing Symposium (IGARSS), (III - 411-III – 414. 7–11 July).

Carlson, T.N., Gillies, R.R., Perry, E.M., 1994. A method to make use of thermal infrared temperature and NDVI measurements to infer surface soil water content and fractional vegetation cover. Remote Sens. Rev. 9, 161–173.

Castro, L.M., Gironás, J., Fernández, B., 2014. Spatial estimation of daily precipitation in regions with complex relief and scarce data using terrain orientation. J. Hydrol. 517, 481–492.

Chai, S.S., Goh, K.L., 2013. Neural Network Ensembles: Combining Multiple Models for Downscaling of Soil Moisture.

Chai, S.-S., Walker, J., Makarynskyy, O., Kuhn, M., Veenendaal, B., West, G., 2009. Use of soil moisture variability in artificial neural network retrieval of soil moisture. Remote Sens. 2, 166.

Chai, S., Walker, J.P., Veenendaal, B., West, G., 2011. An artificial neural network model for downscaling of passive microwave soil moisture. In: 6th IASME/WSEAS International Conference on Water Resources, Hydraulics & Hydrology (WHH'11) (Marc Rosen, Roy Perryman, Stephen Dodds and Francesco Muzi 23 February 2011 to 25 February 2011). WSEAS Press-World Scientific and Engineering Academy and Society, pp. 26–31.

Chakrabarti, S., Bongiovanni, T., Judge, J., Nagarajan, K., Principe, J.C., 2015. Downscaling satellite-based soil moisture in heterogeneous regions using high-resolution remote sensing products and information theory: a synthetic study. IEEE Trans. Geosci. Remote Sens. 53, 85–101.

Chakrabarti, S., Judge, J., Bongiovanni, T., Rangarajan, A., Ranka, S., 2016. Disaggregation of remotely sensed soil moisture in heterogeneous landscapes using holistic structure-based models. IEEE Trans. Geosci. Remote Sens. 54, 4629–4641.

Chan, S.K., Bindlish, R., Neill, P.E.O., Njoku, E., Jackson, T., Colliander, A., Chen, F., Burgin, M., Dunbar, S., Piepmeier, J., Yueh, S., Entekhabi, D., Cosh, M.H., Caldwell, T., Walker, J., Wu, X., Berg, A., Rowlandson, T., Pacheco, A., Mcnairn, H., Thibeault, M., Martínez-Fernández, J., -Z, Á.G., Seyfried, M., Bosch, D., Starks, P., Goodrich, D., Prueger, J., Palecki, M., Small, E.E., Zreda, M., Calvet, J.C., Crow, W.T., Kerr, Y., 2016. Assessment of the SMAP passive soil moisture product. IEEE Trans. Geosci. Remote Sens. 54, 4994–5007.

Chauhan, N.S., 1997. Soil moisture estimation under a vegetation cover: combined active passive microwave remote sensing approach. Int. J. Remote Sens. 18, 1079–1097.

Chauhan, N.S., Miller, S., Ardanuy, P., 2003. Spaceborne soil moisture estimation at high resolution: a microwave-optical/IR synergistic approach. Int. J. Remote Sens. 24, 4599–4622.

Chen, N., He, Y., Zhang, X., 2017. Nir-red spectra-based disaggregation of SMAP soil moisture to 250 m resolution based on smapex-4/5 in Southeastern Australia. Remote Sens. 9, 51.

Choi, M., Hur, Y., 2012. A microwave-optical/infrared disaggregation for improving spatial representation of soil moisture using AMSR-E and MODIS products. Remote Sens. Environ. 124, 259–269.

Choudhury, B.J., Tucker, C.J., Golus, R.E., Newcomb, W.W., 1987. Monitoring vegetation using Nimbus-7 scanning multichannel microwave radiometer's data. Int. J. Remote Sens. 8, 533–538.

Coleman, M.L., Niemann, J.D., 2013. Controls on topographic dependence and temporal instability in catchment-scale soil moisture patterns. Water Resour. Res. 49, 1625–1642.

Coppola, A., Basile, A., Menenti, M., Buonanno, M., Colin, J., De Mascellis, R., Esposito, M., Lazzaro, U., Magliulo, V., Manna, P., 2007. Spatial distribution and structure of remotely sensed surface water content estimated by a thermal inertia approach. IAHS Publ. 316, 3.

Cowley, G.S., Niemann, J.D., Green, T.R., Seyfried, M.S., Jones, A.S., Grazaitis, P.J., 2017. Impacts of precipitation and potential evapotranspiration patterns on downscaling soil moisture in regions with large topographic relief. Water Resour. Res. 53, 1553–1574.

Crow, W.T., Berg, A.A., Cosh, M.H., Loew, A., Mohanty, B.P., Panciera, R., Rosnay, P., Ryu, D., Walker, J.P., 2012. Upscaling sparse ground-based soil moisture observations for the validation of coarse-resolution satellite soil moisture products. Rev. Geophys. 50.

Dalal, R., Henry, R., 1986. Simultaneous determination of moisture, organic carbon, and

total nitrogen by near infrared reflectance spectrophotometry. Soil Sci. Soc. Am. J. 50, 120–123.
Das, N.N., Entekhabi, D., Njoku, E.G., 2011. An algorithm for merging SMAP radiometer and radar data for high-resolution soil-moisture retrieval. IEEE Trans. Geosci. Remote Sens. 49, 1504–1512.
Das, N.N., Entekhabi, D., Njoku, E.G., Shi, J.J.C., Johnson, J.T., Colliander, A., 2014. Tests of the SMAP combined radar and radiometer algorithm using airborne field campaign observations and simulated data. IEEE Trans. Geosci. Remote Sens. 52, 2018–2028.
De Jeu, R.A.M., Holmes, T.R.H., Parinussa, R.M., Owe, M., 2014. A spatially coherent global soil moisture product with improved temporal resolution. J. Hydrol. 516, 284–296.
De Lannoy, G.J.M., Reichle, R.H., 2016a. Assimilation of SMOS brightness temperatures or soil moisture retrievals into a land surface model. Hydrol. Earth Syst. Sci. 20, 4895–4911.
De Lannoy, G.J.M., Reichle, R.H., 2016b. Global assimilation of multiangle and multi-polarization SMOS brightness temperature observations into the GEOS-5 catchment land surface model for soil moisture estimation. J. Hydrometeorol. 17, 669–691.
De Lannoy, G.J., Reichle, R.H., Houser, P.R., Pauwels, V., Verhoest, N.E., 2007. Correcting for forecast bias in soil moisture assimilation with the ensemble Kalman filter. Water Resour. Res. 43.
Djamai, N., Magagi, R., Goita, K., Merlin, O., Kerr, Y., Walker, A., 2015. Disaggregation of SMOS soil moisture over the Canadian Prairies. Remote Sens. Environ. 170, 255–268.
Djamai, N., Magagi, R., Goïta, K., Merlin, O., Kerr, Y., Roy, A., 2016. A combination of DISPATCH downscaling algorithm with CLASS land surface scheme for soil moisture estimation at fine scale during cloudy days. Remote Sens. Environ. 184, 1–14.
Dobson, M.C., Ulaby, F.T., 1986. Active microwave soil moisture research. IEEE Trans. Geosci. Remote Sens. GE-24, 23–36.
Dorigo, W., De Jeu, R., Chung, D., Parinussa, R., Liu, Y., Wagner, W., Fernández-Prieto, D., 2012. Evaluating global trends (1988–2010) in harmonized multi-satellite surface soil moisture. Geophys. Res. Lett. 39, L18405.
Draper, C., Reichle, R., 2015. The impact of near-surface soil moisture assimilation at subseasonal, seasonal, and inter-annual timescales. Hydrol. Earth Syst. Sci. 19, 4831–4844.
Draper, C.S., Mahfouf, J.F., Walker, J.P., 2009. An EKF assimilation of AMSR-E soil moisture into the ISBA land surface scheme. J. Geophys. Res. Atmos. 114 (n/a-n/a).
Du, Y., Ulaby, F.T., Dobson, M.C., 2000. Sensitivity to soil moisture by active and passive microwave sensors. IEEE Trans. Geosci. Remote Sens. 38, 105–114.
Engman, E.T., Chauhan, N., 1995. Status of microwave soil moisture measurements with remote sensing. Remote Sens. Environ. 51, 189–198.
Entekhabi, D., 1995. Recent advances in land-atmosphere interaction research. Rev. Geophys. 33, 995–1003.
Entekhabi, D., Rodriguez-Iturbe, I., Castelli, F., 1996. Mutual interaction of soil moisture state and atmospheric processes. J. Hydrol. 184, 3–17.
Entekhabi, D., Asrar, G.R., Betts, A.K., Beven, K.J., Bras, R.L., Duffy, C.J., Dunne, T., Koster, R.D., Lettenmaier, D.P., Mclaughlin, D.B., Shuttleworth, W.J., Van Genuchten, M.T., Wei, M.-Y., Wood, E.F., 1999. An agenda for land surface hydrology research and a call for the second International hydrological decade. Bull. Am. Meteorol. Soc. 80, 2043–2058.
Entekhabi, D., Jackson, T.J., Njoku, E., O'neill, P., Entin, J., 2008a. Soil Moisture Active/Passive (SMAP) Mission Concept. 70850H-70850H-6.
Entekhabi, D., Njoku, E., O'neill, P., Spencer, M., Jackson, T., Entin, J., Im, E., Kellogg, K., 2008b. The soil moisture active/passive mission (SMAP). In: Geoscience and Remote Sensing Symposium, 2008. IGARSS 2008. IEEE International, pp. 7–11 (July).
Entekhabi, D., Njoku, E.G., O'neill, P.E., Kellogg, K.H., Crow, W.T., Edelstein, W.N., Entin, J.K., Goodman, S.D., Jackson, T.J., Johnson, J., Kimball, J., Piepmeier, J.R., Koster, R.D., Martin, N., Mcdonald, K.C., Moghaddam, M., Moran, S., Reichle, R., Shi, J.C., Spencer, M.W., Thurman, S.W., Leung, T., Van Zyl, J., 2010. The soil moisture active passive (SMAP) mission. Proc. IEEE 98, 704–716.
Fan, L., Xiao, Q., Wen, J., Liu, Q., Jin, R., You, D., Li, X., 2015. Mapping high-resolution soil moisture over heterogeneous cropland using multi-resource remote sensing and ground observations. Remote Sens. 7, 13273.
Fang, B., Lakshmi, V., 2014a. AMSR-E soil moisture disaggregation using MODIS and NLDAS data. In: Remote Sensing of the Terrestrial Water Cycle. John Wiley & Sons, Inc..
Fang, B., Lakshmi, V., 2014b. Soil moisture at watershed scale: remote sensing techniques. J. Hydrol. 516, 258–272.
Fang, B., Lakshmi, V., Bindlish, R., Jackson, T.J., Cosh, M., Basara, J., 2013. Passive microwave soil moisture downscaling using vegetation index and skin surface temperature. Vadose Zone J. 12.
Franke, J., Häntzschel, J., Goldberg, V., Bernhofer, C., 2008. Application of a trigonometric approach to the regionalization of precipitation for a complex small-scale terrain in a GIS environment. Meteorol. Appl. 15, 483–490.
Friedl, M.A., Davis, F.W., 1994. Sources of variation in radiometric surface temperature over a tallgrass prairie. Remote Sens. Environ. 48, 1–17.
Gao, B.-C., 1996. NDWI—A normalized difference water index for remote sensing of vegetation liquid water from space. Remote Sens. Environ. 58, 257–266.
Garcia, M., Fernández, N., Villagarcía, L., Domingo, F., Puigdefábregas, J., Sandholt, I., 2014. Accuracy of the temperature–vegetation dryness index using MODIS under water-limited vs. energy-limited evapotranspiration conditions. Remote Sens. Environ. 149, 100–117.
Geudtner, D., 2012. Sentinel-1 system overview and performance. In: Proc. SPIE 8528, Earth Observing Missions and Sensors: Development, Implementation, and Characterization II.
Geudtner, D., Torres, R., 2012. Sentinel-1 system overview and performance. In: Geoscience and Remote Sensing Symposium (IGARSS), 2012 IEEE International. IEEE, pp. 1719–1721.
Gevaert, A.I., Parinussa, R.M., Renzullo, L.J., Van Dijk, A.I.J.M., De Jeu, R.A.M., 2015. Spatio-temporal evaluation of resolution enhancement for passive microwave soil moisture and vegetation optical depth. Int. J. Appl. Earth Obs. Geoinf. 45 (Part B), 235–244.
Gillies, R.R., Carlson, T.N., 1995. Thermal remote sensing of surface soil water content with partial vegetation cover for incorporation into climate models. J. Appl. Meteorol. 34, 745–756.
Goward, S.N., Xue, Y., Czajkowski, K.P., 2002. Evaluating land surface moisture conditions from the remotely sensed temperature/vegetation index measurements: an exploration with the simplified simple biosphere model. Remote Sens. Environ. 79, 225–242.
Hain, C.R., Mecikalski, J.R., Anderson, M.C., 2009. Retrieval of an available water-based soil moisture proxy from thermal infrared remote sensing. Part I: methodology and validation. J. Hydrometeorol. 10, 665–683.
Hansen, L.K., Salamon, P., 1990. Neural network ensembles. IEEE Trans. Pattern Anal. Mach. Intell. 993–1001.
Hanson, C.L., 1982. Distribution and stochastic generation of annual and monthly precipitation on a mountainous watershed in Southwest Idaho. J. Am. Water Resour. Assoc. 18, 875–883.
Hemakumara, M., Kalma, J., Walker, J., Willgoose, G., 2004. Downscaling of low resolution passive microwave soil moisture observations. In: Proceedings of the 2nd International CAHMDA Workshop on: The Terrestrial Water Cycle: Modeling and Data Assimilation Across Catchment Scales, pp. 25–27.
Hirschi, M., Seneviratne, S.I., Alexandrov, V., Boberg, F., Boroneant, C., Christensen, O.B., Formayer, H., Orlowsky, B., Stepanek, P., 2011. Observational evidence for soil-moisture impact on hot extremes in southeastern Europe. Nat. Geosci. 4, 17–21.
Hoehn, D.C., Niemann, J.D., Green, T.R., Jones, A.S., Grazaitis, P.J., 2017. Downscaling soil moisture over regions that include multiple coarse-resolution grid cells. Remote Sens. Environ. 199, 187–200.
Huete, A., Jackson, R., Post, D., 1985. Spectral response of a plant canopy with different soil backgrounds. Remote Sens. Environ. 17, 37–53.
Im, J., Park, S., Rhee, J., Baik, J., Choi, M., 2016. Downscaling of AMSR-E soil moisture with MODIS products using machine learning approaches. Environ. Earth Sci. 75, 1120.
Ines, A.V.M., Mohanty, B.P., Shin, Y., 2013. An unmixing algorithm for remotely sensed soil moisture. Water Resour. Res. 49, 408–425.
Jackson, T.J., 1993. III. Measuring surface soil moisture using passive microwave remote sensing. Hydrol. Process. 7, 139–152.
Jana, R.B., 2010. Scaling Characteristics of Soil Hydraulic Parameters at Varying Spatial Resolutions. Texas A&M University.
Jiang, L., Islam, S., 2003. An intercomparison of regional latent heat flux estimation using remote sensing data. Int. J. Remote Sens. 24, 2221–2236.
Jiang, H., Shen, H., Li, H., Lei, F., Gan, W., Zhang, L., 2017. Evaluation of multiple downscaled microwave soil moisture products over the central Tibetan plateau. Remote Sens. 9, 402.
Jung, M., Reichstein, M., Ciais, P., Seneviratne, S.I., Sheffield, J., Goulden, M.L., Bonan, G., Cescatti, A., Chen, J., De Jeu, R., Dolman, A.J., Eugster, W., Gerten, D., Gianelle, D., Gobron, N., Heinke, J., Kimball, J., Law, B.E., Montagnani, L., Mu, Q., Mueller, B., Oleson, K., Papale, D., Richardson, A.D., Roupsard, O., Running, S., Tomelleri, E., Viovy, N., Weber, U., Williams, C., Wood, E., Zaehle, S., Zhang, K., 2010. Recent decline in the global land evapotranspiration trend due to limited moisture supply. Nature 467, 951–954.
Kaheil, Y.H., Gill, M.K., Mckee, M., Bastidas, L.A., Rosero, E., 2008. Downscaling and assimilation of surface soil moisture using ground truth measurements. IEEE Trans. Geosci. Remote Sens. 46, 1375–1384.
Kerr, Y.H., Waldteufel, P., Wigneron, J.P., Martinuzzi, J., Font, J., Berger, M., 2001. Soil moisture retrieval from space: the soil moisture and ocean salinity (SMOS) mission. IEEE Trans. Geosci. Remote Sens. 39, 1729–1735.
Kerr, Y.H., Waldteufel, P., Richaume, P., Wigneron, J.P., Ferrazzoli, P., Mahmoodi, A., Bitar, A.A., Cabot, F., Gruhier, C., Juglea, S.E., Leroux, D., Mialon, A., Delwart, S., 2012. The SMOS soil moisture retrieval algorithm. IEEE Trans. Geosci. Remote Sens. 50, 1384–1403.
Kim, G., Barros, A.P., 2002a. Downscaling of remotely sensed soil moisture with a modified fractal interpolation method using contraction mapping and ancillary data. Remote Sens. Environ. 83, 400–413.
Kim, G., Barros, A.P., 2002b. Space–time characterization of soil moisture from passive microwave remotely sensed imagery and ancillary data. Remote Sens. Environ. 81, 393–403.
Kim, J., Hogue, T.S., 2012. Improving spatial soil moisture representation through integration of AMSR-E and MODIS products. IEEE Trans. Geosci. Remote Sens. 50, 446–460.
Kim, S., Balakrishnan, K., Liu, Y., Johnson, F., Sharma, A., 2017. Spatial disaggregation of coarse soil moisture data by using high-resolution remotely sensed vegetation products. IEEE Geosci. Remote Sens. Lett. 14, 1604–1608.
Knipper, R., Hogue, S., Franz, K., SCOTT, R., 2017. Downscaling SMAP and SMOS soil moisture with moderate-resolution imaging spectroradiometer visible and infrared products over southern Arizona. J. Appl. Remote. Sens. 11 (2), 026021.
Kornelsen, K.C., Cosh, M.H., Coulibaly, P., 2015. Potential of bias correction for downscaling passive microwave and soil moisture data. J. Geophys. Res. Atmos. 120, 6460–6479.
Koster, R.D., Suarez, M.J., Ducharne, A., Stieglitz, M., Kumar, P., 2000. A catchment-based approach to modeling land surface processes in a general circulation model: 1. Model structure. J. Geophys. Res. Atmos. 105, 24809–24822.
Koster, R.D., Dirmeyer, P.A., Guo, Z., Bonan, G., Chan, E., Cox, P., Gordon, C.T., Kanae, S., Kowalczyk, E., Lawrence, D., Liu, P., Lu, C.-H., Malyshev, S., Mcavaney, B., Mitchell,

K., Mocko, D., Oki, T., Oleson, K., Pitman, A., Sud, Y.C., Taylor, C.M., Verseghy, D., Vasic, R., Xue, Y., Yamada, T., 2004. Regions of strong coupling between soil moisture and precipitation. Science 305, 1138–1140.
Kyriakidis, P.C., Kim, J., Miller, N.L., 2001. Geostatistical mapping of precipitation from rain gauge data using atmospheric and terrain characteristics. J. Appl. Meteorol. 40, 1855–1877.
Lakshmi, V., 2013. Remote sensing of soil moisture. ISRN Soil Sci. 2013, 33.
Lee, T.J., Pielke, R.A., 1992. Estimating the soil surface specific humidity. J. Appl. Meteorol. 31, 480–484.
Leone, A.P., Sommer, S., 2000. Multivariate analysis of laboratory spectra for the assessment of soil development and soil degradation in the southern Apennines (Italy). Remote Sens. Environ. 72, 346–359.
Liang, X., Lettenmaier, D.P., Wood, E.F., Burges, S.J., 1994. A simple hydrologically based model of land surface water and energy fluxes for general circulation models. J. Geophys. Res. Atmos. 99, 14415–14428.
Liang, X., Wood, E.F., Lettenmaier, D.P., 1996. Surface soil moisture parameterization of the VIC-2L model: evaluation and modification. Glob. Planet. Chang. 13, 195–206.
Liang, X., Wood, E.F., Lettenmaier, D.P., 1999. Modeling ground heat flux in land surface parameterization schemes. J. Geophys. Res. Atmos. 104, 9581–9600.
Lievens, H., Tomer, S.K., Al Bitar, A., De Lannoy, G.J.M., Drusch, M., Dumedah, G., Hendricks Franssen, H.J., Kerr, Y.H., Martens, B., Pan, M., Roundy, J.K., Vereecken, H., Walker, J.P., Wood, E.F., Verhoest, N.E.C., Pauwels, V.R.N., 2015. SMOS soil moisture assimilation for improved hydrologic simulation in the Murray Darling Basin, Australia. Remote Sens. Environ. 168, 146–162.
Lievens, H., Reichle, R.H., Liu, Q., De Lannoy, G.J.M., Dunbar, R.S., Kim, S.B., Das, N.N., Cosh, M., Walker, J.P., Wagner, W., 2017. Joint Sentinel-1 and SMAP data assimilation to improve soil moisture estimates. Geophys. Res. Lett. 44 (12), 6145–6153. http://dx.doi.org/10.1002/2017GL073904.
Liu, J.G., 2000. Smoothing filter-based intensity modulation: a spectral preserve image fusion technique for improving spatial details. Int. J. Remote Sens. 21, 3461–3472.
Liu, W., Baret, F., Xingfa, G., Qingxi, T., Lanfen, Z., Bing, Z., 2002. Relating soil surface moisture to reflectance. Remote Sens. Environ. 81, 238–246.
Lloyd, C.D., 2005. Assessing the effect of integrating elevation data into the estimation of monthly precipitation in Great Britain. J. Hydrol. 308, 128–150.
Loew, A., Mauser, W., 2008. On the disaggregation of passive microwave soil moisture data using emphasis emphasistype a priori knowledge of temporally persistent soil moisture fields. IEEE Trans. Geosci. Remote Sens. 46, 819–834.
Mahfouf, J.F., Bergaoui, K., Draper, C., Bouyssel, F., Taillefer, F., Taseva, L., 2009. A comparison of two off-line soil analysis schemes for assimilation of screen level observations. J. Geophys. Res. Atmos. 114.
Malbéteau, Y., Merlin, O., Molero, B., Rüdiger, C., Bacon, S., 2016. DisPATCh as a tool to evaluate coarse-scale remotely sensed soil moisture using localized in situ measurements: application to SMOS and AMSR-E data in Southeastern Australia. Int. J. Appl. Earth Obs. Geoinf. 45 (Part B), 221–234.
Mallick, K., Bhattacharya, B.K., Patel, N.K., 2009. Estimating volumetric surface moisture content for cropped soils using a soil wetness index based on surface temperature and NDVI. Agric. For. Meteorol. 149, 1327–1342.
Maltese, A., Bates, P., Capodici, F., Cannarozzo, M., Ciraolo, G., La Loggia, G., 2013. Critical analysis of thermal inertia approaches for surface soil water content retrieval. Hydrol. Sci. J. 58, 1144–1161.
Mao, K.-B., Ma, Y., Xia, L., Tang, H.-J., Han, L.-J., 2012. The monitoring analysis for the drought in China by using an improved MPI method. J. Integr. Agric. 11, 1048–1058.
Mascaro, G., Vivoni, E.R., Deidda, R., 2010. Downscaling soil moisture in the southern Great Plains through a calibrated multifractal model for land surface modeling applications. Water Resour. Res. 46 (n/a-n/a).
Mascaro, G., Vivoni, E.R., Deidda, R., 2011. Soil moisture downscaling across climate regions and its emergent properties. J. Geophys. Res. Atmos. 116.
McFarland, M.J., Miller, R.L., Neale, C.M.U., 1990. Land surface temperature derived from the SSM/I passive microwave brightness temperatures. IEEE Trans. Geosci. Remote Sens. 28, 839–845.
Mecikalski, J.R., Diak, G.R., Anderson, M.C., Norman, J.M., 1999. Estimating fluxes on continental scales using remotely sensed data in an atmospheric–land Exchange model. J. Appl. Meteorol. 38, 1352–1369.
Meesters, A.G.C.A., Jeu, R.A.M.D., Owe, M., 2005. Analytical derivation of the vegetation optical depth from the microwave polarization difference index. IEEE Geosci. Remote Sens. Lett. 2, 121–123.
Merlin, O., Chehbouni, A.G., Kerr, Y.H., Njoku, E.G., Entekhabi, D., 2005. A combined modeling and multispectral/multiresolution remote sensing approach for disaggregation of surface soil moisture: application to SMOS configuration. IEEE Trans. Geosci. Remote Sens. 43, 2036–2050.
Merlin, O., Chehbouni, A., Kerr, Y.H., Goodrich, D.C., 2006. A downscaling method for distributing surface soil moisture within a microwave pixel: application to the Monsoon '90 data. Remote Sens. Environ. 101, 379–389.
Merlin, O., Chehbouni, A., Walker, J.P., Panciera, R., Kerr, Y.H., 2008a. A simple method to disaggregate passive microwave-based soil moisture. IEEE Trans. Geosci. Remote Sens. 46, 786–796.
Merlin, O., Walker, J.P., Chehbouni, A., Kerr, Y., 2008b. Towards deterministic downscaling of SMOS soil moisture using MODIS derived soil evaporative efficiency. Remote Sens. Environ. 112, 3935–3946.
Merlin, O., Al Bitar, A., Walker, J.P., Kerr, Y., 2009. A sequential model for disaggregating near-surface soil moisture observations using multi-resolution thermal sensors. Remote Sens. Environ. 113, 2275–2284.
Merlin, O., Al Bitar, A., Walker, J.P., Kerr, Y., 2010. An improved algorithm for disaggregating microwave-derived soil moisture based on red, near-infrared and thermal-infrared data. Remote Sens. Environ. 114, 2305–2316.
Merlin, O., Rudiger, C., Al Bitar, A., Richaume, P., Walker, J.P., Kerr, Y.H., 2012. Disaggregation of SMOS soil moisture in Southeastern Australia. IEEE Trans. Geosci. Remote Sens. 50, 1556–1571.
Merlin, O., Escorihuela, M.J., Mayoral, M.A., Hagolle, O., Al Bitar, A., Kerr, Y., 2013. Self-calibrated evaporation-based disaggregation of SMOS soil moisture: an evaluation study at 3 km and 100 m resolution in Catalunya, Spain. Remote Sens. Environ. 130, 25–38.
Merlin, O., Malbéteau, Y., Notfi, Y., Bacon, S., Khabba, S., Jarlan, L., 2015. Performance metrics for soil moisture downscaling methods: application to DISPATCH data in Central Morocco. Remote Sens. 7, 3783–3807.
Minacapilli, M., Iovino, M., Blanda, F., 2009. High resolution remote estimation of soil surface water content by a thermal inertia approach. J. Hydrol. 379, 229–238.
Mohanty, B.P., Cosh, M.H., Lakshmi, V., Montzka, C., 2017. Soil moisture remote sensing: state-of-the-science. Vadose Zone J. 16.
Molero, B., Merlin, O., MALBÉTEAU, Y., Al Bitar, A., Cabot, F., Stefan, V., Kerr, Y., Bacon, S., Cosh, M.H., Bindlish, R., Jackson, T.J., 2016. SMOS disaggregated soil moisture product at 1 km resolution: processor overview and first validation results. Remote Sens. Environ. 180, 361–376.
Montzka, C., Hasan, S., Bogena, H., Hajnsek, I., Horn, R., Jagdhuber, T., Reigber, A., Hermes, N., Rüdiger, C., Vereecken, H., 2012. Active and passive airborne microwave remote sensing for soil moisture retrieval in the Rur catchment, Germany. In: 2012 IEEE International Geoscience and Remote Sensing Symposium, 22–27 July 2012, pp. 6956–6959.
Montzka, C., Jagdhuber, T., Horn, R., Bogena, H.R., Hajnsek, I., Reigber, A., Vereecken, H., 2016. Investigation of SMAP fusion algorithms with airborne active and passive L-band microwave remote sensing. IEEE Trans. Geosci. Remote Sens. 54, 3878–3889.
Moran, M.S., Clarke, T.R., Inoue, Y., Vidal, A., 1994. Estimating crop water deficit using the relation between surface-air temperature and spectral vegetation index. Remote Sens. Environ. 49, 246–263.
Moran, M.S., Hymer, D.C., Qi, J., Sano, E.E., 2000. Soil moisture evaluation using multi-temporal synthetic aperture radar (SAR) in semiarid rangeland. Agric. For. Meteorol. 105, 69–80.
Muller, E., Décamps, H., 2001. Modeling soil moisture–reflectance. Remote Sens. Environ. 76, 173–180.
Narayan, U., Lakshmi, V., 2008. Characterizing subpixel variability of low resolution radiometer derived soil moisture using high resolution radar data. Water Resour. Res. 44 (n/a-n/a).
Narayan, U., Lakshmi, V., Jackson, T.J., 2006. High-resolution change estimation of soil moisture using L-band radiometer and Radar observations made during the SMEX02 experiments. IEEE Trans. Geosci. Remote Sens. 44, 1545–1554.
Neale, C.M.U., Mcfarland, M.J., CHANG, K., 1990. Land-surface-type classification using microwave brightness temperatures from the special sensor microwave/imager. IEEE Trans. Geosci. Remote Sens. 28, 829–838.
Nemani, R., Pierce, L., Running, S., Goward, S., 1993. Developing satellite-derived estimates of surface moisture status. J. Appl. Meteorol. 32, 548–557.
Njoku, E.G., Entekhabi, D., 1996. Passive microwave remote sensing of soil moisture. J. Hydrol. 184, 101–129.
Njoku, E.G., Wilson, W.J., Yueh, S.H., Rahmat-Samii, Y., 2000. A large-antenna microwave radiometer-scatterometer concept for ocean salinity and soil moisture sensing. IEEE Trans. Geosci. Remote Sens. 38, 2645–2655.
Njoku, E., Yunjin, K., Spencer, M., Rahmat-Samii, Y., Thomson, M.W., 2001. A spaceborne L-band radiometer-radar concept for land and ocean surface monitoring. In: Aerospace Conference, IEEE Proceedings. vol. 4. pp. 4/1841–4/1848.
Njoku, E.G., Wilson, W.J., Yueh, S.H., Dinardo, S.J., Fuk, K.L., Jackson, T.J., Lakshmi, V., Bolten, J., 2002. Observations of soil moisture using a passive and active low-frequency microwave airborne sensor during SGP99. IEEE Trans. Geosci. Remote Sens. 40, 2659–2673.
Noilhan, J., Planton, S., 1989. A simple parameterization of land surface processes for meteorological models. Mon. Weather Rev. 117, 536–549.
Notarnicola, C., Angiulli, M., Posa, F., 2008. Soil moisture retrieval from remotely sensed data: neural network approach versus Bayesian method. IEEE Trans. Geosci. Remote Sens. 46, 547–557.
O'neill, P.E., Chauhan, N., 1992. Synergistic use of active and passive microwave in soil moisture estimation. In: International Geoscience and Remote Sensing Symposium, 1992. IGARSS '92., 26–29 May 1992, pp. 492–494.
O'neill, P.E., Chauhan, N.S., Jackson, T.J., 1996. Use of active and passive microwave remote sensing for soil moisture estimation through corn. Int. J. Remote Sens. 17, 1851–1865.
Owe, M., Van De Griend, A.A., 2001. On the relationship between thermodynamic surface temperature and high-frequency (37 GHz) vertically polarized brightness temperature under semi-arid conditions. Int. J. Remote Sens. 22, 3521–3532.
Owe, M., De Jeu, R., Holmes, T., 2008. Multisensor historical climatology of satellite-derived global land surface moisture. J. Geophys. Res. Earth Surf. 113.
Pablos, M., Piles, M., Sánchez, N., Vall-Llossera, M., Martínez-Fernández, J., Camps, A., 2016. Impact of day/night time land surface temperature in soil moisture disaggregation algorithms. Eur. J. Remote. Sens. 49, 899–916.
Paloscia, S., Pettinato, S., Santi, E., Notarnicola, C., Pasolli, L., Reppucci, A., 2013. Soil moisture mapping using Sentinel-1 images: algorithm and preliminary validation. Remote Sens. Environ. 134, 234–248.
Pampaloni, P., Paloscia, S., 1985. Experimental relationships between microwave emission and vegetation features. Int. J. Remote Sens. 6, 315–323.
Panciera, R., Walker, J.P., Jackson, T.J., Gray, D.A., Tanase, M.A., Ryu, D., Monerris, A., Yardley, H., Rüdiger, C., Wu, X., Gao, Y., Hacker, J.M., 2014. The soil moisture active passive experiments (SMAPEx): toward soil moisture retrieval from the SMAP mission. IEEE Trans. Geosci. Remote Sens. 52, 490–507.
Parada, L.M., Liang, X., 2003. A downscaling framework for L band radiobrightness temperature imagery. J. Geophys. Res. Atmos. 108 (n/a-n/a).

Parinussa, R.M., Yilmaz, M.T., Anderson, M.C., Hain, C.R., De Jeu, R.A.M., 2014. An intercomparison of remotely sensed soil moisture products at various spatial scales over the Iberian Peninsula. Hydrol. Process. 28, 4865–4876.
Park, S., Im, J., Park, S., Rhee, J., 2015. AMSR2 soil moisture downscaling using multi-sensor products through machine learning approach. In: 2015 IEEE International Geoscience and Remote Sensing Symposium (IGARSS), 26–31 July 2015, pp. 1984–1987.
Patel, N.R., Anapashsha, R., Kumar, S., Saha, S.K., Dadhwal, V.K., 2009. Assessing potential of MODIS derived temperature/vegetation condition index (TVDI) to infer soil moisture status. Int. J. Remote Sens. 30, 23–39.
Pellenq, J., Kalma, J., Boulet, G., Saulnier, G.M., Wooldridge, S., Kerr, Y., Chehbouni, A., 2003. A disaggregation scheme for soil moisture based on topography and soil depth. J. Hydrol. 276, 112–127.
Peng, J., Niesel, J., Loew, A., 2015. Evaluation of soil moisture downscaling using a simple thermal-based proxy – the REMEDHUS network (Spain) example. Hydrol. Earth Syst. Sci. 19, 4765–4782.
Peng, J., Loew, A., Shiqiang, Z., Jie, W., Niesel, J., 2016. Spatial downscaling of satellite soil moisture data using a vegetation temperature condition index. IEEE Trans. Geosci. Remote Sens. 54, 558–566.
Peng, J., Loew, A., Merlin, O., Verhoest, N.E.C., 2017. A review of spatial downscaling of satellite remotely sensed soil moisture. Rev. Geophys. 55 (2), 341–366.
Perry, M.A., Niemann, J.D., 2007. Analysis and estimation of soil moisture at the catchment scale using EOFs. J. Hydrol. 334, 388–404.
Perry, M.A., Niemann, J.D., 2008. Generation of soil moisture patterns at the catchment scale by EOF interpolation. Hydrol. Earth Syst. Sci. 12, 39–53.
Petropoulos, G.P., Ireland, G., Barrett, B., 2015. Surface soil moisture retrievals from remote sensing: current status, products & future trends. Phys. Chem. Earth A/B/C 83–84, 36–56.
Piles, M., Camps, A., Vall-Llossera, M., Talone, M., 2009a. Spatial-resolution enhancement of SMOS data: a deconvolution-based approach. IEEE Trans. Geosci. Remote Sens. 47, 2182–2192.
Piles, M., Entekhabi, D., Camps, A., 2009b. A change detection algorithm for retrieving high-resolution soil moisture from SMAP radar and radiometer observations. IEEE Trans. Geosci. Remote Sens. 47, 4125–4131.
Piles, M., Camps, A., Vall-Llossera, M., Corbella, I., Panciera, R., Rudiger, C., Kerr, Y.H., Walker, J., 2011. Downscaling SMOS-derived soil moisture using MODIS visible/infrared data. IEEE Trans. Geosci. Remote Sens. 49, 3156–3166.
Piles, M., Vall-Llossera, M., Laguna, L., Camps, A., 2012. A downscaling approach to combine SMOS multi-angular and full-polarimetric observations with MODIS VIS/IR data into high resolution soil moisture maps. In: IEEE International Geoscience and Remote Sensing Symposium (IGARSS), pp. 1247–1250 (22–27 July).
Piles, M., Vall-Llossera, M., Camps, A., Sánchez, N., Martínez-Fernández, J., Martínez, J., González-Gambau, V., Riera, R., 2013. On the synergy of SMOS and Terra/Aqua MODIS: high resolution soil moisture maps in near real-time. In: IEEE International Geoscience and Remote Sensing Symposium (IGARSS), pp. 3423–3426 (21–26 July).
Piles, M., Sanchez, N., Vall-Llossera, M., Camps, A., Martinez-Fernandez, J., Martinez, J., Gonzalez-Gambau, V., 2014. A downscaling approach for SMOS land observations: evaluation of high-resolution soil moisture maps over the Iberian Peninsula. IEEE J. Sel. Top. Appl. Earth Obs. Remote Sens. 7, 3845–3857.
Piles, M., Petropoulos, G.P., Sánchez, N., González-Zamora, Á., Ireland, G., 2016. Towards improved spatio-temporal resolution soil moisture retrievals from the synergy of SMOS and MSG SEVIRI spaceborne observations. Remote Sens. Environ. 180, 403–417.
Quesney, A., Le Hégarat-Mascle, S., Taconet, O., Vidal-Madjar, D., Wigneron, J.P., Loumagne, C., Normand, M., 2000. Estimation of watershed soil moisture Index from ERS/SAR data. Remote Sens. Environ. 72, 290–303.
Ranney, K.J., Niemann, J.D., Lehman, B.M., Green, T.R., Jones, A.S., 2015. A method to downscale soil moisture to fine resolutions using topographic, vegetation, and soil data. Adv. Water Resour. 76, 81–96.
Reichle, R.H., 2000. Variational Assimilation of Remote Sensing Data for Land Surface Hydrologic Applications. Massachusetts Institute of Technology.
Reichle, R.H., Entekhabi, D., Mclaughlin, D.B., 2001. Downscaling of radio brightness measurements for soil moisture estimation: a four-dimensional variational data assimilation approach. Water Resour. Res. 37, 2353–2364.
Reichle, R., Koster, R., De Lannoy, G., Crow, W., Kimball, J., 2014. SMAP Algorithm Theoretical Basis Document (ATBD): Level 4 Surface and Root Zone Soil Moisture (L4_SM) Data Product [Online]. Jet Propulsion Lab, Pasadena, CA Available: https://nsidc.org/sites/nsidc.org/files/technical-references/272_L4_SM_RevA_web.pdf (Accessed 2017).
Reichle, R.H., Lannoy, G.J.M.D., Liu, Q., Ardizzone, J.V., Colliander, A., Conaty, A., Crow, W., Jackson, T.J., Jones, L.A., Kimball, J.S., Koster, R.D., Mahanama, S.P., Smith, E.B., Berg, A., Bircher, S., Bosch, D., Caldwell, T.G., Cosh, M., González-Zamora, Á., Collins, C.D.H., Jensen, K.H., Livingston, S., Lopez-Baeza, E., Martínez-Fernández, J., Mcnairn, H., Moghaddam, M., Pacheco, A., Pellarin, T., Prueger, J., Rowlandson, T., Seyfried, M., Starks, P., Su, Z., Thibeault, M., Velde, R.V.D., Walker, J., Wu, X., Zeng, Y., 2017. Assessment of the SMAP level-4 surface and root-zone soil moisture product using in situ measurements. J. Hydrometeorol. 0 (null).
Remesan, R., Shamim, M.A., Han, D., Mathew, J., 2009. Runoff prediction using an integrated hybrid modelling scheme. J. Hydrol. 372, 48–60.
Richardson, A.J., Wiegand, C., 1977. Distinguishing vegetation from soil background information. Photogramm. Eng. Remote. Sens. 43, 1541–1552.
Robinson, D., Campbell, C., Hopmans, J., Hornbuckle, B., Jones, S.B., Knight, R., Ogden, F., Selker, J., Wendroth, O., 2008. Soil moisture measurement for ecological and hydrological watershed-scale observatories: a review. Vadose Zone J. 7, 358–389.
Rouse, J.W., Haas, R., Schell, J., Deering, D., 1974. Monitoring Vegetation Systems in the Great Plains with ERTS.
Rüdiger, C., Su, C.H., Ryu, D., Wagner, W., 2016. Disaggregation of low-resolution L-band radiometry using C-band radar data. IEEE Geosci. Remote Sens. Lett. 13, 1425–1429.
Sahoo, A.K., De Lannoy, G.J.M., Reichle, R.H., Houser, P.R., 2013. Assimilation and downscaling of satellite observed soil moisture over the Little River Experimental Watershed in Georgia, USA. Adv. Water Resour. 52, 19–33.
Salvia, M., Grings, F., Ferrazzoli, P., Barraza, V., Douna, V., Perna, P., Bruscantini, C., Karszenbaum, H., 2011. Estimating flooded area and mean water level using active and passive microwaves: the example of Paraná River Delta floodplain. Hydrol. Earth Syst. Sci. 15, 2679–2692.
Sánchez-Ruiz, S., Piles, M., Sánchez, N., Martínez-Fernández, J., Vall-Llossera, M., Camps, A., 2014. Combining SMOS with visible and near/shortwave/thermal infrared satellite data for high resolution soil moisture estimates. J. Hydrol. 516, 273–283.
Sandholt, I., Rasmussen, K., Andersen, J., 2002. A simple interpretation of the surface temperature/vegetation index space for assessment of surface moisture status. Remote Sens. Environ. 79, 213–224.
Santi, E., 2010. An application of the SFIM technique to enhance the spatial resolution of spaceborne microwave radiometers. Int. J. Remote Sens. 31, 2419–2428.
Schmugge, T., Gloersen, P., Wilheit, T., Geiger, F., 1974. Remote sensing of soil moisture with microwave radiometers. J. Geophys. Res. 79, 317–323.
Schmugge, T., Jackson, T., Mckim, H., 1980. Survey of methods for soil moisture determination. Water Resour. Res. 16, 961–979.
Schmugge, T.J., Kustas, W.P., Ritchie, J.C., Jackson, T.J., Rango, A., 2002. Remote sensing in hydrology. Adv. Water Resour. 25, 1367–1385.
Seneviratne, S.I., Corti, T., Davin, E.L., Hirschi, M., Jaeger, E.B., Lehner, I., Orlowsky, B., Teuling, A.J., 2010. Investigating soil moisture–climate interactions in a changing climate: a review. Earth Sci. Rev. 99, 125–161.
Shevenell, L., 1999. Regional potential evapotranspiration in arid climates based on temperature, topography and calculated solar radiation. Hydrol. Process. 13, 577–596.
Shi, H., Fu, X., Chen, J., Wang, G., Li, T., 2014a. Spatial distribution of monthly potential evaporation over mountainous regions: case of the Lhasa River basin, China. Hydrol. Sci. J. 59, 1856–1871.
Shi, J., Guo, P., Zhao, T., Du, J., 2014b. Soil Moisture downscaling algorithm for combining radar and radiometer observations for SMAP mission. In: 2014 XXXIth URSI General Assembly and Scientific Symposium (URSI GASS), 16–23 Aug. 2014, pp. 1–4.
Shin, Y., Mohanty, B.P., 2013. Development of a deterministic downscaling algorithm for remote sensing soil moisture footprint using soil and vegetation classifications. Water Resour. Res. 49, 6208–6228.
Song, C., Jia, L., Menenti, M., 2012. A method for retrieving high-resolution surface soil moisture by downscaling AMSR-E brightness temperature. In: 2012 IEEE International Geoscience and Remote Sensing Symposium, 22–27 July 2012, pp. 730–733.
Song, C., Jia, L., Menenti, M., 2014. Retrieving high-resolution surface soil moisture by downscaling AMSR-E brightness temperature using MODIS LST and NDVI data. IEEE J. Sel. Top. Appl. Earth Obs. Remote Sens. 7, 935–942.
Srivastava, P., Han, D., Ramirez, M., Islam, T., 2013. Machine learning techniques for downscaling SMOS satellite soil moisture using MODIS land surface temperature for hydrological application. Water Resour. Manag. 27, 3127–3144.
Stisen, S., Sandholt, I., Nørgaard, A., Fensholt, R., Jensen, K.H., 2008. Combining the triangle method with thermal inertia to estimate regional evapotranspiration—applied to MSG-SEVIRI data in the Senegal River basin. Remote Sens. Environ. 112, 1242–1255.
Taylor, C.M., 2015. Detecting soil moisture impacts on convective initiation in Europe. Geophys. Res. Lett. 42, 4631–4638.
Temimi, M., Leconte, R., Brissette, F., Chaouch, N., 2007. Flood and soil wetness monitoring over the Mackenzie River Basin using AMSR-E 37 GHz brightness temperature. J. Hydrol. 333, 317–328.
Temimi, M., Leconte, R., Chaouch, N., Sukumal, P., Khanbilvardi, R., Brissette, F., 2010. A combination of remote sensing data and topographic attributes for the spatial and temporal monitoring of soil wetness. J. Hydrol. 388, 28–40.
Theis, S.W., Blanchard, B.J., Blanchard, A.J., 1986. Utilization of active microwave roughness measurements to improve passive microwave soil moisture estimates over bare soils. IEEE Trans. Geosci. Remote Sens. GE-24, 334–339.
Torres, R., Snoeij, P., Geudtner, D., Bibby, D., Davidson, M., Attema, E., Potin, P., Rommen, B., Floury, N., Brown, M., 2012. GMES sentinel-1 mission. Remote Sens. Environ. 120, 9–24.
Tuttle, S.E., Salvucci, G.D., 2014. A new approach for validating satellite estimates of soil moisture using large-scale precipitation: comparing AMSR-E products. Remote Sens. Environ. 142, 207–222.
Ulaby, F.T., Moore, R.K., Fung, A.K., 1981. Microwave remote sensing: Active and passive. In: Microwave Remote Sensing Fundamentals and Radiometry. vol. 1.
Ulaby, F.T., Moore, R.K., Fung, A.K., 1982. Microwave Remote Sensing: Active and Passive, in Radar Remote Sensing and Surface Scattering and Emission Theory, Reading. Addison-Wesley, MA, USA.
Ulaby, F.T., Dobson, M.C., Brunfeldt, D.R., 1983. Improvement of moisture estimation accuracy of vegetation-covered soil by combined active/passive microwave remote sensing. IEEE Trans. Geosci. Remote Sens. GE-21, 300–307.
Ulaby, F.T., Dubois, P.C., Van Zyl, J., 1996. Radar mapping of surface soil moisture. J. Hydrol. 184, 57–84.
Van Der Velde, R., Salama, M., Eweys, O., Wen, J., Wang, Q., 2015. Soil moisture mapping using combined active/passive microwave observations over the East of the Netherlands. IEEE J. Sel. Top. Appl. Earth Obs. Remote Sens. 1–18.
Van Doninck, J., Peters, J., De Baets, B., De Clercq, E.M., Ducheyne, E., Verhoest, N.E.C., 2011. The potential of multitemporal Aqua and Terra MODIS apparent thermal inertia as a soil moisture indicator. Int. J. Appl. Earth Obs. Geoinf. 13, 934–941.
Vanderlinden, K., Giráldez, J.V., Meirvenne, M.V., 2008. Spatial estimation of reference

evapotranspiration in Andalusia, Spain. J. Hydrometeorol. 9, 242–255.
Vereecken, H., Huisman, J.A., Bogena, H., Vanderborght, J., Vrugt, J.A., Hopmans, J.W., 2008. On the value of soil moisture measurements in vadose zone hydrology: a review. Water Resour. Res. 44.
Verhoef, A., Van Den Hurk, B.J.J.M., Jacobs, A.F.G., Heusinkveld, B.G., 1996. Thermal soil properties for vineyard (EFEDA-I) and savanna (HAPEX-Sahel) sites. Agric. For. Meteorol. 78, 1–18.
Verhoest, N.E.C., Van Den Berg, M.J., Martens, B., Lievens, H., Wood, E.F., Ming, P., Kerr, Y.H., Al Bitar, A., Tomer, S.K., Drusch, M., Vernieuwe, H., De Baets, B., Walker, J.P., Dumedah, G., Pauwels, V.R.N., 2015. Copula-based downscaling of coarse-scale soil moisture observations with implicit bias correction. IEEE Trans. Geosci. Remote Sens. 53, 3507–3521.
Wagner, W., Scipal, K., 2000. Large-scale soil moisture mapping in western Africa using the ERS scatterometer. IEEE Trans. Geosci. Remote Sens. 38, 1777–1782.
Wagner, W., Lemoine, G., Rott, H., 1999. A method for estimating soil moisture from ERS scatterometer and soil data. Remote Sens. Environ. 70, 191–207.
Wagner, W., Sabel, D., Doubkova, M., Bartsch, A., Pathe, C., 2009. The potential of Sentinel-1 for monitoring soil moisture with a high spatial resolution at global scale. In: Earth Observation and Water Cycle Science Symposium. Frascati, Italy.
Wagner, W., Hahn, S., Kidd, R., Melzer, T., Bartalis, Z., Hasenauer, S., Figa-Saldaña, J., De Rosnay, P., Jann, A., Schneider, S., Komma, J., Kubu, G., Brugger, K., Aubrecht, C., Züger, J., Gangkofner, U., Kienberger, S., Brocca, L., Wang, Y., Blöschl, G., Eitzinger, J., Steinnocher, K., Zeil, P., Rubel, F., 2013. The ASCAT soil moisture product: a review of its specifications, validation results, and emerging applications. Meteorol. Z. 22, 5–33.
Walker, J.P., Houser, P.R., 2004. Requirements of a global near-surface soil moisture satellite mission: accuracy, repeat time, and spatial resolution. Adv. Water Resour. 27, 785–801.
Walker, J.P., Willgoose, G.R., Kalma, J.D., 2001. One-dimensional soil moisture profile retrieval by assimilation of near-surface measurements: a simplified soil moisture model and field application. J. Hydrometeorol. 2, 356–373.
Walker, J.P., Houser, P.R., Willgoose, G.R., 2004. Active microwave remote sensing for soil moisture measurement: a field evaluation using ERS-2. Hydrol. Process. 18, 1975–1997.
Wan, Z., Wang, P., Li, X., 2004. Using MODIS land surface temperature and normalized difference vegetation index products for monitoring drought in the southern Great Plains, USA. Int. J. Remote Sens. 25, 61–72.
Wang, L., Qu, J.J., 2007. NMDI: a normalized multi-band drought index for monitoring soil and vegetation moisture with satellite remote sensing. Geophys. Res. Lett. 34.
Wang, L., Qu, J.J., 2009. Satellite remote sensing applications for surface soil moisture monitoring: a review. Front. Earth Sci. China 3, 237–247.
Wang, J., Ling, Z., Wang, Y., Zeng, H., 2016. Improving spatial representation of soil moisture by integration of microwave observations and the temperature–-vegetation–drought index derived from MODIS products. ISPRS J. Photogramm. Remote Sens. 113, 144–154.
Werbylo, K.L., Niemann, J.D., 2014. Evaluation of sampling techniques to characterize topographically-dependent variability for soil moisture downscaling. J. Hydrol. 516, 304–316.
Western, A.W., Grayson, R.B., Blöschl, G., 2002. Scaling of soil moisture: a hydrologic perspective. Annu. Rev. Earth Planet. Sci. 30, 149–180.
Wilson, D.J., Western, A.W., Grayson, R.B., 2005. A terrain and data-based method for generating the spatial distribution of soil moisture. Adv. Water Resour. 28, 43–54.
Wu, X., Walker, J.P., Das, N.N., Panciera, R., Rüdiger, C., 2014. Evaluation of the SMAP brightness temperature downscaling algorithm using active–passive microwave observations. Remote Sens. Environ. 155, 210–221.
Wu, X., Walker, J.P., Rudiger, C., Panciera, R., Gray, D.A., 2015. Simulation of the SMAP data stream from SMAPEx field campaigns in Australia. IEEE Trans. Geosci. Remote Sens. 53, 1921–1934.
Wu, X., Walker, J.P., Rüdiger, C., Panciera, R., Gao, Y., 2016. Intercomparison of alternate soil moisture downscaling algorithms using active-passive microwave observations. IEEE Geosci. Remote Sens. Lett. 1–5.
Wu, X., Walker, J.P., Rudiger, C., Gao, Y., 2017. Medium-resolution soil moisture retrieval using bayesian merging method. IEEE Geosci. Remote Sens. Lett. 55 (11), 6482–6493.
Xia, Y., Sheffield, J., Ek, M.B., Dong, J., Chaney, N., Wei, H., Meng, J., Wood, E.F., 2014. Evaluation of multi-model simulated soil moisture in NLDAS-2. J. Hydrol. 512, 107–125.
Yee, M., Walker, J.P., Rüdiger, C., Parinussa, R.M., Koike, T., Kerr, Y.H., 2017. A comparison of SMOS and AMSR-2 soil moisture using representative sites of the OzNet monitoring network. Remote Sens. Environ. 195, 297–312.
Zhan, X., Miller, S., Chauhan, N., Di, L., Ardanuy, P., Running, S., 2002. Soil Moisture Visible/Infrared Imager/Radiometer Suite Algorithm Theoretical Basis Document.
Zhan, X., Houser, P.R., Walker, J.P., Crow, W.T., 2006. A method for retrieving high-resolution surface soil moisture from hydros L-band radiometer and Radar observations. IEEE Trans. Geosci. Remote Sens. 44, 1534–1544.
Zhang, Y., Wegehenkel, M., 2006. Integration of MODIS data into a simple model for the spatial distributed simulation of soil water content and evapotranspiration. Remote Sens. Environ. 104, 393–408.
Zhang, D., Tang, R., Zhao, W., Tang, B., Wu, H., Shao, K., Li, Z.-L., 2014. Surface soil water content estimation from thermal remote sensing based on the temporal variation of land surface temperature. Remote Sens. 6, 3170.
Zhao, W., Li, A., 2013a. A downscaling method for improving the spatial resolution of AMSR-E derived soil moisture product based on MSG-SEVIRI data. Remote Sens. 5, 6790.
Zhao, W., Li, Z.-L., 2013b. Sensitivity study of soil moisture on the temporal evolution of surface temperature over bare surfaces. Int. J. Remote Sens. 34, 3314–3331.
Zhou, Z., Zhao, S., Chen, Z., Jiang, L., 2015. Comparison of different downscaling methods of soil moisture in Luan he Watershed. In: 2015 IEEE International Geoscience and Remote Sensing Symposium (IGARSS), 26–31 July 2015, pp. 1980–1983.